Mechanisms and Treatment of Blood-Brain Barrier Dysfunction and Related Pathology During Aging

by

Vladimir Senatorov

A dissertation submitted in partial satisfaction of the

requirements for the degree of

Doctor of Philosophy

in

Neuroscience

in the

Graduate Division

of the

University of California, Berkeley

Committee in charge:

Dr. Daniela Kaufer, Chair
Dr. Andrew Dillin
Dr. Ellen Robey
Dr. David Schaffer

Spring 2018

Abstract

Mechanisms and Treatment of Blood-Brain Barrier Dysfunction and Related Pathology During Aging

by

Vladimir Senatorov

Doctor of Philosophy in Neuroscience

University of California, Berkeley

Dr. Daniela Kaufer, Chair

Aging involves a decline in neural function that contributes to cognitive impairment and disease. However, the causes of the transition from a “young-and-healthy” to “aged-and-dysfunctional” brain are not well understood. The following studies all address the mechanisms by which the blood-brain barrier (BBB) declines during aging, and how genetic and pharmacological inhibition of inflammatory signaling ameliorates aging-related neuropathology. Chapter 2 describes how the blood-brain barrier (BBB) deteriorates during aging, starting as early as middle age and continuing to the end of the lifespan. This vascular damage activates inflammatory transforming growth factor β (TGFβ) signaling in astrocytes. Using gain-of-function and loss-of-function manipulations in mice, we show that astrocytic TGFβ signaling is necessary and sufficient to cause neural dysfunction and pathological outcomes, including aberrant electrocorticographic activity, vulnerability to seizures, and cognitive impairment. Furthermore, inhibition of TGFβ signaling reverses these symptomatic hallmarks of aging. Chapter 3 delves deeper into the mechanism by which molecular correlates of neurosynaptic transmission become dysregulated during aging, focusing specifically on how TGFβ signaling contributes to aging-related cognitive decline via selective remodeling of glutamatergic and GABAergic receptor subunits. Chapter 4 investigates the core mechanism of decline of the transcriptional machinery that governs BBB permeability during aging, and also explores the potential of a novel pharmacological approach aimed at restoring the structural and functional integrity of the BBB. Together, these studies reveal the neurovascular unit as one of the earliest triggers of neurological aging, indicating that the aging brain may retain considerable latent capacity which can be revitalized by therapeutic inhibition against TGFβ signaling.

Table of Contents

Chapter 1. Introduction

Adapted from: Senatorov VV Jr, Friedman AR, Milikovsky DZ, Ofer J, Saar-Ashkenazy R, Charbash A, Jahan N, Chin G, Mihaly E, Lin JM, Ramsay HJ, Moghbel A, Preininger MK, Eddings CR, Harrison HV, Veksler R, Becker A, Hart B, Rogawski MA, Dillin A, Friedman A, and Kaufer D, 2018. Blood-brain barrier breakdown during aging causes chronic but reversible neural dysfunction via TGF-beta signaling. Manuscript in preparation.

Aging is accepted as one of the strongest drivers of cognitive decline, which is thought to result from underlying hallmarks of brain aging including synaptic loss and other impairments in neural function [1,2]. This predictable decline has been shown across mammalian species, especially in humans, who are heterogenous in their experience. Some elderly people have only subtle deficits, while some experience much more severe, neurodegenerative decline, as in Alzheimer's disease (AD) and in other types of dementias. It is unknown whether the "natural" cognitive decline that is widespread and apparently normal in aging is functionally distinct from severe forms of dementia, or alternatively, whether the early stages of mild cognitive impairment (MCI) may be the first step on a pathway leading to severe neurodegenerative disease. We also have a severely limited understanding of how the brain transitions from a youthful, healthy organ into an old and more dysfunctional one. The neurobiological mechanisms that work in concert to govern this enormously complex transition, have been especially elusive.

The blood-brain barrier (BBB) forms one of the most essential and tightly-regulated interfaces of the body. Composed of specialized endothelial cells, pericytes and astrocytic end-feet that sheathe the brain capillaries, the BBB restricts the diffusion of molecules from the blood to create a highly privileged and controlled environment that is absent in other tissues. As such, the BBB establishes the exacting milieu that enables brain function, including the precise ionic concentrations needed for neural activity, the compartmentalization of brain-specific growth factors and signaling molecules, and the immune-privileged brain environment [3,4].

As early as the 1970s, clinical researchers began to report alarming observations of BBB dysfunction in aging patients [5], raising the possibility of a new form of biological senescence involving vascular leakiness, which would be expected to cause neurological complications [4,6–9]. While these reports generated controversy, including debate over how to accurately measure BBB status in living subjects[10], meta-analysis across clinical BBB studies concluded that BBB dysfunction is not only widely prevalent in aging individuals, but also strongly correlated with neurological disease [11], including Alzheimer's disease [9,12–14]. Furthermore, BBB dysfunction in aging patients was found to be highly associated with mild cognitive impairment when localized in the hippocampus [15]. This regional specificity suggests that vascular leakiness may directly cause impairments in affected brain regions. These clinical findings raise the possibility that BBB dysfunction may be a major contributor to age-related neurological diseases including dementias [16]. Yet remarkably there have been very few animal studies investigating BBB dysfunction during aging.

Notably, age-related cognitive impairments share a remarkably similar set of symptomatic outcomes to head injury and trauma: both aging and acute insults to the brain involve initial BBB disruption followed by secondary neural dysfunction and cognitive impairment [17–19]. Especially on the levels of molecular, cellular and systems mechanisms, the connections may be even stronger. There is strong evidence that the earliest stages of mild cognitive impairment, which can precede significant dementia-like pathology, may be caused by an imbalance in excitation and inhibition (E/I) mechanisms, as well as hyperexcitability in hippocampal and cortical circuits [20–23]. In rodent head injury studies, such imbalance stems from molecular and cellular pathology at the interactions of the neurovascular unit, which involves a complex intermingling of different brain cell types and various forms of signaling factors.

It has been shown that exogenous application of albumin to the brain triggers its uptake into glial cells and causes TGFβ signaling activation [24,25]. This subsequent dysfunction directly effects neuronal communication and leads to a remodeling of neural circuits to cause hyperexcitability and E/I imbalance [26,27]. Therefore, we reasoned that in aging, BBB dysfunction may play a similar role, in which TGFβ signaling causes neural dysfunction and hyperexcitability that could account for a range of age-related symptoms including increased seizure vulnerability and cognitive impairment.

To identify candidate mechanisms through which BBB dysfunction might cause age-related impairments, we turned to other disease contexts where the role of BBB disruption has been studied more extensively. Head trauma causes pronounced BBB dysfunction, which can persist for months or even years after the initial injury [28–30]. About 5-40% of traumatic head injury patients go on to develop secondary post-traumatic epilepsy (PTE) after a silent period of epileptogenesis [31]. In rodent studies, we previously found that inducing BBB disruption in otherwise healthy animals is sufficient to cause epileptogenesis via the signaling action of blood molecules that leak into the brain, in particular blood serum albumin [31]. Following BBB disruption, albumin induces an inflammatory TGFβ signaling cascade, primarily by TGFβR binding and endocytosis into astrocytes [32,33]. In turn, activated astrocytes produce pro-inflammatory cytokines, including TGFβ1 ligand (thus amplifying the TGFβ signaling cascade), IL-6, and IL-1β [32,34,35], propagating a signaling response that enacts physiological changes in neighboring neurons – including changes in expression of genes governing neurotransmission and excitability/inhibitory (E/I) balance, and alterations in connectivity and plasticity [24,26,27,36–38]. This reorganization of local neural networks, and associated neural dysfunction causes lower seizure threshold and spontaneous seizures [24,36,37], as well as delayed reduction in dendritic arborization and cell loss [39].

This work provoked us to investigate whether BBB dysfunction, and consequent activation of TGFβ signaling, may play a similarly central role in the neurobiology of aging. In further support of this candidate pathway, TGFβ signaling is elevated in aging rodents [40–44]and human AD patients [45–47]. However, the cause of this elevated signaling, and whether it is beneficial or pathological, has remained controversial and poorly understood. For example, elevated TGFβ signaling from activated astrocytes increases pathological outcomes in various disease models, including Alzheimer's disease [48–50], ALS [51,52], and age-related dysfunction in hypothalamic glucose homeostasis [53]. In contrast, other studies have suggested that TGFβ signaling promotes neural survival in the aging brain [54–56]. These conflicting results may arise

from the fact that the TGFβ signaling pathway is a ubiquitous and pleiotropic regulatory pathway, which exerts a wide variety of effects that are specific to cell-type and context.

These studies seek to shed light on this controversy and provide the first evidence for a mechanism that directly links brain microvascular pathology and BBB dysfunction, which occur widely in mammalian aging, to age-related neural and cognitive dysfunction. We show that astrocytic TGFβ signaling functions as a regulatory cascade that induces changes in molecular, electrophysiological, and behavioral outcomes. Key findings are that 1) BBB dysfunction appears as early as middle age, with a time course that is well-matched to first appearance of mild age-related symptoms and precedes late-stage disease; 2) induction of TGFβ signaling with albumin in young mice is sufficient to cause the neurological outcomes observed in old mice; and 3) intervention against TGFβ signaling, either by targeted genetic KO in astrocytes or by small molecule drug, are sufficient to reverse neurological markers, BBB breakdown, and functional outcomes in aging. Furthermore, comparative analysis in humans indicated that this mechanism appears to be conserved in mammals, and hence is highly likely to be relevant in aging human populations.

Chapter 2. Blood-brain barrier breakdown during aging causes chronic but reversible neural dysfunction via TGF-beta signaling

Adapted from: Senatorov VV Jr, Friedman AR, Milikovsky DZ, Ofer J, Saar-Ashkenazy R, Charbash A, Jahan N, Chin G, Mihaly E, Lin JM, Ramsay HJ, Moghbel A, Preininger MK, Eddings CR, Harrison HV, Veksler R, Becker A, Hart B, Rogawski MA, Dillin A, Friedman A, and Kaufer D, 2018. Blood-brain barrier breakdown during aging causes chronic but reversible neural dysfunction via TGF-beta signaling. Manuscript in preparation.

2.1 Introduction

Aging is often accompanied by cognitive decline, even in the absence of dementia or measurable neurodegeneration [1,2]. Our investigations focused on naturally aging mice, allowing us to observe the relative sequence of biological changes associated with brain aging. We found that BBB dysfunction and consequent albumin extravasation appears as early as middle age, placing it among the earliest known hallmarks of the aging brain. Consistent with our findings, changes in the expression of key neurotransmission proteins have been widely observed in humans and other mammals as one of the first signs of neurological aging [1,2,57,58], and these changes in neurotransmission are associated with hippocampal hyperexcitability that is thought to be one of the earliest events in the progression of mild cognitive impairment [22,23,59]. However, the regulatory pathways that trigger or control these changes are unknown. We found that microvascular BBB dysfunction allows serum albumin to enter into the brain, where it binds to astrocytic TGFβR [34] and leads to abnormally increased TGFβ signaling [24]. Activation of this signaling cascade in turn causes transcriptional down-regulation of GABAergic and glutamatergic neurotransmission proteins. Inhibition of astrocytic TGFβ signaling in aging mice was sufficient to reverse these age-induced changes in expression. This suggests a straight-forward mechanism through which BBB dysfunction may cause dysfunction in the aging brain, by altering the levels of the foundational proteins controlling neural signaling.

We explore the hypothesis that BBB dysfunction is itself a trigger of TGFβ signaling in aging, and that in turn this TGFβ signaling transduces an inflammatory cascade that directly causes pathological outcomes associated with neurological decline in aging. Rather than relying on in vitro and transgenic models (which may exhibit intrinsic, cell-autonomous effects that do not generalize to the whole organism), we instead characterized the relationship between BBB dysfunction and TGFβ signaling across the lifespan of naturally aging mice, finding that BBB breakdown appears as early as middle age, and advances in step with progressively increasing astrocytic TGFβ signaling. We then genetically and pharmacologically manipulated TGFβ signaling and found that activation of TGFβ signaling is sufficient to induce aged-like neuropathological outcomes in otherwise healthy, young rodents, including aberrant neural activity, cognitive impairment, and seizure vulnerability. Furthermore, genetic and pharmacological interventions to restore a healthy level of baseline TGFβ signaling dramatically reverse outcomes in aged mice, restoring youthful neural activity and cognitive capacity. Finally, we performed comparative analysis indicating that the same mechanism, triggered by vascular decline, translates to the aging human brain. Together, our results comprehensively describe a novel mechanism underlying a broad range of age-related neurological impairments,

controlled by complex interactions between vasculature, astrocytes, and neurons within the neurovascular unit. They also reveal an untapped potential for targeting vascular pathology as therapeutic strategy to prevent and reverse changes in the core neuro-regulatory machinery at the foundation of age-associated brain dysfunction.

2.2 Results

Aging mice experience progressive BBB dysfunction that is associated with TGFβ signaling and aberrant neural activity

Rodent models offer an ideal system to investigate the underlying mechanisms and outcomes of BBB dysfunction in age-related disease; however, there have been very few studies investigating BBB status in naturally aging rodents [60]. Thus, our initial analysis focused on comprehensively characterizing the time course of BBB dysfunction during natural aging, to establish the temporal relationship between vascular leakiness and the onset of age-related neural dysfunction. Given the putative role of astrocytes in BBB-induced TGFβ signaling, we used a transgenic mouse line labeling astrocytes via the Aldh1L1 promoter (Rep-Aldh1L1) [61]. This pan-astrocytic promoter labels a greater number and variety of astrocytes than traditional approaches using markers such as GFAP, enabling more comprehensive analysis of the aging astrocyte population [62,63]. We found that expression of this marker was stable and did not change across the lifespan (Figure S2.1). Using Rep-Aldh1L1 mice, we quantified albumin extravasation and astrocytic uptake of albumin at time points across the mouse lifespan, with analysis focused on the hippocampus, given its essential roles in age-related memory decline and implication as one of the earliest areas of BBB decline in aging humans [15]. Albumin was effectively absent from the hippocampus of young mice, but appeared in the aging hippocampus starting as early as 7 months (“middle age”) with levels increasing in aging up to two years, near the end of life (Figure 2.1A-B). To estimate the specificity of albumin uptake in different other cell types, we performed separate stains for markers of microglia (Iba1), oligodendrocytes (CAII), and neurons (NeuN), and counted the percent of all albumin+ cells for each cell type. Albumin was taken up predominantly by Aldh1L1-positive astrocytes, accounting for approximately 60% of albumin uptake, with a lower fraction of albumin uptake seen in all other cell types (Figure S2.1). These findings in aged mice correspond to previous reports that albumin uptake occurs primarily in astrocytes in vitro and following experimentally-induced BBB disruption in vivo [32,64]. In these studies, albumin endocytosis into astrocytes is mediated by direct binding to the TGFβ receptor II (TGFβR) subunit, which activates the TGFβR ALK5 [24,37] and induces the phosphorylation of Smad2 (pSmad2), the primary signal transduction protein that initiates the ALK5-TGFβ signaling cascade. Further, this activation also increases the production of TGFβ1 in astrocytes [37] and activation of latent TGFβ1 protein from extra-cellular matrix [26], yielding an increase in the canonical ligand of TGFβR and therefore amplification of the TGFβ cascade. Hence, we focused our subsequent analysis on astrocytes and investigated the relationship between albumin uptake and TGFβ signaling in the aged mouse brain. Concurrent with the time course of albumin extravasation, aging mice showed a progressive increase in the levels of pSmad2, co-localized with albumin-positive astrocytes (Figure 2.1C-E). Activation of the TGFβ pathway was further quantified via Western blot showing increased levels of pSmad2

in the hippocampus of old mice, compared to young, as well as increases in active TGFβ1 (Figure 2.1F).

Based on the mechanistic insights from rodent head injury models, in which TGFβ signaling induced by BBB dysfunction causes reorganization of neural networks and hyperexcitability, we predicted that TGFβ signaling may similarly account for abnormal excitability associated with aging in both rodents and humans [20,21,23,41]. Thus, we performed telemetric electrocorticography (ECoG) to search for evidence of network dysfunction in aging mice. In comparing recordings taken from young and old mice over a 5 day period in the home cage, we found that aged mice showed an increase in the relative power of slow wave activity (<5 Hz) (Figure S2.2A), similar to EEG slowing described in human dementia patients [65–67], which is thought to reflect dysfunctional neural networks. Detailed analysis of this aberrant ECoG signal revealed that the slow-wave activity was not continuous, but rather manifested in discrete, transient paroxysmal slow wave episodes (SWEs, median frequency < 5 Hz; Figure S2.2B). Strikingly, approximately half of the aged mice showed a highly elevated number of SWEs with thousands of paroxysmal events per day (Figure S2.2C). Using an unbiased Gaussian mixed model clustering approach, we found that the aged mice stratified into two statistically distinct clusters, one with high number of SWE per day (h-SWE) and one with low number of SWE (l-SWE) per day (Figure 1G and Figure S2.2D-E). In contrast, the young mice group formed in a single cluster, with a low average number of SWEs per day, similar to the l-SWE aged group (Figure S2.2D). The duration of SWEs was not different across groups (Figure S2.2F), indicating that the increases in the h-SWE group were driven by an increase in the number, not in duration, of SWEs. Furthermore, the h-SWE activity was not associated with circadian fluctuations in ECoG activity, but rather occurred consistently across the day-night cycle (Figure S2.2G). Based on this clustering, we analyzed relative power across the broader ECoG spectrum to compare activity across the three subgroups (young, old l-SWE, and old h-SWE), further showing that old h-SWE have increased low-frequency power (delta band) and corresponding decreases in higher frequency activity (theta – beta), whereas the spectral power of the old l-SWE mice did not differ from that of young mice (Figure 2.1H). These results suggest that ECoG analysis of discrete SWEs can provide a “fingerprint” characterizing a sub-population of aged mice that are affected by recurrent episodes of transient, hyper-synchronized pathological neural network activity. In turn, this may provide a useful biomarker to assess whether therapeutic interventions are effective in restoring healthy neural network activity.

Beyond abnormal ECoG activity, hyperexcitability caused by TGFβ signaling would be predicted to cause seizure vulnerability in aged mice, which could provide a mechanistic explanation for the phenomenon of high epilepsy risk observed in aging humans [68,69]. However, the time course of age-related seizure vulnerability has not been rigorously characterized in naturally-aging mice [70]. We examined seizure vulnerability at time points across the lifespan of aging mice to establish the temporal relationship between declining BBB function and seizure threshold. We assessed seizure vulnerability by injecting a single dose of pentylenetetrazol (PTZ), a non-competitive GABA receptor blocker, and used the modified Racine scale to quantify the severity of induced seizures on a scale of 1 (immobility) to 6 (status epilepticus)[71,72]. Compared to 3-month-old mice, aged mice showed increased vulnerability to induced seizures, beginning at the 12-month-old (middle-aged) time point (Figure 2.1I-J), and corresponding to the age at which significant levels of albumin and TGFβ signaling appear in the brain.

Furthermore, old mice were highly vulnerable to mortality from severe seizures, with a significantly shorter latency to mortality (Figure 2.1K).

Transgenic inhibition of astrocytic TGFβ signaling reverses pathological outcomes in aging mice

Our initial experiments established that BBB dysfunction occurs relatively early in aging, and is tightly linked with astrocytic TGFβ signaling and the onset of neural dysfunction. We next performed targeted experimental interventions to determine if TGFβ signaling plays a causal role in these outcomes. We generated a transgenic mouse line (aTGFβR2/KO) expressing inducible Cre recombinase under the astrocyte-specific GLAST promoter. This enables targeted knock-out of the floxed TGFβR with temporal precision, specifically in astrocytes (Figure 2.2A), allowing us to interrogate the role of astrocytic TGFβ signaling in mediating pathological outcomes. Treatment with tamoxifen (tam) efficiently induced recombination in approximately 40% of hippocampal astrocytes but not in neurons (Figure S2.3), and significantly reduced levels of astrocytic TGFβR (Figure 2.2B). We aged cohorts of aTGFβR2/KO mice to early (12-16 months) and late (17-24 months) stages of aging, and then induced TGFβR2 KO in astrocytes to test their role in age-related seizure vulnerability and cognitive dysfunction (Figure 2.2C). Following induction, aged KO mice showed a significant decrease in TGFβ1 in the brain (Figure 2.2D). In early aging, control mice that were heterozygous for the floxed TGFβR2 (fl/+), and hence retained intact astrocytic TGFβ signaling, showed a profile of high vulnerability to PTZ induced seizures (Figure 2.2E-G), similar to that seen in the cohort of aged Rep-Aldh1L1 mice (Figure 2.1I-K). As an additional control, we included a cohort of aTGFβR2/KO that were homozygous for floxed TGFβR2 but were given corn oil (vehicle) injections instead of tam. These mice, which are genetically identical to the KO group, but retain two intact copies and physiological expression levels of aTGFβR2 (+/+), showed high seizure vulnerability similar to the other aged cohorts. In contrast, mice with homozygous induced KO of the aTGFβR2 (fl/fl) were protected against PTZ-induced seizures, with a profile of vulnerability and seizure mortality similar to young mice (Figure 2.2E-G). When induced in late aging, KO of aTGFβR2 again reversed age-related pathology: aged aTGFβR2 heterozygote (fl/+) controls showed typical age-related vulnerability to induced seizures, whereas aTGFβR2 KO (fl/fl) displayed low vulnerability and mortality to PTZ challenge (Figure 2.2H-J), similar to the phenotype of young mice.

To assess the role of astrocytic TGFβ signaling in age-related cognitive decline, we first attempted to assess cognitive status via the Morris water maze (MWM task); however, we found that in our hands aged mice were unable to learn this task effectively due in part to physical disability (decrepitude and poor swimming ability). Instead, we tested aged transgenic mice for spontaneous alternation in the T-maze, a hippocampal working memory task [73] that is impaired in aging rodents [74]. The task is optimal for assessing aging rodents because it can be performed rapidly without extensive training, is sensitive to even mild impairments in hippocampal function [75,76], and yet it is not affected by motor and vision impairments that may be present in aging mice [73]. At both early and late aging time points, aTGFβR2 KO mice performed significantly better than heterozygous controls (Figure 2.2K-L). We observed that at the early aging time point, several control mice showed notably high individual performance scores, and the overall mean performance of control mice decreased from early to late aging –

in line with an expected age-related decline. This suggests that during early aging, there may be significant individual heterogeneity, with some individuals developing early BBB dysfunction, TGFβ signaling, and cognitive impairment, while others retain intact BBB and healthy levels of TGFβ signaling. To assess this, we performed T-maze in an additional cohort of early aging (12-16 month old) aTGFβR2 KO and heterozygous controls, and collected dissected hippocampi to assess individual molecular outcomes. Using Western blot, we then quantified the level of hippocampal pSmad2 in each individual and correlated this biomarker of TGFβ signaling to the T-maze cognitive performance outcomes. Across both heterozygous (fl/+) and homozygous (fl/fl) genotypes, pSmad2 levels were negatively correlated with T-maze performance (Figure 2.2M). Together, these results show that targeted inhibition of the TGFβ signaling pathway, via induced KO in astrocytes, is sufficient to reverse the outcomes of seizure vulnerability and cognitive impairment in hippocampal spatial working memory in old mice, and that cognitive outcomes in a heterogeneous "mildly impaired" early aging cohort are correlated with the individual levels of TGFβ signaling.

Infusion of albumin into the brains of young rodents is sufficient to reproduce the neurological phenotype of aged mice.

Our KO studies in aging mice show that TGFβ signaling – and specifically astrocytic TGFβ signaling – is necessary for age-related seizure vulnerability and cognitive impairment. To test if TGFβ signaling, as induced by BBB dysfunction, is sufficient to cause the aberrant neural activity (apart from other potential aging factors), we infused albumin (iAlb) or artificial cerebrospinal fluid (aCSF) into the brain ventricles (icv) of healthy, young adult rats and mice via osmotic mini-pump for 7 days. Following icv infusion, the exogenous albumin diffused readily into the ipsilateral hippocampus, and was taken up by astrocytes within 48 hours of infusion (Figure S2.4A-B), similar to uptake seen in previous studies [33,77]. Albumin infusion induced an increase in the levels of GFAP and pSmad2 protein in the rat hippocampus (Figure 2.3A), similar to levels of increase observed in old mice. We next conducted the PTZ seizure challenge in young mice 48 hours after iAlb. At 48 hours, iAlb mice showed significantly increased seizure severity and mortality induced by PTZ compared to aCSF controls (Figure 2.3B-D), fully reprising the seizure vulnerability observed in naturally aged mice. Finally, recordings of ECoG activity in iAlb rats showed an increase in slow-wave power, including an increase in slow-wave delta and decrease in alpha and beta power (Figure 2.3E), mirroring the aberrant activity seen in old h-SWE mice. Like old h-SWE mice, slow-wave activity in iAlb rats was characterized by SWEs, which were significantly increased in the ipsilateral hemisphere receiving iAlb, compared to contralateral hemisphere (Figure S2.4C-G).

We next used young aTGFβR KO to test the necessity and sufficiency of TGFβ signaling in cognitive impairment. Following induction with tamoxifen, we implanted young aTGFβR KO and control mice with iAlb (or aCSF control) osmotic pumps for one week. One month later, we tested mice in the Morris water maze (MWM) spatial memory task. In mice that were heterozygous for floxed TGFβR2 ($Tgfbr2^{fl/+}$), and hence had intact TGFβ signaling, iAlb infusion caused significantly impaired memory performance over 9 days of MWM training (Figure 2.3F). Furthermore, aTGFβR KO partially rescued this deficit, with iAlb $Tgfbr2^{fl/fl}$ KO mice showing an intermediate learning curve between the performance levels of iAlb and aCSF $Tgfbr2^{fl/+}$ mice.

Together, these data show that experimental induction of TGFβ signaling by albumin infusion is sufficient to confer a dramatic "aged" phenotype in young mice, including gliosis, aberrant neural activity, seizure vulnerability, and cognitive impairment. Furthermore, selective knock out of TGFβR expression in astrocytes in young mice rescues albumin-induced cognitive impairment, indicating that activation of astrocytic TGFβR is required to attain the aged brain cognitive phenotype.

A novel small molecule inhibitor of TGFβ signaling reverses molecular and functional outcomes in aging mice

These findings demonstrate the role of astrocytic TGFβ signaling in the pathogenesis of age-related neurological vulnerability, and suggest the potential of TGFβR as a therapeutic target. Considering these therapeutic implications, we next tested the efficacy of a novel small molecule TGFβR1 kinase inhibitor, IPW. IPW has a promising clinical profile – including ability to cross the BBB and good stability following oral dosing (Figure S2.5), making it suitable for once-per-day dosing to achieve inhibition of TGFβR signaling. We first tested IPW in young mice with TGFβ signaling induced by iAlb, treating them with daily i.p. injections (20 mg/kg) of IPW for two days after pump implant. IPW treatment significantly reduced pSmad2 levels measured in the dissected hippocampus of treated mice, compared to mice treated with vehicle control (Figure 2.4A-B). When examining vulnerability to PTZ, iAlb mice treated with vehicle showed high seizure vulnerability – replicating our previous results – whereas IPW treatment reversed this vulnerability, reducing both seizure severity and mortality to the level seen in the control aCSF infused mice (Figure 2.4C-E). These data supported the likelihood for IPW efficacy in naturally aged mice, since it showed not only excellent target engagement, but also that inhibition of TGFβ signaling was sufficient to reverse iAlb seizure vulnerability.

Based on these validation studies, we then tested IPW as an intervention against TGFβ signaling in mice aged to 2 years old, near the end of the mouse lifespan. Immunofluorescent analysis of hippocampal sections from aged mice revealed that 5 days of treatment with IPW (20 mg/kg i.p.) reduced the number of astrocytes co-labeled with pSmad2 (Figure 2.5A). Western blot showed that old mice had significantly elevated levels of pSmad2, and 5 days of IPW treatment in aged mice reduced pSmad2 back to the baseline level seen in healthy, young mice (Figure 2.5B). Furthermore, IPW treatment reduced the downstream outputs associated with astrocytic TGFβ signaling, including levels of TGFβ1 and the marker of astrocyte activation, GFAP (Figure 2.5C-D). To examine outcomes related to network dysfunction, we performed a longitudinal study on the young and old mice that had been segmented by GMM clustering into l-SWE and h-SWE subgroups, to assess their individual trajectories following treatment. After 5 days of baseline recording (same cohort as Figure 2.2), mice were treated for 5 days with IPW, followed by 5 days of "washout" after halting IPW treatment (Figure 2.5E). IPW treatment had no effect on the l-SWE old or on young mice, which continued to show normal ECoG activity. In contrast, IPW treatment ameliorated aberrant ECoG activity in the h-SWE group, reducing the number of SWEs to a level seen in young mice. This effect of IPW persisted throughout the 5-day washout period. A separate cohort of old mice, classified with h-SWE ECoG activity,

underwent the same experiment, except with administration of vehicle control; vehicle injection had no effect on aberrant slow-wave activity (Figure S2.6A-B).

Given the effects of IPW on inhibiting TGFβ signaling and reversing associated outcomes in molecular and electrophysiological markers of neural network dysfunction, we next assessed functional outcomes in naturally aged mice. To assess seizure vulnerability, old mice were treated with IPW for 7 days, followed by PTZ challenge. As in aTGFβR KO genetic intervention, mice treated with IPW were more resilient to PTZ, showing lower seizure severity and mortality compared to aged control mice treated with vehicle (Figure 2.5F-H). Following 7 days of IPW treatment, aged mice also showed significant improvement in the spontaneous alternation T-maze task (Figure 2.5I), again consistent with the findings from genetic aTGFβR KO mice. To further assess cognitive outcomes, we performed the novel object recognition task, which is also sensitive to age-related memory decline, but is less dependent on hippocampal function than spatial maze tasks [79,80]. After 7 days of IPW treatment, aged mice showed significant improvement in object memory versus vehicle-treated controls (Figure 2.5J).

Progressive BBB dysfunction in human aging is associated with astrocytic TGFβ signaling

In our rodent studies, we directly measured albumin extravasation and TGFβ signaling that progresses across the lifespan. In aging humans, BBB dysfunction has also been widely reported, but these studies depend on indirect measures from CSF sampling or imaging that can be technically challenging and may produce conflicting results [10]. Thus, we sought to independently confirm age-related BBB dysfunction in human subjects, validating and expanding on results reported elsewhere [11,13,15]. We used dynamic contrast-enhanced MRI scanning (DCE-MRI) to quantify BBB permeability in 113 healthy human subjects ranging in age from 21 to 83 years old (Figure 2.6A). We first established normal levels of brain permeability based on permeability values in healthy, young patients (age 21-40), setting an upper value for "normal permeability" at the 95th percentile (i.e. 95% of brain voxels in the averaged healthy young brain were below this value; Figure S2.6A). Permeability maps demonstrated increased likelihood for BBB dysfunction in aged individuals (Figure 2.6A), with a linear increase in the percentage of voxels showing supra-threshold permeability values (Figure 2.6B). Notably, while BBB dysfunction has been reported previously in aging humans [11,15], our study specifically focused on healthy subjects, excluding individuals with any MRI abnormality or neurological indication, including mild cognitive impairment. To estimate the percent of the population affected by BBB dysfunction across age groups, we applied a threshold to classify individuals as either BBB-intact (BBB-I; supra-threshold permeability in less than 5% of brain volume) or BBB-disrupted (BBB-D; supra-threshold permeability in more than 5% of brain volume). By age 60, nearly half of the population was affected (Figure S2.6B). Our finding that BBB leakiness is frequently found at relatively early time points during normal aging, suggests that BBB dysfunction may precede subsequent cognitive decline and neuropathology.

Next, to investigate the relationship between BBB dysfunction and astrocytic TGFβ signaling in aging human brains, we examined post-mortem tissue from young (31.3 ± 5 years old) and aging (70.6 ± 5.6 years) human subjects with no history of brain disorder, and directly measured co-localization of albumin extravasation, TGFβ signaling and astrocytes as performed in our rodent studies, thus providing an important complement to the indirect MRI approach. We

found high levels of the serum protein albumin in the old hippocampus, which was absent in the young (Figure 2.6C). Albumin was detected mostly in astrocytes (identified by the astrocytic marker GFAP), and colocalized with phosphorylated Smad2 (pSmad2), the primary signaling protein of the canonical TGFβ signaling cascade. The number of albumin-pSmad2 co-labeled astrocytes was significantly increased in old vs. young individuals (Figure 2.6D). Using a human gene expression database generated by the UK Brain Expression Consortium (NCBI accession # GSE46706) [81], we further examined the expression levels of candidate set of glutamatergic and GABAergic genes that we quantified in mouse. Comparing expression in the young and aging human hippocampus, we found significant downregulation of key genes controlling neurotransmission and plasticity, including GABA receptor (Gabra5, Gabra4, and Gabrb2) and NMDA receptor (Nr2A and Nr2B) subunits (Figure 2.6E). Together, these data show that outcomes of BBB dysfunction characterized in rodent models, including astrocytic TGFβ pathway/pSmad2 signaling and associated changes in glutamatergic/gabaergic genes, are also present in the aged human brain.

2.3 Discussion

The results of this study provide the first evidence for a mechanism that directly links brain microvascular pathology and BBB dysfunction, which occur widely in mammalian aging, to age-related neural and cognitive dysfunction. We showed that astrocytic TGFβ signaling functions as a regulatory cascade that induces changes in molecular, electrophysiological, and behavioral outcomes. We show that 1) BBB dysfunction appears during middle age, with a time course that is well-matched to first appearance of mild age-related symptoms and precedes late-stage disease; 2) induction of TGFβ signaling with albumin in young mice is sufficient to cause similar outcomes observed in old mice; and 3) intervention against TGFβ signaling is sufficient to reverse pathology in aging.

In line with this putative mechanism, we used telemetric ECoG to directly record abnormal neural network activity during aging. We found slowing of EEG/ECoG activity, consistent with other reports in the context of aging [65–67]. We further showed that this slowing of activity in mice is characterized as discrete, paroxysmal transient events (SWEs), occuring frequently and spontaneously against a backdrop of “normal” ECoG activity. These SWEs are reminiscent of paroxysmal events that appear during epileptogenic network reorganization (prior to the onset of spontaneous seizures) in rodent models of epilepsy [82], and of aberrant EEG activity that has been observed and diagnosed as subclinical epileptiform activity and/or “silent seizures” in aging human patients [83–85]. These data support the suggestion, proposed elsewhere [17–19], that there may be common mechanistic links between age-related dementia and epilepsy, which has a remarkably high incidence in the elderly [68,86,87]. We emphasize that changes in neurotransmission machinery, triggered by BBB dysfunction and TGFβ signaling, provide a simple, parsimonious model for how this dysfunction may arise in aging. Indeed, along with molecular changes, we found that TGFβ inhibition reversed aberrant ECoG activity, increased seizure threshold, and improved cognitive outcomes in aged mice, suggesting efficacy in the myriad symptoms that would be expected to arise from a dysfunctional neural network.

By uncovering a foundational mechanism linking BBB decline to neural dysfunction, our study raises several critical questions: what causes BBB decline itself? And is BBB decline causal to, concurrent with, or an outcome of (or independent from) other well-known mechanisms of aging such as inflammation, reactive oxidation stress and metabolic failures, proteasome senescence, DNA degradation, etc. [88–93]? Our work, while novel in focusing on microvascular integrity and interactions within the neurovascular unit, can be placed in context of some of these mechanisms. For example, activation of astrocytes and gliosis has been shown to be a key step in many different aging diseases, with astrocytes playing potent roles in controlling neuroinflammation, neural functions including synaptic plasticity, senescence, and neurodegeneration [94–98]; we show that BBB dysfunction may be an early step causing or contributing to activation of astrocytes and the ensuing inflammatory response. Similarly, several previous studies have reported increased TGFβ signaling in aging [42,41,40,43], and suggested that it could be a primary regulatory factor inducing aged neural phenotypes; we show that astrocytic uptake of albumin may be one of the earliest steps first inducing this age-related TGFβ cascade. But beyond such mechanistic rodent studies, only large-scale human epidemiological studies will provide the necessary and critical insight into the relationship between BBB status, other known biomarkers, and disease outcomes. We argue that such translation of this research to the human context holds exciting potential for age-related diseases, like dementia and epilepsy, that contine to be poorly understood and go without effective treatment.

2.4 Methods

BBB imaging. Imaging protocol was approved by the Soroka University Medical Center Helsinki institutional review board, and written informed consent was given by all participants. BBB status was assessed by DCE-MRI in n=105 subjects with an age range of 21 to 83 years old. MRI scans were performed using a 3T Philips Ingenia scanner, and included: T1-weighted anatomical scan (3D gradient echo, TE/TR = 3.7/8.2 ms, acquisition matrix 432x432, voxel size: 0.5x0.5x1 mm), T2-weighted imaging (TE/TR = 90/3000 ms, voxel size 0.45x0.45x4 mm). For the calculation of pre-contrast longitudinal relaxation times (T_{10}), variable flip angle (VFA) method was used (3D T1w-FFE, TE/TR = 2/10 ms, acquisition matrix: 256x256, voxel size: 0.89x0.89x6 mm, flip angles: 10, 15, 20, 25 and 30°). Dynamic contrast-enhanced (DCE) sequence was then acquired (Axial, 3D T1w-FFE, TE/TR = 2/4 ms, acquisition matrix: 192x187 (reconstructed to 256x256), voxel size: 0.9x0.9x6 mm, flip angle: 20°, Δt = 10 Sec, temporal repetitions: 100, total scan length: 16.7 minutes). An intravenous bolus injection of gadoterate meglumine (Gd-DOTA, Dotarem, Guerbet, France) was administered using an automatic injector after the first five DCE repetitions. Data preprocessing included image registration and normalization to MNI coordinates (using SPM (http://www.fil.ion.ucl. ac.uk/spm)). BBB permeability was calculated for each brain voxel using in-house MATLAB script (Mathworks, USA), as described[99–101]. Briefly, a linear fit is applied to the later part of the concentration curve of each voxel; the slope is then divided by the slope at the superior sagittal sinus, to compensate for physiological (e.g., heart rate, blood flow) and technical (e.g., contrast agent injection rate) variability.

Immunostaining. Postmortem hippocampus was obtained from young (n=3, mean age = 31.3 ± 5 years) and old patients (n=10, mean age = 70.6 ± 5.6 years). All participants gave informed and written consent and all procedures were conducted in accordance with the Declaration of Helsinki and approved by the University of Bonn ethics committee. Resected hippocampi were fixed in 4% formalin and processed into liquid paraffin. All specimens were sliced at 4 µm with a microtome (Microm, Heidelberg, Germany), mounted on slides, dried, and deparaffined in descending alcohol concentration. For mouse samples, mice were anesthetized with Euthasol euthanasia solution and transcardially perfused with ice cold heparinized physiological saline (10 units heparin/mL physiological saline) followed by 4% paraformaldehyde (PFA, Fisher Scientific #AC416785000) in 0.1 M phosphate buffered saline (PBS). Brains were removed, post-fixed in 4% PFA for 24 hours at 4° C, and cryoprotected in 30% sucrose in PBS. Brains were then embedded in Tissue-Tek O.C.T. compound (Sakura, Torrance, CA), frozen, and sliced on a cryostat into 20 µm coronal sections, mounted on slides. All samples were immunostained under the following protocol. Slides were treated for antigen retrieval (for human, 5 min incubation at 100° C in sodium citrate buffer, pH 6.0); for mouse, 15 min incubation at 65 °C in Tris-EDTA buffer (10mM Tris Base, 1 mM EDTA solution, 0.05% Tween 20, pH 9.0), then incubated in blocking solution (5% Normal Donkey Serum in 0.1% Triton X-100/TBS) for 1 hour at room temperature. Samples were then stained with primary antibody at 4° C, followed by fluorescent-conjugated secondary antibody for 1 hour at room temperature, and then incubated with DAPI (900 nM; Sigma-Aldrich) to label nuclei. For human, primary antibodies were rabbit anti-phosphorylated Smad2 (Millipore AB3849-I, 1:500), chicken anti-Albumin (Abcam ab106582, 1:500), and mouse anti-GFAP (Millipore MAB3402, 1:500); for mouse, the same were used except goat anti-GFAP (Abcam ab53554, 1:1000). Secondary antibodies were anti- rabbit Alexa Fluor 568, anti-chicken Alexa Fluor 647, anti-goat Alexa Fluor 488, anti-mouse Alexa Fluor 488 (1:500, Jackson ImmunoResearch), and anti-goat Alexa Fluor 647 (Abcam ab150131, 1:500). All antibodies dilutions were in blocking solution. For tissue from old human patients and aged mice, slide- mounted brain sections for treated with TrueBlack Lipofuscin Autofluorescence Quencher (Biotium #23007) before coverslip mounting.

Microscopy. Images were acquired at 20X or 40X magnification using a Zeiss Axio Observer Research microscope (Carl Zeiss AG) and Metamorph software (version 7.7.7.0), and analyzed using ImageJ software (NIH). For human samples, counts were performed in 10 of randomly selected sampling areas per subject. For mouse, imaging was performed in at least 3 hippocampal sections per mouse. Cell counts for each individual marker, and colabeling, were calculated manually by an observer blind to experimental conditions, and normalized to the total number of DAPI-positive cells. For each subject, counts from each sampling area were averaged.

Western Blot. Hippocampal tissue was homogenized and protein lysates were extracted using RIPA buffer (50 mM Tris-HCl, 150 mM NaCl, 1% NP-40, 0.5% Sodium deoxycholate, 0.1% SDS) including a protease (Calbiochem #539134) and phosphatase inhibitor cocktail (Roche PhoStop Ref: 4906845001). Protein samples were run under reducing conditions. 20 µg of protein lysate was mixed with Laemmli buffer (Bio-Rad #161-0737), containing 5% 2-mercaptoethanol (Sigma M6250), and fractionated by SDS-PAGE using the Mini-PROTEAN Tetra System and pre-cast TGXTM Gels (Bio-Rad #456-1096); Following separation, samples were transferred to a nitrocellulose membrane (0.45 µm, Bio-Rad #1620115). Membranes were

blocked for 1 hr at room temperature with 5% non-fat dry milk (Apex #20-241) in TBST (10 mM Tris, 150 mM NaCl, 0.5% Tween 20, pH 8.0), and incubated overnight at 4 °C with primary antibody. Membranes were then washed 3x10 min with TBST and incubated with secondary antibodies for 1 hr at room temperature. Membranes were washed with TBST 3x10min and visualized using chemiluminescence SuperSignal West Dura Extended Substrate (ThermoFisher Scientific #34075), and Bio-Rad Chemidoc system with Bio-Rad Image Lab software (version 4.0.1). Densitometry analysis was done using Image J (NIH). The following primary and secondary antibodies were used: rabbit anti-β-Actin (1:2000, Cell Signaling #4970), rabbit anti-GAPDH (1:2000, Cell Signaling #2118), rabbit anti-TGFβR2 (1:1500, Abcam ab186838), rabbit anti-phosphorylated Smad2 (1:1000, Millipore AB3849-I), rabbit anti-phosphorylated Smad2 (1:1000, Millipore AB3849), rabbit anti-NMDAR2A (1:1000, Cell Signaling #4205), rabbit anti-NMDAR2B (1:1000, Cell Signaling #4207), chicken anti-Albumin (1:1500, Abcam ab106582), goat anti-GFAP (1:1000, Abcam ab53554), anti-goat HRP (1:1000, R&D systems HAF109), anti-mouse HRP (1:2000, Cell Signaling #7076), anti-rabbit HRP (1:2000, Cell Signaling #4970), and anti-chicken HRP (1:2000, ThermoFisher Scientific A16054)**.**

RT-qPCR. Total RNA was extracted from 200-250 mg of frozen mouse hippocampal tissue using TRIzol reagent (ThermoFisher Scientific #15596026), and further purified with DNA-free DNA Removal Kit (ThermoFisher Scientific AM1906). First-strand cDNA synthesis was performed from 1 µg isolated RNA template using iScript RT supermix (Bio-Rad #1708841). PCR products were amplified using a CFX96 Real-Time PCR System (Bio-Rad), and threshold cycles were detected using SsoAdvanced Universal SYBR Green Supermix (Bio-Rad #172-5271). Mean threshold cycles were normalized to 18s internal control, and relative gene expression levels were quantified using the 2-ΔΔCT method. Primer sequences were obtained from the NCI/NIH qPrimerDepot.

Human transcriptome analysis. Human gene expression data was downloaded from the NCBI GEO database, accession number GSE46706, and the data columns pertaining to hippocampus were extracted. The majority of the header information was removed, but the age of the donor was maintained along with the GEO ID linking each column to its donor. The values for each probe set were log 2 transformed, and assigned to their respective genes using the vendor supplied annotation file. This generated a probe set/transcript level data matrix. Since many genes are measured by multiple probe sets, expression values across these probe sets were combined. This led to a gene level data matrix which was further simplified by retaining only target genes of interest. We then used the age of the donor to sort the data columns and generate graphs of the expression levels for subsets of individuals (young vs old -- bottom and top 33% of all patients sorted by age). Normal differential expression testing was performed to compare old and young.

Osmotic pump implants. For mice, pumps were implanted as previously described[102]. Briefly, surgery was performed on adult male mice under isofluorane anesthesia (2%). Using a stereotaxic frame, a hole was drilled through the skull at 0.5 mm posterior, 1 mm lateral to bregma, and a cannula was placed into the right lateral cerebral ventricle, fixed with surgical glue. Cannulas (Brain infusion kit BIK 3, #0008851, Alzet, Cupertino, CA) were attached to micro-osmotic pumps (Model 2001, ALZET) filled with 200 µL of either 0.4 mM bovine serum albumin (Alb; Sigma-Aldrich) solution or artificial cerebrospinal fluid (aCSF) as previously described [103], and implanted subcutaneously in the right flank. In a subset of animals, 10% of

the Alb was replaced with Alexa Fluor 647 conjugated BSA (2.68 g/L; ThermoFisher Scientific A34785). Pumps infused at a rate of 1.0 µL/hr for the duration described in each experiment. For rats, 10 week-old male Wistar rats were used, and surgeries were performed the same way, using the following coordinates: -1 mm posterior and 1.5 mm lateral to bregma. For rats, albumin was used at a concentration of 0.2 mM and infused for 7 days at a rate of 10 µL/hr via larger micro-osmotic pumps (Model 2ML1, Alzet).

ECoG. ECoG was recorded as previously reported [104] from 9- to 12-wk-old Wistar male rats implanted with osmotic pumps, and from young (3 months, n = 5) and old (18-22 months, n = 20) mice. In brief, under stereotaxic surgery and 2% isoflurane anesthesia, two screw electrodes were implanted in each hemisphere (rat coordinates: 4.8 mm posterior, 2.7 mm anterior, and 2.2 mm lateral; mouse coordinates: 0.5 and 3.5 mm posterior and 1 mm lateral, all relative to bregma). A wireless transmitter (Data Science International, Saint Paul, MN, US) was placed in a dorsal subcutaneous pocket, and leads connected to the screws. Connections were isolated and fixed by bone cement such that one ECoG channel was associated with each hemisphere. For rat surgeries, a cannula (-1 mm caudal, 1.5 lateral, 4 mm depth) and osmotic pump (infusing at 2.4 µl/h) were also implanted[37]. Animals were treated with post-operative buprenorphine (0.1 mg/Kg) and allowed to recover for at least 72 hrs prior to recording. Continuous, bichannel ECoG (sampling rate, 500Hz) was recorded wirelessly from freely roaming animals in the home cage for the duration of experiments described. Rats were recorded during the first and the fourth week following surgery. Mice were recorded for 15 days, starting 1 week after surgery, and administered IPW (20 mg/kg) on days 6-10 of recording. To detect SWE, ECoG signals were buffered into 2 sec long epochs with an overlap of 1 sec. Fast Fourier Transform (FFT) was applied and the frequency of median power was extracted for each epoch. Thus, an event was considered as a SWE if its frequency of median power was less than 5 Hz for 10 consecutive seconds or more. FFT was also applied for the entire recording period to analyze relative power across the frequency spectrum of 1-20 Hz.

Animal care and transgenic mice. All animal procedures were approved by the institutional animal care committees. Animals were housed with a 12:12 light:dark cycle with food and water available ad libitum. Aldh1L1-eGFP mice were bred from STOCK Tg(Aldh1l1-EGFP)OFC789Gsat/Mmucd (identification number 011015-UCD), purchased from the Mutant Mouse Regional Resource Center. These FVB/N mice were crossed to a C57BL/6 genetic background. The resulting strain exhibits constitutive astrocytic expression of eGFP protein under the astrocytic promoter Aldehyde Dehydrogenase 1 Family, Member L1 (Aldh1L1). Triple transgenic aTGFβR/KO mice were bred from strains purchased from the Jackson Laboratory to generate mice that express CreERT under the astrocytic promoter glial high affinity glutamate transporter (GLAST), with a floxed exon 4 of TGF-βR2 ($tgfbr2^{fl}$), and a transgenic LacZ reporter gene inhibited by a floxed neomycin cassette. Tamoxifen induction thus induces activation of astrocytic CreERT resulting in a null TGFβR2 allele (tgfbr2null) and LacZ expression ($R26R^{-/-}$). The parental strain STOCK Tg(Slc1a3-cre/ERT)1Nat/J mice were outcrossed with B6;129-Tgfbr2tm1Karl/J and B6.129S4-Gt(ROSA)26Sortm1Sor/J mice to produce males, while B6;129-Tgfbr2tm1Karl/J and B6.129S4-Gt(ROSA)26Sortm1Sor/J mice were outcrossed to produce females. The resulting GLAST-CreERT; $tgfbr2^{fl/+}$ males were bred with tgfbr2fl/+; R26R-/- and $tgfbr2^{fl/fl}$; $R26R^{-/-}$ females to produce triple transgenic offspring. Subsequent generations were incrossed to produce experimental triple transgenic mice of genotypes GLAST-CreERT; $tgfbr2^{fl/fl}$;

R26R$^{-/-}$, GLAST-CreERT; tgfbr2$^{fl/+}$; R26R$^{-/-}$, GLAST-CreERT; tgfbr2$^{fl/fl}$; R26R$^{-/+}$, and GLAST-CreERT; tgfbr2$^{fl/+}$; R26R$^{-/-}$. All mice were genotyped via PCR analysis of tissue biopsy samples (Table S4). The inducible Cre/lox system was activated by 5 days of tamoxifen injection (Sigma-Aldrich, 160 mg/kg dissolved in corn oil, i.p). Control GLAST-CreERT; tgfbr2$^{fl/+}$ heterozygotes received the same dosage of tamoxifen and control GLAST-CreERT; tgfbr2$^{fl/fl}$ mice received i.p. injection of corn oil vehicle at equivalent volumes. Mice were weighed daily to ensure accurate dosage.

Seizure induction. Seizures were induced by a single injection of pentylenetetrazole (PTZ; Sigma, P6500, 85 mg/kg s.c.). Video recordings were taken for 30 minutes following induction, which were then scored by a blind observer, using a modified Racine scale to quantify progression of seizure severity, as follows: 0 – No Seizures; 1 – Immobility; 2 – Straub's tail; 3 – Forelimb Clonus; 4 – Generalized Clonus; 5 – Bouncing Seizure; 6 - Status Epilepticus. Latency to first appearance of each Racine stage was quantified, as was latency to mortality (when occurring prior to the 30 min endpoint).

Behavior assessments. Spatial working memory was tested by spontaneous alternation in a T-maze constructed of black plastic, with stem (50 x 16 cm) and two arms (50 x 10 cm). A vertical divider was placed at the midline of the stem exit, thus creating two entryways leading to either the right or left arms. Naïve mice were placed at the beginning of the stem and allowed to freely roam until opting to enter either the right or left arm. Upon crossing the threshold of the chosen arm, a door was lowered, and the mouse was contained to the chosen arm for 30 sec. Then, the mouse was returned to the stem and the door raised, allowing the next choice trial to commence immediately. After 10 sequential trials, the mouse was returned to the home cage. "Correct" alternation choices were scored when the mouse chose the arm opposite of that chosen in the previous trial, and percent correct was calculated as (total correct choices) / (total number of completed trials). In the event that a mouse did not leave the stem within 60 sec, it was removed from the apparatus for 30 sec, and then reset in the stem to start a new trial. These "incomplete" trials were not counted in scoring. Spatial memory in young mice was assessed in the Morris Water Maze (MWM) task[105]. For each trial, mice were placed at randomized starting locations in a MWM pool filled with opaque water (colored with non-toxic white acrylic paint), with visual cues placed on the pool walls. Mice were allowed to swim freely until locating a hidden platform under the surface of the water (or guided to the platform after 40 seconds of failed searching), and then left on the platform for 10 seconds prior to starting a new trial. Spatial learning was quantified by measuring latency to reach the platform, averaged from four trials per day, with training over 9 consecutive days of learning. Object memory was tested in the novel object task, using a 3-day protocol consisting of a 10 min trial on each day, recorded by overhead video. On day 1 mice were habituated to a square testing chamber, constructed of white plastic (50 x 50 cm), with two unfamiliar objects placed inside. On day 2, the previous objects were removed and 3 new objects were placed in a "L" configuration, equidistant from each other and the walls. On day 3, one of the objects was removed and replaced by a new object, thus leaving 2 familiar objects and 1 novel object. A blind observer quantified duration of time spent investigating each object (scoring criteria were mouse nose oriented towards object at a distance of 1 cm or less), and percentage of time at the novel object was quantified as (duration investigating novel object) / (total duration investigating all three objects). The set objects were chosen from common items such as lab bottles, pipette boxes, cups (placed open-side down), etc., that were of similar dimensions but

varied in shape, color, and material. The sequence and position of objects across trials was identical for all mice.

IPW pharmacokinetics. Brain concentration measurement of IPW-5371 was performed by Jubilant Biosys. The experiment was approved by the Jubilant Biosys Institutional Animal Ethics Committee, Bangalore, India (IAEC/JDC/2015/72) and were in accordance with the Committee for the Purpose of Control and Supervision of Experiments on Animals (CPCSEA), Ministry of Social Justice and Environment, Government of India. Twelve Balb/C mice (age 6-7 weeks) were procured from Bioneeds, Bangalore, India. Animals were housed in Jubilant Biosys animal care facility in a temperature and humidity controlled room with a 12:12 h light:dark cycles, had free access to food (Provimin, India) and water for one week before experimental use. Following ~4 h fasting (during fasting period animals had free access to water) mice received IPW-5371 orally at a dose of 20 mg/kg (dissolved in 0.5% methylcellulose and saline). Mice were euthanized under isofluorane and the brain was removed and weighed. Brain tissue homogenates were prepared with 10% tetrahydrofuran in acetonitrile [tissue was homogenated with 4 mL/g of 10% tetradhydrofuran in acetonitrile containing IS (100 ng/mL)]. Subsequently, 250 µL of brain homogenate was centrifuged at 14,000 rpm for 5 min at 10 °C. An aliquot of 10 µL was injected onto an API 4000 LC-MS/MS system for analysis.

Statistics and data. Data collection and preparation was performed by researchers who were blind to experimental conditions, and the lead and corresponding authors were responsible for experiment design, conducting statistical analysis, and unblinding the final results. All graphs are plotted showing mean and SE. Two sample comparisons were performed by student's t-test or Mann-Whitney test, and multiple group comparisons were conducted by ANOVA or Kruskal–Wallis test, followed by post-hoc testing to compare individual groups when a main effect was detected. Multiple correction comparisons were used as described in figure legends. Seizure progression in the PTZ experiments was analyzed by two-way ANOVA, and linear regression was used to calculate regression slopes. Differences in regression slope were also compared by ANOVA. Different subgroups that were observed in ECoG recordings were first classified by an unbiased Gaussian mixed model, and then inferential statistics were performed on the subsequent groups. For all inferential statistics, two-tailed tests were used and significance thresholds were set at $p<0.05$.

2.5 Figures

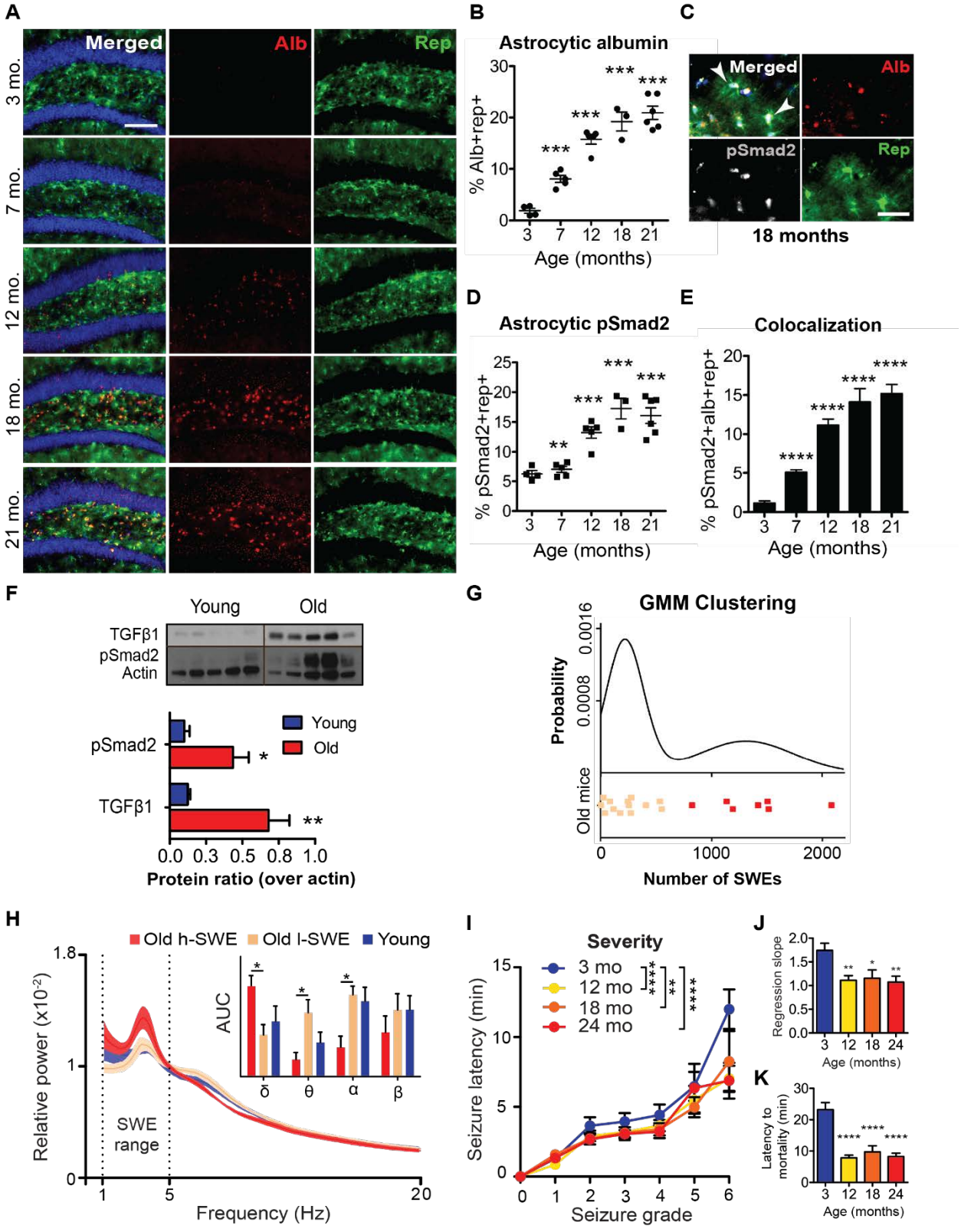
A
Merged
Alb
Rep
3 mo.
7 mo.
12 mo.
18 mo.
21 mo.
B
Astrocytic albumin
% Alb+rep+
Age (months)
C
Merged
Alb
pSmad2
Rep
18 months
D
Astrocytic pSmad2
% pSmad2+rep+
Age (months)
E
Colocalization
% pSmad2+alb+rep+
Age (months)
F
Young
Old
TGFβ1
pSmad2
Actin
Young
Old
pSmad2
TGFβ1
Protein ratio (over actin)
G
GMM Clustering
Probability
Old mice
Number of SWEs
H
Old h-SWE
Old l-SWE
Young
Relative power (x10⁻²)
SWE range
Frequency (Hz)
AUC
δ
θ
α
β
I
Severity
3 mo
12 mo
18 mo
24 mo
Seizure latency (min)
Seizure grade
J
Regression slope
Age (months)
K
Latency to mortality (min)
Age (months)

Figure 2.1. Progressive BBB dysfunction in aging mice is associated with elevated TGFβ signaling and aberrant network activity. (A) Immunofluorescent staining used to quantify progression of BBB decline in the aging mouse hippocampus at 3, 7, 12, 17, and 21 months old. Astrocytes are labeled by GFP expressed transgenically under the pan-astrocytic promoter Aldh1L1 (Rep-aldh1L1-eGFP), albumin is labeled by immunostaining, and cell nuclei by DAPI (blue). Scale bar = 100 μm. (B) Albumin localized in astrocytes increases with age (ANOVA, $p < 0.0001$). (C) Co-localization of albumin and pSmad2 (arrows), visualized by immunostaining (Scale bar = 30 μm). Aging mice show an increase in the level of (D) pSmad2 colabeled with astrocytes (ANOVA, $p = <0.0001$), and (E) the percentage of astrocytes co-localizing with both albumin and pSmad2 (ANOVA, $p < 0.0001$). For all measures, groups were compared by Bonferroni post-hoc test. Sample sizes are n = 4 (3 mo); 5 (7 and 12 mo); 3 (18 mo); and 6 (21 mo). (F) Western blot analyzing TGFβ1 and pSmad2, outputs of the TGFβ signaling pathway, in hippocampus from young and old mice. Western blot densitometry shows that pSmad2 ($p=0.019$) and TGFβ ($p = 0.005$) protein levels were elevated in the aged mouse hippocampus (t-test with Bonferroni correction, $p=0.019$ and 0.005 respectively, n = 5). (G) Slow-wave episodes were quantified from continuous ECoG recordings in young and old mice, and GMM clustering was used to classify old mice into h-SWE and l-SWE subgroups. (H) Relative power was compared across the frequency spectrum from 1-20 Hz for all groups. Area under the curve (AUC) measures for each frequency band (δ, 1-5 Hz; θ, 6-8 Hz; α, 9-12 Hz; β, 13-20 Hz) showed that h-SWE old mice exhibited an increase in power in the slow-wave δ band and a decrease in θ and α (ANOVA, interaction $p < 0.01$, with Bonferroni posttest, n = 6 h-SWE, 6 l-SWE, 5 young). (I) At 3, 12, 18, and 24 months seizures were induced in mice by PTZ injection, and progression through the modified Racine scale was used to score seizure severity (latency to the first seizure at each level of severity). Aged mice (12-24 months) had greater severity in seizures (2-way ANOVA, main effect of seizure progression $p < 0.0001$; main effect of age $p = 0.005$, n = 13 (3 mo), 10 (12 mo), 8 (18 mo and 24 mo)), with (J) decreased linear regression slopes indicating faster progression through all stages of seizures (ANOVA, $p = 0.0011$ with Bonferroni posttest). (K) Latency to mortality caused by severe seizures was significantly faster in 12-24 month groups compared to young mice (ANOVA, $p < 0.0001$ with Bonferroni posttest).

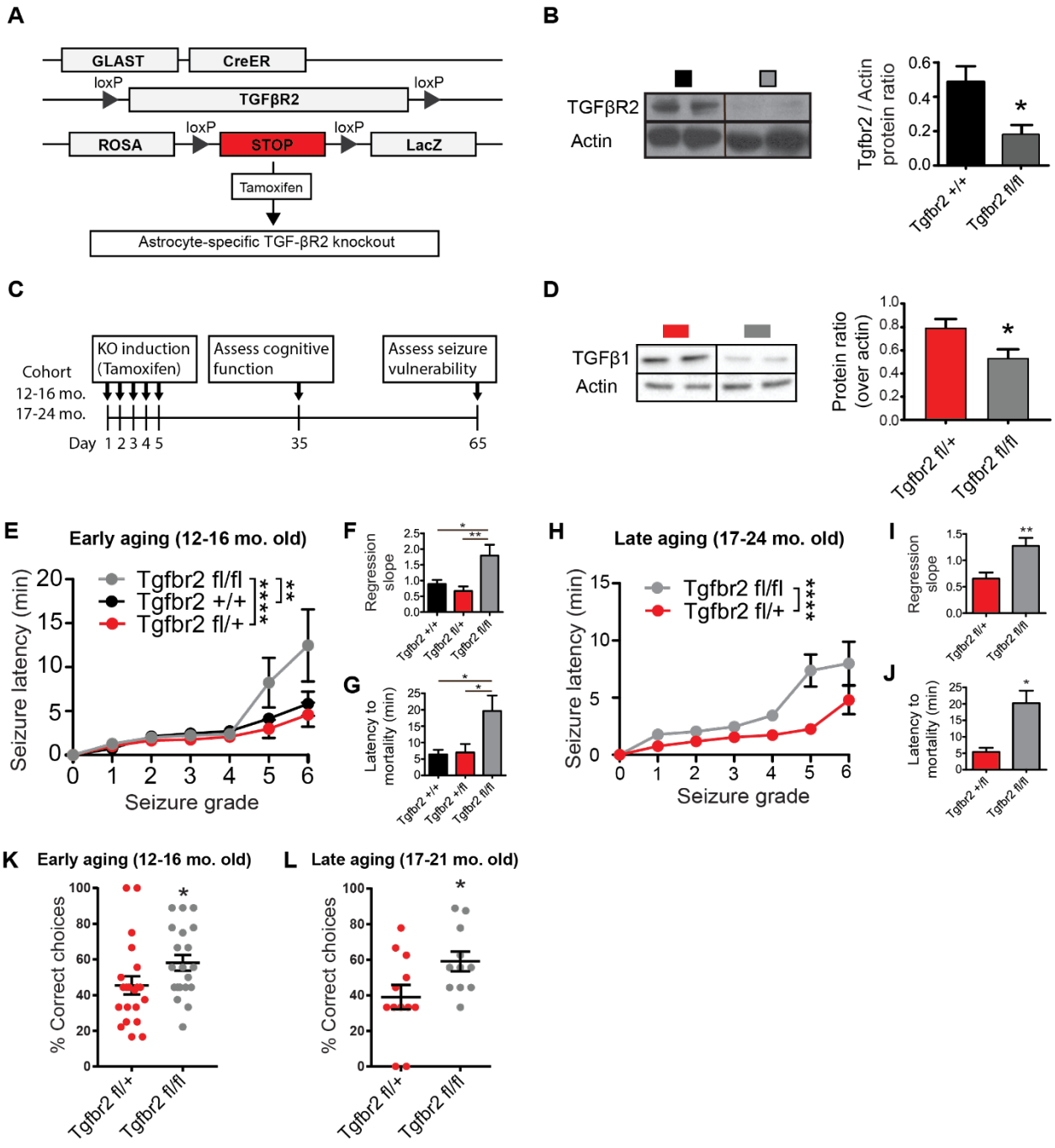

Figure 2.2. Knock-out of astrocytic TGFβ reverses neurological outcomes in aging mice. (A) Schematic of the transgenic aTGFβR KO system. The astrocytic GLAST promoter drives expression of Cre recombinase in astrocytes. Following induction with tamoxifen injection, activated Cre excises the TGFβR gene at inserted loxP sites. LacZ reporter expression provides a readout of Cre activity. (B) Western blot with densitometry confirmed significant reduction in levels of TGFβR in the hippocampus following tamoxifen induction. (C) Experimental timeline. KO was induced in early (12- 16 mo.) and late (17-24 mo.) aged mice, and T-maze testing was

performed 35 days later. (D) aTGFβ KO reduced the protein levels of pSmad2 and TGFβ1 in the hippocampus of early aging mice, compared to heterozygotes. At 65 days post-induction, mice were tested for vulnerability to PTZ- induced seizures. aTGFβR KO ($Tgfbr2^{fl/fl}$) reversed seizure vulnerability in 12-16 mo old mice, significantly slowing (E-F) progression through the Racine scale (2-way ANOVA, main effect of seizure progression $p < 0.0001$; main effect of genotype $p = 0.0053$; interaction $p = 0.0214$, with Bonferroni posttest, n = 5 $Tgfbr2^{+/+}$, 6 $Tgfbr2^{fl/+}$ and $Tgfbr2^{fl/fl}$) and (G) latency to mortality (ANOVA, $p = 0.022$, with Bonferroni posttest), compared to control heterozygous mice ($Tgfbr2^{fl/+}$) and mice given oil control rather than tamoxifen induction ($Tgfbr^{+/+}$). (H-I) 17-24 month old mice with aTGFβ KO were similarly protected against PTZ seizure vulnerability with less severe seizures (2-way ANOVA, main effect of seizure progression $p < 0.0001$; main effect of genotype $p < 0.0001$; interaction $p = 0.026$) and (J) delayed mortality ($p = 0.016$). (K-L) In T-maze, aTGFβR KO mice showed significantly better working memory performance compared to heterozygous controls at in both early aging (12-16 months old, Mann-Whitney test, $p = 0.0273$, n = 21 $Tgfbr2^{fl/+}$, 20 $Tgfbr2^{fl/fl}$) and late aging assessments (t-test, $p = 0.035$ n = 12 $Tgfbr2^{fl/+}$, 11 $Tgfbr2^{fl/fl}$).

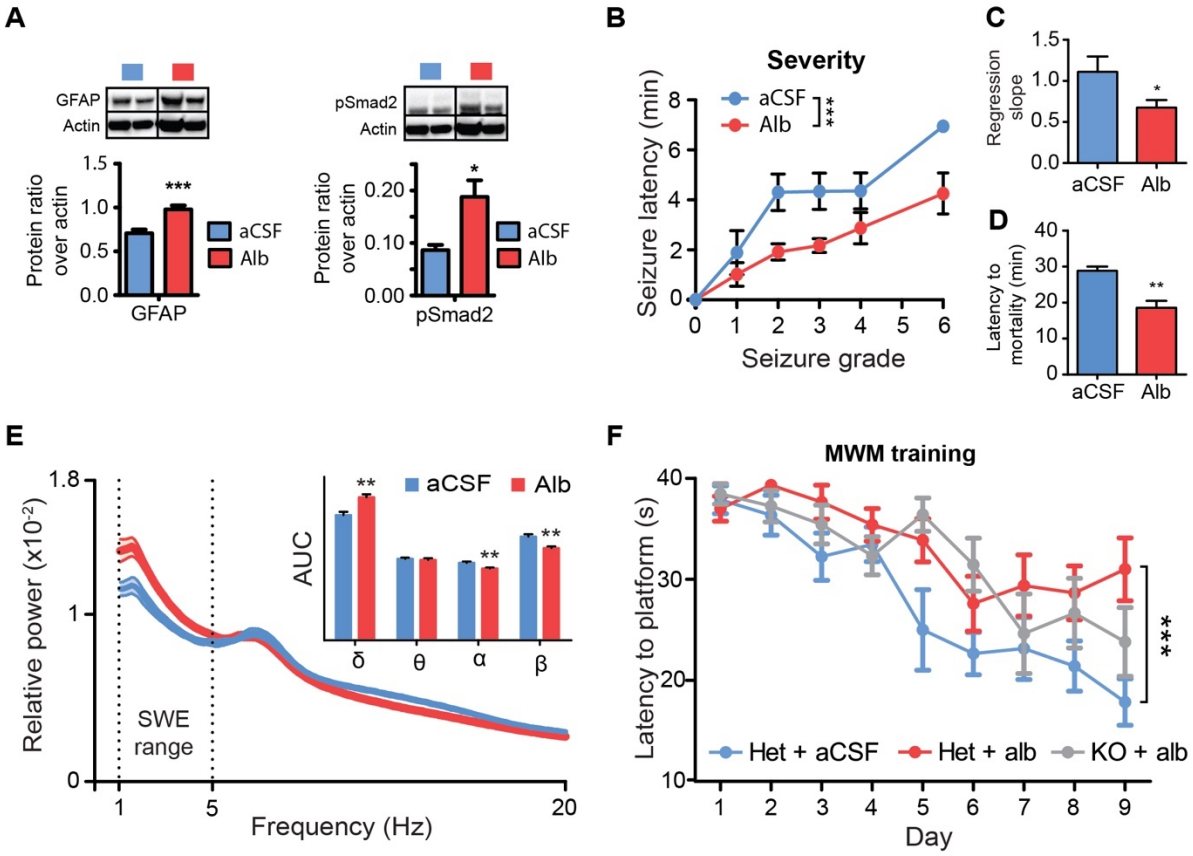

Figure 2.3. Aberrant network activity, vulnerability to induced seizures, and cognitive impairment is conferred in young rodents by albumin infusion. (A) Young adult rats were given icv albumin infusion (iAlb) for 7 days. iAlb increased protein levels of the activated astrocyte marker GFAP (t-test, p = 0.004, n = 4) and (g) pSmad2 (p = 0.022). (B) Young mice received icv infusion of either albumin or aCSF control for 48 hours, followed by PTZ seizure induction. Albumin infusion caused increased severity in induced seizures (2-way ANOVA, main effect of seizure progression p < 0.0001; main effect of treatment p = 0.0001, n = 4), with (C) and regression slopes showing faster seizure progression (t- test, p = 0.032), and (D) faster latency to mortality (t-test, p=0.004), compared to aCSF controls. (E) ECoG activity was recorded from iAlb rats. AUC measures showed that albumin caused an increase in relative power in δ, with a corresponding decrease in α and β power (Mann-Whitney test, n = 5 aCSF, 8 alb). (F) Following induction with tamoxifen, young aTGFβR KO and control mice were given iAlb surgery and then tested in the MWM task one month later. Compared to aCSF controls, iAlb Tgfbr2$^{fl/+}$ mice had significantly poorer learning performance, and KO (Tgfbr2$^{fl/fl}$) partially rescued performance following iAlb (2-way repeated measure ANOVA, main effect of learning over time p < 0.0001, main effect of group p = 0.0093, with Bonferroni posttest on day 9 showing significant differences between aCSF and iAlb Tgfbr2$^{fl/+}$, p < 0.001, but not between iAlb and KO. n = 9 aCSF Tgfbr2$^{fl/+}$, 10 iAlb Tgfbr2$^{fl/+}$, and 8 iAlb Tgfbr2$^{fl/fl}$). For all tests, *p<0.05, **p<0.01, ***p<0.005, ****p<0.001.

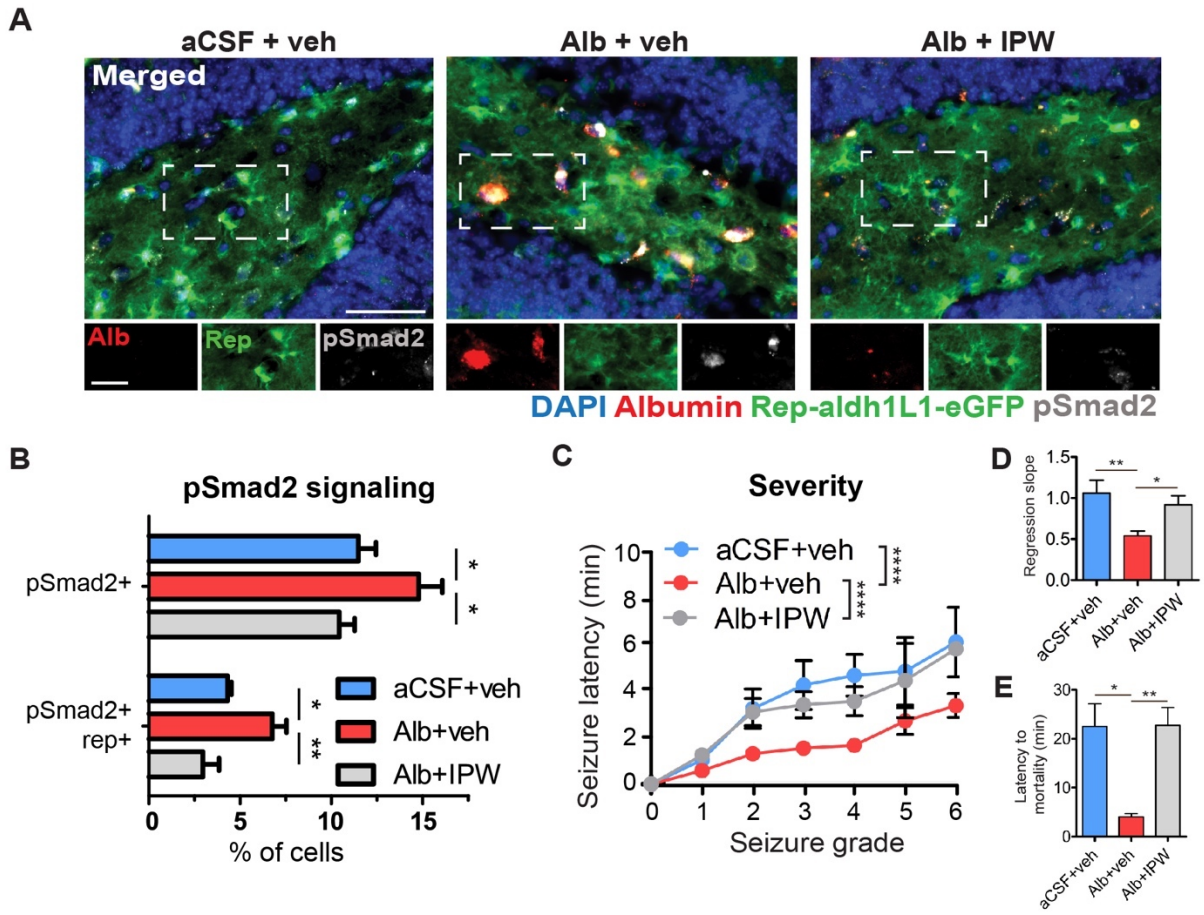

Figure 2.4. IPW reduces pSmad2 signaling and seizure vulnerability in young mice infused with albumin. (A) Immunofluorescent images from iAlb mice after treatment with IPW or vehicle injections during 7 days of icv albumin infusion (Scale bar = 50 µm main image, 25 µm inset). (B-C) iAlb mice showed elevated levels pSmad2 signaling localized in astrocytes (compared to aCSF controls) and IPW reduced pSmad2 (ANOVA: % pSmad2, $p = 0.027$; % pSmad2+ rep+, $p = 0.0048$; $n = 6$). (C) IPW treatment reduced seizure vulnerability conferred by iAlb (2-way ANOVA, main effect of seizure progression $p < 0.0001$; main effect of treatment $p < 0.0001$, $n = 6$ (aCSF+veh and Alb+veh), 7 (Alb+IPW)), restoring seizure profile to aCSF control levels as quantified by (D) slopes of linear regression of progression through the Racine scale (ANOVA, main effect of treatment $p = 0.004$, with Bonferroni's posttest). (E) IPW treatment also reversed the vulnerability to seizure mortality conferred by iAlb.

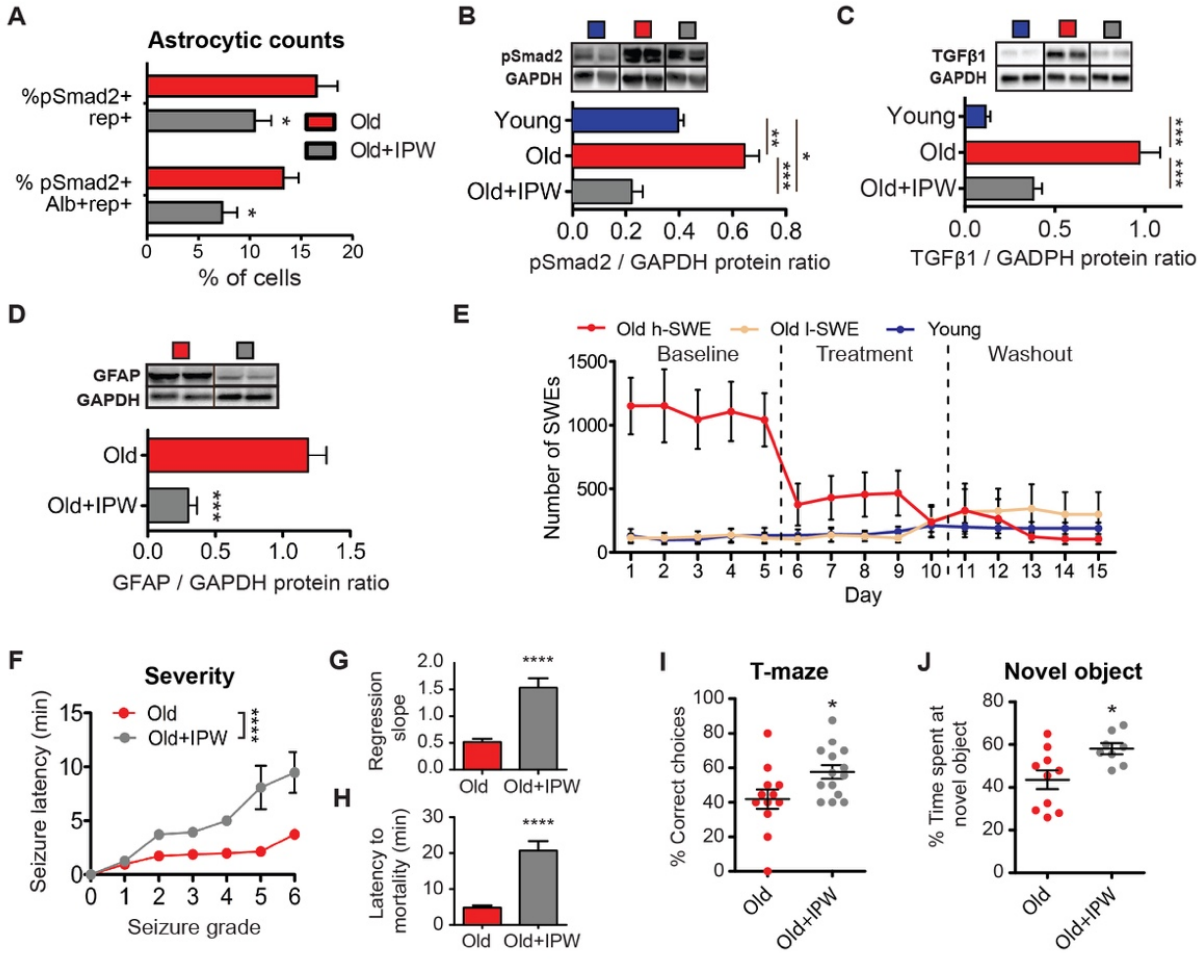

Figure 2.5. IPW reverses TGFβ signaling, aberrant neural activity, seizure vulnerability, and cognitive impairment in aged mice. (A) Aged Rep-Aldh1L1 mice were treated 7 days of IPW (20 mg/kg, i.p.) or vehicle, followed by immunofluorescent staining for pSmad2 and albumin (Alb). IPW significantly reduced fraction of astrocytes (rep+) that co-labeled with pSmad2, and the fraction of cells triple labeled with pSmad2, Alb, and rep (t-test with Holm-Bonferroni correction, n = 5 old, 6 old+IPW). (B) Densitometry of Western blot shows that IPW restored levels of elevated pSmad2 protein in old mice, to the level of young mice (ANOVA, main effect $p<0.0001$, with Tukey's posttest, n = 4). IPW treatment also reduced levels of (C) TGFβ1 in aged mice (ANOVA, main effect $p<0.0001$, with Tukey's posttest, n = 4) and (D) GFAP protein, a marker of activated astrocytes (t-test, $p = 0.0004$, n = 4 old, 5 old+IPW). (E) Continuous ECoG recording over 15 days was used to investigate effects of IPW on aberrant network activity. During 5 days of baseline recording, clustering analysis was used to classify old mice as affected by high numbers of SWEs (h-SWE, n = 6), or low numbers of SWEs (l-SWE, n = 6), similar to the level of young mice (n = 5). In the subsequent 5 days of recording, IPW treatment restored a youthful ECoG profile in the affected mice, reducing SWEs (Dunn's multiple comparisons test $p = 0.0098$) to the level of young mice. After IPW dosing was halted, the old mice retained a l-SWE ECoG profile throughout the "washout" period (Dunn's multiple comparisons test baseline

vs washout p = 0.0002). (F) 7 days of albumin treatment reversed seizure vulnerability in aged mice, reducing seizure severity in Racine scale (2-way ANOVA, main effect of seizure progression $p < 0.0001$; main effect of drug treatment $p < 0.0001$; interaction $p = 0.0001$, with Bonferroni posttest, n = 9) and (G) linear regression slope measures (t-test, $p < 0.0001$), and reducing the onset of (H) seizure induced mortality (t-test, $p < 0.0001$). 7 days of IPW treatment improved cognitive scores of old mice in the (I) T-maze (t-test, $p = 0.028$, n = 12 vehicle, 14 IPW) and (J) novel object memory tasks (t-test, $p = 0.017$, n = 10 vehicle, 8 IPW).

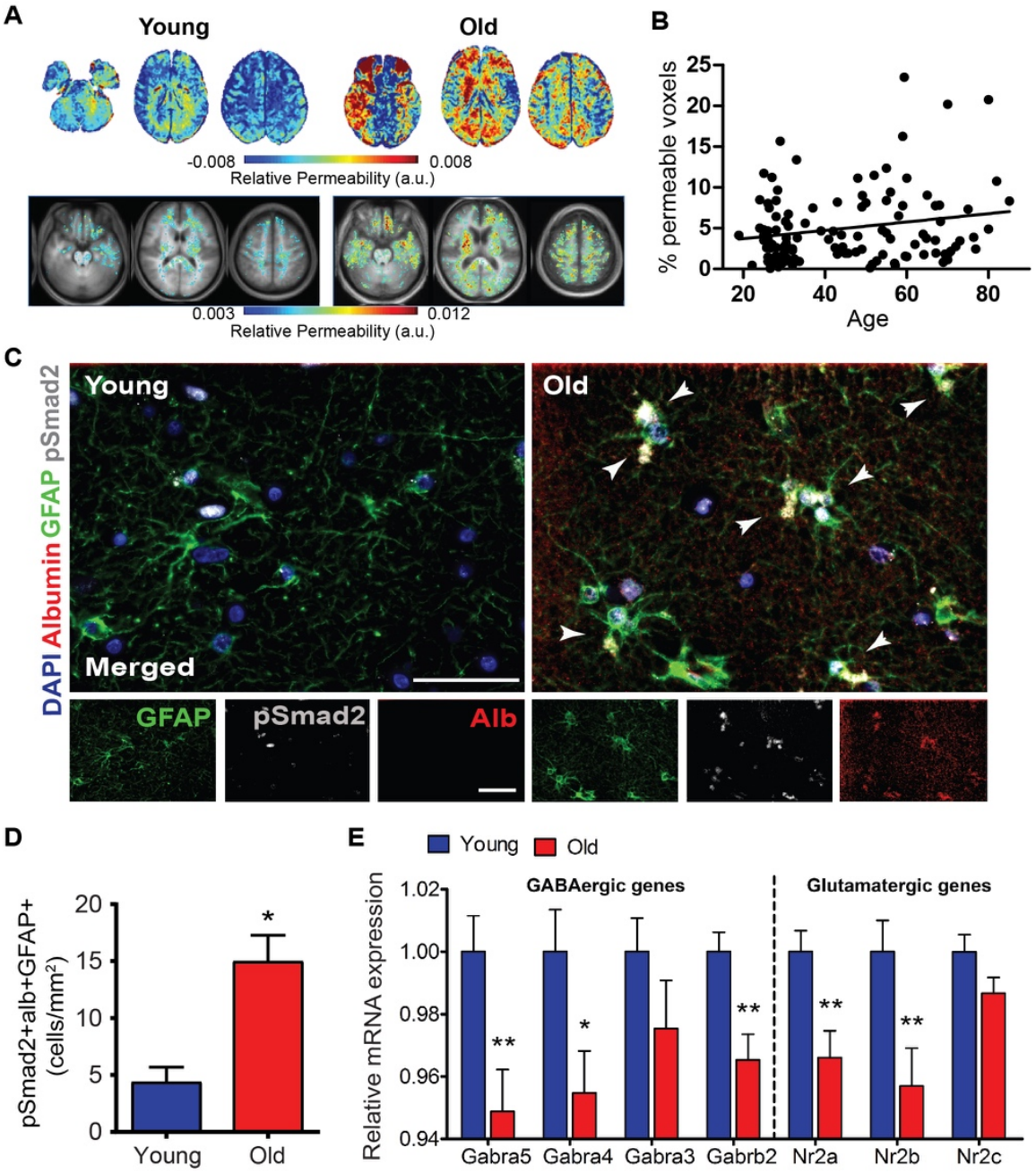
A
Young
Old
-0.008
0.008
Relative Permeability (a.u.)
0.003
0.012
Relative Permeability (a.u.)
B
% permeable voxels
Age
C
DAPI Albumin GFAP pSmad2
Young
Old
Merged
GFAP
pSmad2
Alb
D
pSmad2+alb+GFAP+ (cells/mm²)
Young
Old
E
Young
Old
GABAergic genes
Glutamatergic genes
Relative mRNA expression
Gabra5
Gabra4
Gabra3
Gabrb2
Nr2a
Nr2b
Nr2c

Figure 2.6. Aging patients show decline in the integrity of the BBB and increased TGFβ signaling. (A) (Top Panel): Representative images from DCE-MRI scans of a young (30 years old) and old (70 years old) subject using an MRI-sensitive contrast agent, Gd-DTPA, which does not cross the intact BBB. Intensity of signal reflects relative BBB permeability (in arbitrary units, a.u.). (Bottom Panel): Average permeability maps from all young (ages 20-40) and old (60-80) subjects. (B) Linear regression was used to model changes in BBB permeability (% of total brain volume with permeability values above the 95^{th} percentile of the averaged young healthy subjects), showing a significant increase with age (n = 113, p=0.0315). (C) Representative images of immunofluorescent staining of post-mortem human hippocampal tissue from young (31.3 ± 5 years) and old (70.6 ± 5.6 years) individuals, showing albumin in the aging hippocampus, localized in astrocytes (GFAP) and co-localized with the TGFβ pathway signaling protein phosphorylated Smad2 (pSmad2), indicated by arrows. Nuclei are visualized by DAPI stain. Scale bar = 50 μm. (D) The aging human hippocampus has significantly elevated numbers of astrocytes that colabel with albumin and pSmad2 (t-test, p=0.0324, n = 3 young, 10 old). (E) Expression of select glutamatergic and GABAergic genes from young and old humans, from the UK Gene Expression Consortium, analyzing subunits of the NMDA receptor (NR2A, NR2B, and NR2C) and $GABA_A$ receptor subunits (GABRA5, GABRA4, GABRA3, and GABRB2). Expression of NR2A, NR2B, GABRA5, GABRA4, and GABRB2 is downregulated in the aging human hippocampus (t-test with Holm- Bonferroni correction for multiple comparisons, n = 27 young, 36 old, *p<0.05, **p<0.01).

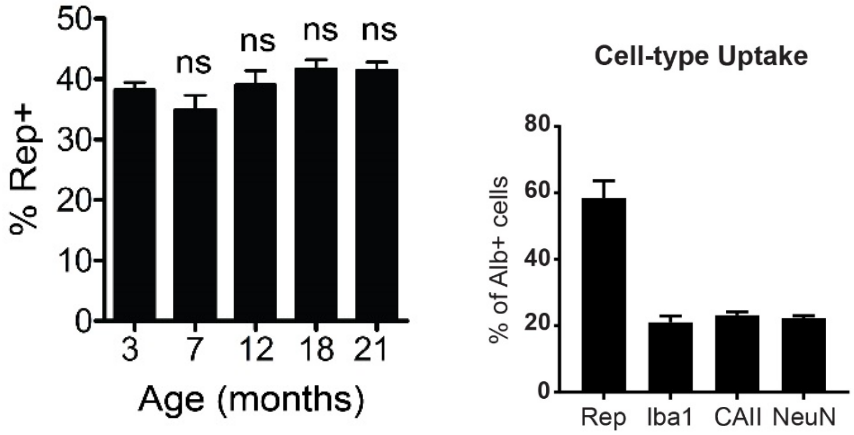

Figure S2.1. Related to Figure 2.1. (Left Panel) Percent of total cells expressing fluorescent reporter (Rep) in the hippocampus of Rep-Aldh1L1 mice. The number of labeled astrocytes did not change across the lifespan. (Right Panel) Co-staining for cell-specific markers was used to estimate the percent of albumin taken up by different cell types in the aged mouse hippocampus, as a percent of all albumin positive cells. Albumin was predominantly taken up by astrocytes (Rep), and was found at lower levels in microglia (Iba1), oligodendrocytes (CAII), and neurons (NeuN).

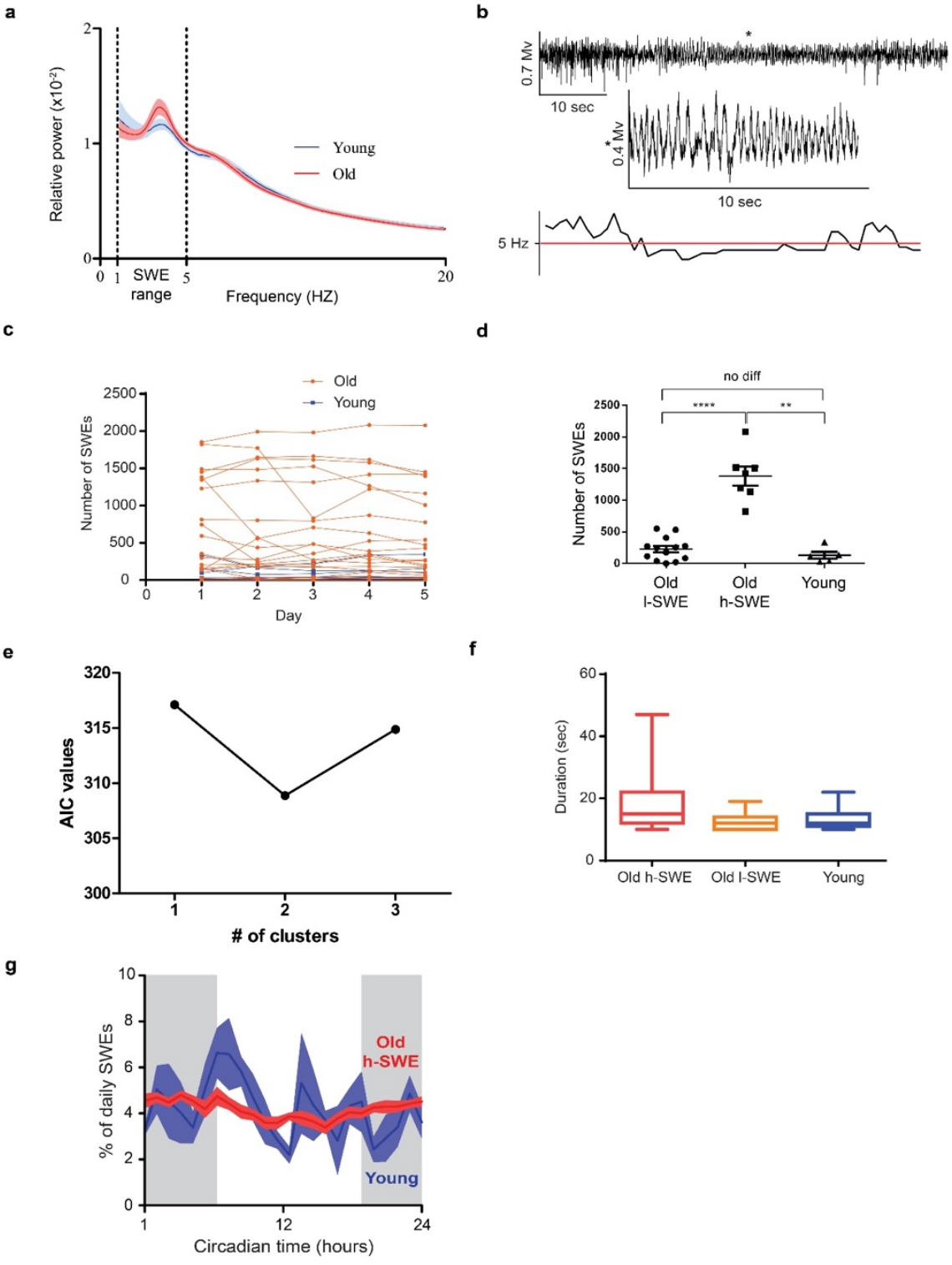
a
Relative power (x10-2)
Young
Old
SWE range
Frequency (HZ)
b
0.7 Mv
10 sec
0.4 Mv
10 sec
5 Hz
c
Old
Young
Number of SWEs
Day
d
no diff
****
**
Number of SWEs
Old l-SWE
Old h-SWE
Young
e
AIC values
# of clusters
f
Duration (sec)
Old h-SWE
Old l-SWE
Young
g
% of daily SWEs
Old h-SWE
Young
Circadian time (hours)

Figure S2.2. Related to Figure 2.1. (a) Spectral analysis of ECoG showed a trend towards increased slow- wave power in aged mice compared to young. Slow-wave activity was examined in greater detail by quantifying discrete SWEs. (b) A representative trace shows a SWE with slow-wave activity less than 5 Hz and a 10 second window of the slow wave event (marked with *). (c) Visualization of individual trajectories over the five day recording period shows that individual mice had a consistent h-SWE or l- SWE phenotype; h-SWE mice continued to show high numbers of SWEs across all days of recording. (d) GMM clustering was performed to segregate the old mice into l-SWE and h-SWE subgroups. The old h-SWE group had significantly more SWEs than the old l-SWE group or young. (e) Akaike information criterion (AIC) was used to compare the goodness-of-fit of GMM clustering models with 1, 2, or 3 clusters. Lower AIC values represent better goodness-of-fit. (f) While the old h-SWE mice had a significantly elevated number of SWEs, the increased number of SWE was not related to duration of individual SWEs; SWEs across all groups were of short, discrete duration with no difference in average of SWE duration between groups. (g) Circadian plot showing occurrence of SWEs throughout the day. Young mice show a circadian oscillation, with the highest percentage of all SWEs occurring after onset of the light cycle, whereas h-SWE mice show SWEs consistently throughout both day and night.

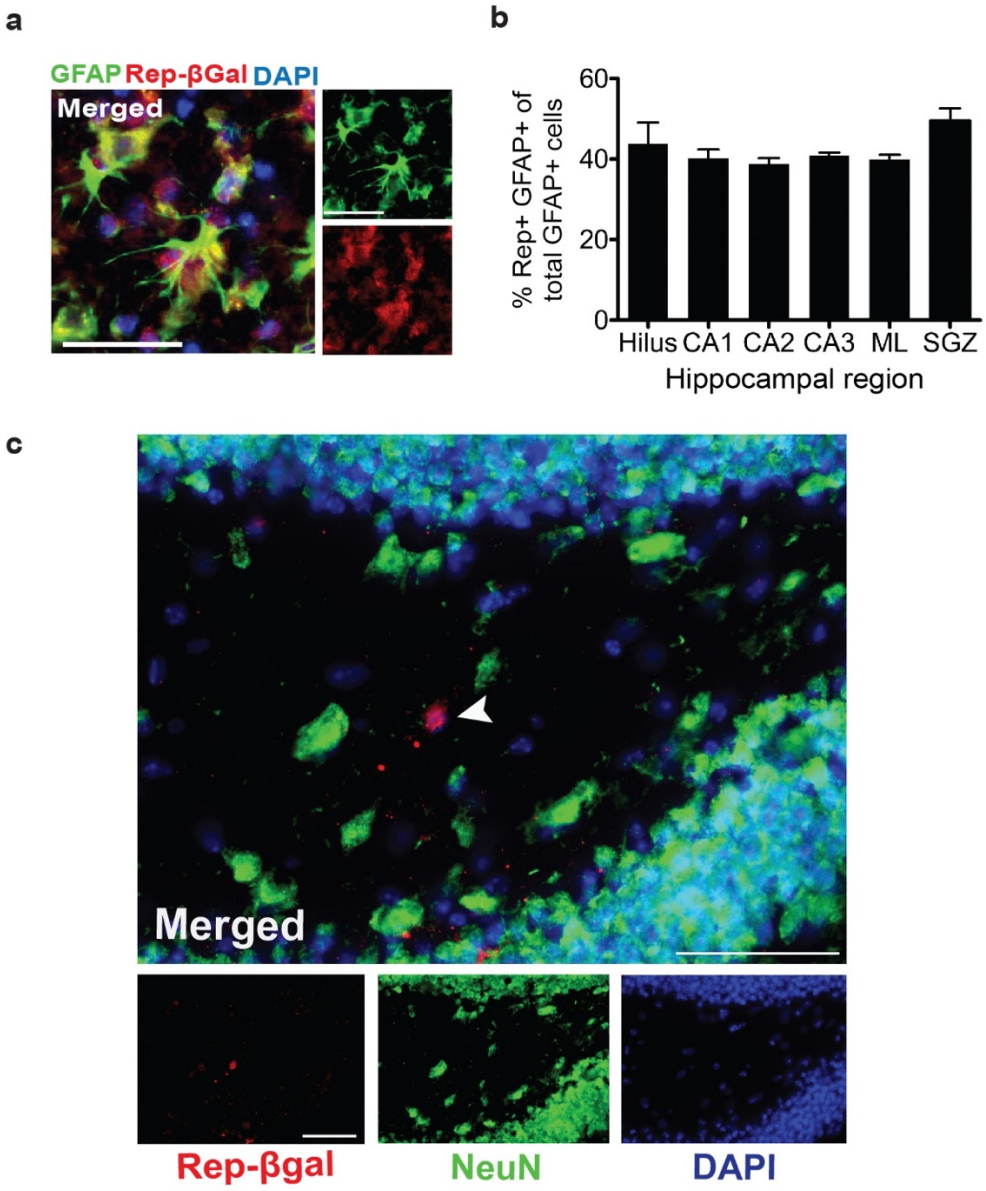

Figure S2.3. Related to Figure 2.2. (a) Representative immunofluorescent image from mouse hippocampus, showing reporter expression (Rep-βGal, red) in astrocytes (GFAP, green) following induction of the Cre recombinase system. Scale Bar = 30 µm. (b) Reporter expression was present in approximately 45% of hippocampal astrocytes, and was consistent throughout all hippocampal subregions (CA: cornu ammonis; ML: molecular layer; SGZ: subgranular zone). (c) No significant reporter expression was observed in mature neurons (NeuN), indicating that hippocampal neural stem cells expressing GLAST did not generate an appreciable lineage of recombinant TGFβR KO neurons. Scale bar = 50 µm.

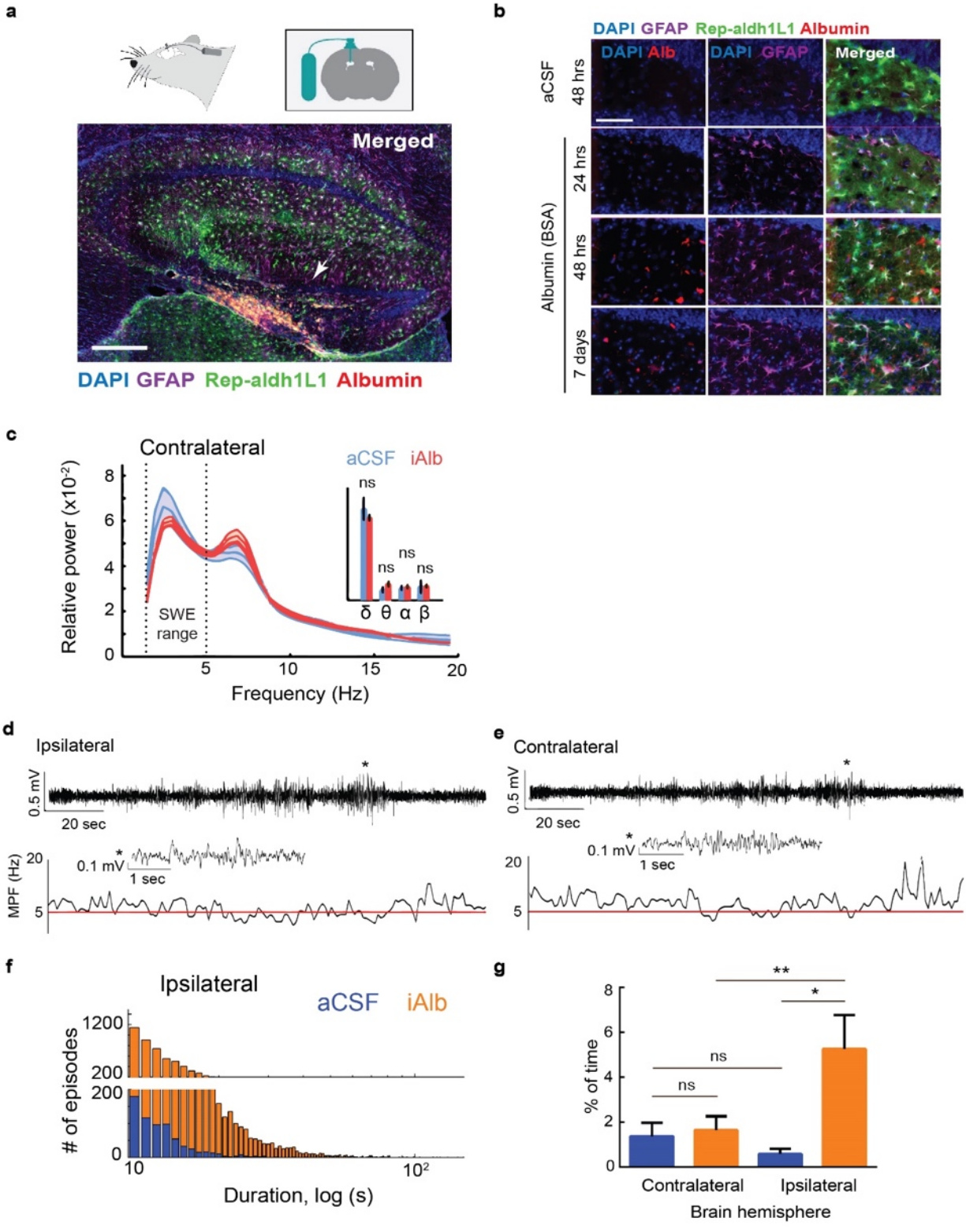
a
Merged
DAPI GFAP Rep-aldh1L1 Albumin
b
DAPI GFAP Rep-aldh1L1 Albumin
aCSF
48 hrs
DAPI Alb
DAPI GFAP
Merged
Albumin (BSA)
24 hrs
48 hrs
7 days
c
Contralateral
aCSF iAlb
Relative power (x10-2)
SWE range
ns
δ θ α β
Frequency (Hz)
d
Ipsilateral
0.5 mV
20 sec
0.1 mV
1 sec
MPF (Hz)
e
Contralateral
f
Ipsilateral
aCSF iAlb
# of episodes
Duration, log (s)
g
% of time
ns
*
**
Contralateral
Ipsilateral
Brain hemisphere

Figure S2.4. Related to Figure 2.3. (a) (Top) Diagrams showing mouse icv pump implants, with cannulas placed to infuse albumin into the brain ventricle; (Bottom) Immunofluorescent image of ipsilateral hemisphere, showing hippocampus (coronal slice). The infused albumin (fluorescent-tagged, in red) diffuses into the ventricle and accumulates in the dentate gyrus (arrowhead indicates the granule cell layer). Scale bar = 700 µm. (b) Representative images from the dentate gyrus show albumin uptake in astrocytes at 24 hours, 48 hours, and 7 days after pump implant (with aCSF control shown at 48 hours; scale bar = 50 µm). (c) No shift in the spectrum of ECoG activity was observed in recordings from contralateral hemisphere of iAlb rats. (d-e) Representative ECoG traces from ipsilateral and contralateral hemisphere, showing discrete SWEs within a 10 second window (marked with *). (f) Histogram showing number of SWEs recorded from ipsilateral cortex, binned by duration of SWEs. iAlb rats had significantly elevated number of SWEs compared to aCSF-infused controls. (g) Elevated SWEs were specific to ipsilateral cortex of iAlb rats, which showed SWEs occurring during nearly 6% of total recording time. In contrast, the contralateral hemisphere of iAlb rats, and both hemispheres of aCSF controls, had much lower percent of SWEs.

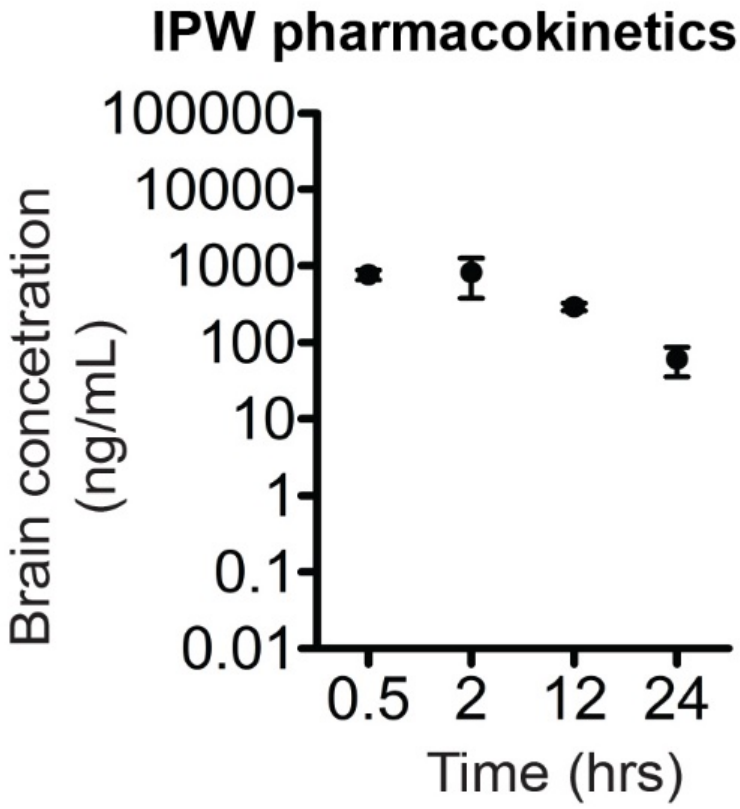

Figure S2.5. Related to Figure 2.4. PK measures of IPW concentration in brain lysates from n = 3 mice at timepoints spanning 24 hours after a single dose (30 mg/kg, po). At 24 hours, IPW concentration remains above the IC_{50} of 75 nM.

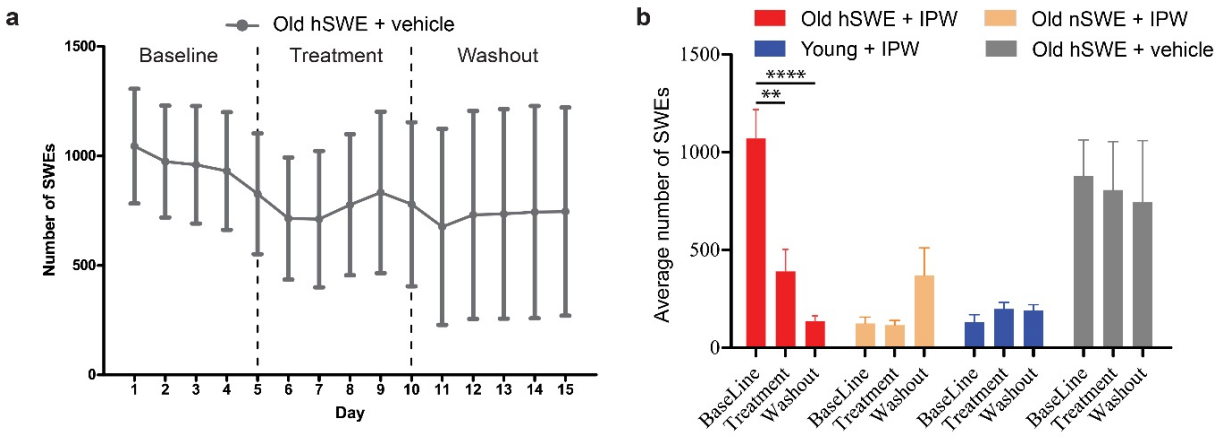

Figure S2.6. Related to Figure 2.5. (a) Mice treated with injection of vehicle (rather than IPW) showed no change in number of SWEs. (b) Average number of SWEs for all groups during the final two days of each treatment period (Baseline prior to injection, treatment with daily injection of IPW or vehicle control, and washout with cessation of injections). Treatment significantly reduces SWEs in the h-SWE group, whereas no changes in SWEs were observed in any other group.

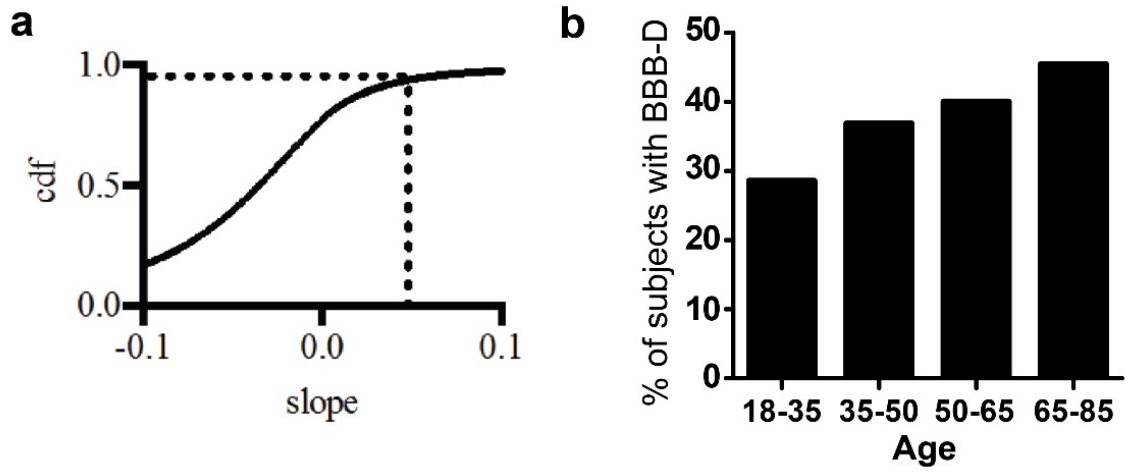

Figure S2.7. Related to Figure 2.6. (a) Classification threshold defining BBB-disrupted (BBB-D) and BBB- intact (BBB-I) subjects following dce-MRI. The cumulative distribution function (cdf) is shown. A threshold was set at 95%, defining the BBB-I group as those showing BBB permeability in less than 5% of total brain volume. (b) Descriptive statistics estimating the percent of individuals affected by BBB-D (defined as suprathreshold permeability in more than 5% all brain voxels) across age groups.

Chapter 3. TGF-beta disrupts neurosynaptic signaling in the hippocampus during aging

Adapted from: Senatorov VV Jr, Friedman AR, Milikovsky DZ, Ofer J, Saar-Ashkenazy R, Charbash A, Jahan N, Chin G, Mihaly E, Lin JM, Ramsay HJ, Moghbel A, Preininger MK, Eddings CR, Harrison HV, Veksler R, Becker A, Hart B, Rogawski MA, Dillin A, Friedman A, and Kaufer D, 2018. Blood-brain barrier breakdown during aging causes chronic but reversible neural dysfunction via TGF-beta signaling. Manuscript in preparation.

3.1 Introduction

Aberrant TGFβ signaling in the brain can promote a wide range of pathology such as increased inflammation, aberrant synaptogenesis, and altered plasticity [32,106] (Chapter 2). Increased levels of TGFβ are linked to a number of age-associated diseases, including Alzheimer's disease [107], type 2 diabetes [108], Huntington's disease [109], and epileptogenesis [27,32]. Altered neurotransmission is often the main symptom of such diseases, and has shown to be modulated by TGFβ1 through changes in synaptic signaling – an essential component of which is the N-methyl-D-aspartate receptor (NMDA-R) – a glutamate-gated ion channel critical for brain plasticity [102,110,111]. Activation of TGFβ signaling has been shown to directly affect glutamatergic signaling and excitatory synaptogenesis [110], as well as Ca^{2+}/calmodulin-dependent protein kinase alpha (CamK2α), a protein kinase critical for NMDA-mediated long term potentiation, and learning and memory [111,112].

NMDARs exist as a tetrameric formation comprised of two NR1 subunits and either two NR2 subunits or one NR2 and one NR3 subunit [113–115]. The identity of the latter two subunits predicates the unique receptor subtype, whose expression in the brain is dynamic, often changing in response to environmental stimuli [113]. For example, sensory deprivation in rodents can drastically alter the balance of NR2A and NR2B subunits in the brain [113,114], demonstrating the sensitivity of these receptors to environmental factors. Indeed, the plasticity of these receptors makes them especially responsive in contexts of aberrant or pathological neural activity [115] and so it makes sense that these core signaling proteins are especially vulnerable to dysregulation in aging [116]. Notably, decreased expression of the NR2B subunit causes impaired synaptic plasticity and age-related cognitive dysfunction [117], while upregulating expression of NR2B through genetic overexpression [118] and viral injection [119] has been shown to improve the performance of old mice in cognitive behavior assays for associative memory and spatial learning. Here, we specifically focus on the two subunits of the NMDAR that have been shown to decline in the human hippocampus during aging (Chapter 2). Furthermore, we expand or focus from molecular characterization of the old brain, to exploring the relationship between NMDAR expression, TGFβ signaling, and cognitive function in an effort to elucidate the complex interaction between them.

To date, no studies have been done investigating the role of TGFβ signaling in age-related remodeling of neurosynaptic markers and cognitive impairment. In this study, we show that inhibition of the TGFβ signaling pathway – either genetically via inducible astrocytic knock-out of TGFβR2 or pharmacologically – has a corrective effect on the age-related decline in neurosynaptic marker expression, correlating with improved cognition in old mice. In doing so,

we provide evidence for a novel mechanism of how dysregulated TGFβ signaling in the aging brain contributes to cognitive decline.

Existing NMDAR-targeted pharmacological approaches focus on direct modulation of glutamatergic signaling, by non-specifically changing expression of the subunit expression levels to broadly increase neurotransmission, or inhibiting its expression to decrease brain excitotoxicity [115,117,119,120]. However, these approaches have been largely ineffective as disease-modifying approaches – and there is no effective treatment for age-related cognitive decline or dementia. For example, clinical trials of NMDA-antagonists such as memantine have indicated only minor and short-lived beneficial effects in the treatment of neurodegenerative disease [121,122]. As a result, such pharmacological approaches have been criticized for being overly "symptomatic" [120]. Fewer therapeutic attempts have focused on regulating NMDARs and GABARs indirectly through upstream targets, by lowering inflammatory load in the brain during aging. Such an approach has the potential to be especially effective in modifying disease etiology, because instead of directly activating or inhibition key neurotransmission proteins, it focuses on dampening inflammatory signaling in the hippocampus to allow protein expression of synaptic markers to recover and stabilize. In this study, we illustrate the therapeutic potential of this approach using a novel small molecule TGFβR1 inhibitor to indirectly modify a profile of neurosynaptic markers in the aging brain, to improve cognitive performance.

3.2 Results

Decreased glutamatergic and GABAergic signaling in the hippocampus of aged mice

A number of studies have reported a decrease in NMDAR expression in the hippocampus of aged animals [116,117]. Our investigation confirms that mice aged to 24 months have significantly reduced levels of hippocampal NR2A and NR2B, shown both through protein and gene expression analyses (Figure 3.1A), compared to young controls (3 months old). Furthermore, protein data indicates that CamKIIα, a downstream protein kinase important for NMDA-mediated LTP, is also reduced in older mice (Figure 3.1A). Following this confirmation, we examined key GABAergic neurotransmission genes that were shown to be regulated by TGFβ signaling [32], and their expression in young and old mice. We found that key genes controlling excitability (Gabra3, Gabrb3, Gabrb2, Gad1, Glur1, and Slc1a2) were down-regulated in aging, compared to young mouse hippocampus (Figure 3.1B). Notably, these genes, in addition to NR2A and NR2B, constitute much of the core machinery that controls neural signaling and plasticity, making them ideal targets to gain a readout of the molecular substrates of neurotransmission.

Effects of astrocytic TGFβR2 knockout on NMDAR subunit expression during middle and late aging

Using a transgenic mouse line with inducible knock-out of TGFβR2 specifically in astrocytes (described in depth in Chapter 2), we examined the role of TGFβ on NMDAR signaling in mice during early aging (12-16) months. In the hippocampus of middle-aged $Tgf\beta r2^{fl/fl}$ animals, we observed a marked decrease in the both the latent and active forms of TGFβ1

compared to heterozygous controls (Tgfβr2 $^{fl/+}$) (Figure 3.2A). We next examined the effect of TGFβR KO on NMDAR expression. Genetic deletion of TGFβR2 significantly increased the expression of both NR2A and NR2B, and downstream CamKIIα (Figure 3.2B). Correlation between protein levels and performance in the T-maze identified a positive association between T-maze performance and higher protein levels of CamKIIα, NR2A, and NR2B. Additionally, higher protein levels of pSmad2 (both isoforms combined), pSmad2 (53kDa isoform only), and latent TGFβ1 were correlated with worse T-maze performance (Figure 3.2C-H), even though total pSmad2 protein level was not significantly different between the two groups (Figure 3.2A). We previously reported that aged astrocytic TGFβR2 KO mice have significantly reduced TGFβ1 protein levels in the hippocampus (Chapter 2). Following our findings in middle-aged mice, we analyzed hippocampal homogenates of aged astrocytic-TGFβR2 KO mice for other markers implicated in TGFβ signaling. Knockout during late aging did not produce significant changes in total hippocampal protein expression of either the latent or active forms of TGFβ1, or pSmad2. NMDAR expression was also unaffected by knockout in the late aging experimental group; however, levels of CamKIIα were slightly elevated following knockout. These findings indicate that middle-aged mice are particularly sensitive to inhibition of astrocytic TGFβ signaling. These data support the idea that the early aging brain retains remarkable latent capacity for plasticity given that NMDAR expression was effectively restored after knock-out. This plasticity may decline during later aging as sensitivity to astrocytic TGFβ inhibition was lost in late aging animals (24 months old) (Figure 3.3A-B).

Both acute and prolonged treatment with a small molecule TGFβ inhibitor restores age-related decline of NMDAR and GABAR subunit expression

In our previous research, a small-molecule TGFβ1 kinase inhibitor, IPW, demonstrated strong efficacy in ameliorating blood-brain barrier pathology in aging. We showed that just one day of IPW treatment could restore "youthful" brain activity in old mice (Chapter 2). Here, we continue to investigate the core mechanism by which TGFβ negatively regulates the molecular correlates of neurotransmission. We investigated the potential of a small-molecule TGFβ1 kinase inhibitor, IPW, as a potential therapeutic intervention for age-related neurosynaptic deficits.

We assessed whether IPW treatment could reverse regulatory gene imbalance in aged mice to a profile typical of younger mice. Twenty-four hours following a single dose, IPW caused significant increases in the expression of NR2A and NR2B subunits, as well as GABAergic and other glutamatergic genes (Figure 3.4A), along with a subset of genes regulating astrocyte function, including connexins that control connectivity within astrocytic networks and at neural synapses [123], and the inward rectifying potassium channel Kir4.1, which regulates neural excitability by buffering extracellular potassium released during neural firing [27,124]. Together, these studies show that inhibition of chronic TGFβ signaling in aged mice can rapidly restore neural and astrocytic gene expression. In line with our previous findings, we then treated aged mice with IPW for 7 days and 2 weeks and examined NMDAR expression compared with old controls. Western blot densitometry analysis shows that after 1 week of treatment, the IPW group had significantly higher expression of both NR2A and NR2B in the hippocampus (Figure 3.4B). Two weeks of IPW treatment produced even greater rescue of NR2A and NR2B

expression (Figure 3.5A), evidenced by gene expression, as well as other glutamatergic receptors such as GluR1, and GABAergic receptors (Gabrb3, Gabrb2, Gabra3, Gabra4, Gabra5, Gad1) (Figure 3.5B). Correlation to T-maze score was significant for Gabrb2, Gabra3, Gabra5, and Gad1 (Figure 3.5C-F). IPW had a region-specific effect, showing changes in hippocampus but not cortex. Protein and RNA analysis of cortical samples revealed no significant changes in NR2A or NR2B after 1 or 2 weeks of treatment (Figure 3.6A, 3.6E), or markers of TGFβ signaling (Smad2, pSmad2, pSmad3, TGFβ1 latent, TGFβ1 active) (Figure 3.6B-D).

3.3 Discussion

Blood-brain barrier deterioration, evidenced by the presence of albumin in the brain, is one of the earliest discoverable hallmarks of age-related neural decline, detectable beginning in middle age (Chapter 2). Since the onset of neurodegeneration is often not prevalent during natural aging until the end of the lifespan, the early biological changes of aging – that begin during middle-age, are often overlooked in the literature. In this study, we characterize changes in hippocampal protein, and their association with cognitive performance, in early aging mice (12 months old) yet there is less variation between individuals during middle age than in old age, making middle-aged mice a valuable experimental group for study. For us, this group yielded the most consistent results: astrocytic knockout of TGFβR downregulated the markers of inflammatory TGFβ1 signaling and upregulated levels of NR2A and NR2B. Furthermore, gene expression could be correlated to behavioral scoring in the T-maze, confirming that inhibition of the TGFβ1 signaling pathway not only rescues NMDAR expression, but also improves cognitive function. These findings elucidate a new framework through which to view pathological NMDAR remodeling in old age, a phenomenon that has been well documented in the literature [113,115,116,118,119], but for which no clear mechanism has been isolated. Previous studies have suggested that age-related changes in NMDARs might be attributed to the build-up of amyloid-β plaques [113,125], augmented levels of extracellular glutamate [115,126], BDNF dysregulation [127], and oxidative damage [128], among others.

No studies have looked at pathological NMDAR remodeling in the context of the TGFβ1 signaling pathway. Yet, TGFβ is thought to play a crucial role in a number of age-associated diseases. Higher numbers of SNPs for TGFβ have been documented in human patients with AD and mild cognitive impairment, independent of ApoE4 status [107], and elevated levels of TGFβ have been shown to disrupt astrocytic function in an epilepsy model [26,102]. The relationship between TGFβ and NMDA expression is especially interesting given the high degree of experience-dependent plasticity in NMDARs: age-related change is more evident in NMDARs than any other glutamate receptor [116].

Our results show that in late aging, astrocytic TGFβR2 knockout did not significantly affect levels of total pSmad2 or TGFβ protein, or alter their downstream NMDAR expression in mice at 24 mo. of age. Interestingly, however, downstream CamKIIα signaling was significantly elevated, indicating that some effect on glutamatergic signaling and synaptic modulation is activated by inhibition of astrocytic TGFβ during late aging. Aging is a complex process, with multiple factors convoluting what might be a more straightforward process in middle age. Since our mice are naturally aged for two years, there might be increased heterogeneity in this modestly-sized cohort. Indeed, the effect of knockout is more apparent in the middle-aged

group. Alternatively, it is possible that astrocytic TGFβ is not alone sufficient to rescue NMDAR expression in late aging. Since other cell types in the brain can also upregulate TGFβ signaling in the old brain, there might be a compensatory mechanism in microglia or other TGFβ-secreting cells to keep elevated levels of inflammatory signaling in the hippocampus.

A recent study reported that middle-aged mice with high levels of hippocampal synaptic NR2B performed better in cognitive function tasks, while old mice demonstrated a reversal in outcome, with high levels of hippocampal synaptic NR2B being found in the worst performers [129]. We find a similar pattern in our results, showing that mice during late aging are less sensitive to astrocytic knock-out of TGFβ. This may be attributed to the possibility that NMDARs lose their plasticity [130] and binding ability [116] in old age, or suffer more oxidative damage or other stressors [116], indicating that NR2B expression in late aging might be compensatory for these receptors' decreased functionality. Additionally, dysregulated neuronal activity itself, has also been shown to increase NR2A and NR2B levels [113]. Within the hippocampus, regional specificity of NMDAR expression may also be important; for example, a previous study in aged rats demonstrated that poor scorers in a cognitive behavior task had upregulated levels of NMDARs only in certain regions of the hippocampus but not in others [131].

Synaptic plasticity in the hippocampus is essential for cognitive function, and has been characterized as an imbalance of excitatory and inhibitory signaling elements, that leads with cognitive impairment in aging [132–135]. Our For example, a reduction in the GAD-1 enzyme, important for the conversion of glutamate to GABA, has been implicated in age-related memory loss through neuronal over-excitation in the hippocampus [134]. Furthermore, a number of studies have determined that hippocampal Gabra5 plays a crucial role in memory acquisition [132–134]. Increasing expression through an allosteric modulator improves the scores of aged rats in cognitive function tasks [132], and the depletion of radixin, a protein important for the synaptic exchange of Gabra5, impairs short-term memory [133]. It has also been reported that in regular aging, a steady decrease in both glutamate and GABA is observed in the hippocampus [135].

Our study demonstrates that pharmacological inhibition of TGFβ with IPW treatment, is effective in rescuing NR2A and NR2B expression in aged mice after just 24 hours. We also treated old mice with IPW for 1 week and 2 weeks and found significant upregulation in levels of NR2A, NR2B, as well as a number of GABAergic genes. Moreover, a positive correlation was determined between high levels of certain GABAergic genes, including glutamate decarboxylase 1 (GAD1) and GABA receptor subunit 5 (Gabra5), and T-maze score. In addition to the rescue of NR2A and NR2B, the upregulation of these key GABAergic subunit genes is interesting, especially since in late aging, animals that performed best on the cognitive function task, also had the highest levels of inhibitory GABAergic signaling. This suggests that reduced hippocampal excitation is important for cognitive function during late aging.

IPW has demonstrated potential not only in elevating NMDAR expression in aging, but also restoring GABAergic signaling elements as well. NMDAR agonists such as memantine, the current NMDA-targeted market drug for moderate to severe AD, or amantadine have been criticized for their nonspecific inhibition of NMDARs, and are only considered moderately effective [115,120–122]. IPW's upstream inhibition of TGFβ signaling may be less symptom-targeted and better able to rescue molecular neurotransmission deficits by altering the transcriptional profile of key genes, instead of acting on individual NMDA or GABA receptors. Furthermore, IPW treatment did not show significant changes in the cortex, suggesting its efficacy may be

specific to the hippocampus – the first brain region reported to decline in aging-related cognitive impairment, and the center of learning and memory in the brain [15]. Notably, this work explores the negative effect of inflammatory TGFβ signaling on glutamatergic and GABAergic signaling in the hippocampus through loss-of-function studies in the aging brain during both middle and late aging, and the small molecule TGFβR inhibitor IPW demonstrated a rapid and potent reversal of age-related pathology.

3.4 Methods

Western Blot. Mouse brain tissue (from the hippocampus, cortex, pre-frontal cortex, and hypothalamus) was homogenized and protein lysates were extracted using RIPA buffer (50 mM Tris-HCl, 150 mM NaCl, 1% NP-40, 0.5% Sodium deoxycholate, 0.1% SDS) including a protease (Calbiochem #539134) and phosphatase inhibitor cocktail (Roche PhoStop Ref: 4906845001). Protein samples were run under reducing conditions. 20 µg of protein lysate was mixed with Laemmli buffer (Bio-Rad #161-0747), containing 5% 2-mercaptoethanol (Sigma M6250), and fractionated by SDS-PAGE using the Mini-PROTEAN Tetra System and pre-cast TGX™ Gels (Bio-Rad #456-1096); Following separation, samples were transferred to a nitrocellulose membrane (0.45 µm, Bio-Rad #1620115). Membranes were blocked for 1 hr at room temperature with 5% non-fat dry milk (Apex #20-241) in TBST (10 mM Tris, 150 mM NaCl, 0.5% Tween 20, pH 8.0), and incubated overnight at 4 °C with primary antibody. Membranes were then washed 3x10 min with TBST and incubated with secondary antibodies for 1 hr at room temperature. Membranes were washed with TBST 3x10min and visualized using chemiluminescence SuperSignal West Dura Extended Substrate (ThermoFisher Scientific #34075), and Bio-Rad Chemidoc system with Bio-Rad Image Lab software (version 4.0.1). Densitometry analysis was done using Image J (NIH). The following primary and secondary antibodies were used: rabbit anti-GAPDH (1:2000, Cell Signaling #2118), rabbit anti-phosphorylated Smad2 (1:1000, Millipore AB3849-I), rabbit anti-phosphorylated Smad3 (1:1000, Cell Signaling #9520S), rabbit anti- TGFβ1 (1:500, Abcam ab92486), rabbit anti-NMDAR2A (1:1000, Cell Signaling #4205), rabbit anti-NMDAR2B (1:1000, Cell Signaling #4207), mouse anti-CamKIIα (1:2000, Millipore #05-532), anti-rabbit HRP (1:2000, Cell Signaling #4970), and anti-mouse HRP (1:2000, Cell Signaling #7076).

RT-qPCR. Total RNA was extracted from 200-250 mg of frozen mouse brain tissue using TRIzol reagent (ThermoFisher Scientific #15596026), and further purified with DNA-free DNA Removal Kit (ThermoFisher Scientific AM1906). First-strand cDNA synthesis was performed from 1 µg isolated RNA template using iScript RT supermix (Bio-Rad #1708841). PCR products were amplified using a CFX96 Real-Time PCR System (Bio-Rad), and threshold cycles were detected using SsoAdvanced Universal SYBR Green Supermix (Bio-Rad #172-5271). Mean threshold cycles were normalized to 18s internal control, and relative gene expression levels were quantified using the 2-ΔΔCT method. Primer sequences were obtained from the NCI/NIH qPrimerDepot.

Animal care and transgenic mice. All animal procedures were approved by the institutional animal care committees. Animals were housed with a 12:12 light:dark cycle with food and water available ad libitum. Triple transgenic astrocytic TGFβR/KO mice were bred from strains purchased from the Jackson Laboratory to generate mice that express CreERT

under the astrocytic promoter glial high affinity glutamate transporter (GLAST), with a floxed exon 4 of TGFβR2 (tgfbr2fl), and a transgenic LacZ reporter gene inhibited by a floxed neomycin cassette. Tamoxifen induction thus induces activation of astrocytic CreERT resulting in a null TGFβR2 allele (tgfbr2null) and LacZ expression ($R26R^{-/-}$). The parental strain STOCK Tg(Slc1a3-cre/ERT)1Nat/J mice were outcrossed with B6;129-Tgfbr2tm1Karl/J and B6.129S4-Gt(ROSA)26Sortm1Sor/J mice to produce males, while B6;129-Tgfbr2tm1Karl/J and B6.129S4-Gt(ROSA)26Sortm1Sor/J mice were outcrossed to produce females. The resulting GLAST-CreERT; $tgfbr2^{fl/+}$ males were bred with $tgfbr2^{fl/+}$; $R26R^{-/-}$ and $tgfbr2^{fl/fl}$; $R26R^{-/-}$ females to produce triple transgenic offspring. Subsequent generations were incrossed to produce experimental triple transgenic mice of genotypes GLAST-CreERT; $tgfbr2^{fl/fl}$; $R26R^{-/-}$, GLAST-CreERT; $tgfbr2^{fl/+}$; $R26R^{-/-}$, GLAST-CreERT; $tgfbr2^{fl/fl}$; $R26R^{-/+}$, and GLAST-CreERT; $tgfbr2^{fl/+}$; $R26R^{-/-}$. The inducible Cre/lox system was activated by 5 days of tamoxifen injection (Sigma-Aldrich, 160 mg/kg dissolved in corn oil, i.p). Control GLAST-CreERT; $tgfbr2^{fl/+}$ heterozygotes received the same dosage of tamoxifen.

T-maze behavior. Spatial working memory was tested by spontaneous alternation in a T-maze constructed of black plastic, with stem (50 x 16 cm) and two arms (50 x 10 cm). A vertical divider was placed at the midline of the stem exit, thus creating two entryways leading to either the right or left arms. Naïve mice were placed at the beginning of the stem and allowed to freely roam until opting to enter either the right or left arm. Upon crossing the threshold of the chosen arm, a door was lowered, and the mouse was contained to the chosen arm for 30 sec. Then, the mouse was returned to the stem and the door raised, allowing the next choice trial to commence immediately. After 10 sequential trials, the mouse was returned to the home cage. "Correct" alternation choices were scored when the mouse chose the arm opposite of that chosen in the previous trial, and percent correct was calculated as (total correct choices) / (total number of completed trials). In the event that a mouse did not leave the stem within 60 sec, it was removed from the apparatus for 30 sec, and then reset in the stem to start a new trial. These "incomplete" trials were not counted in scoring.

3.5 Figures

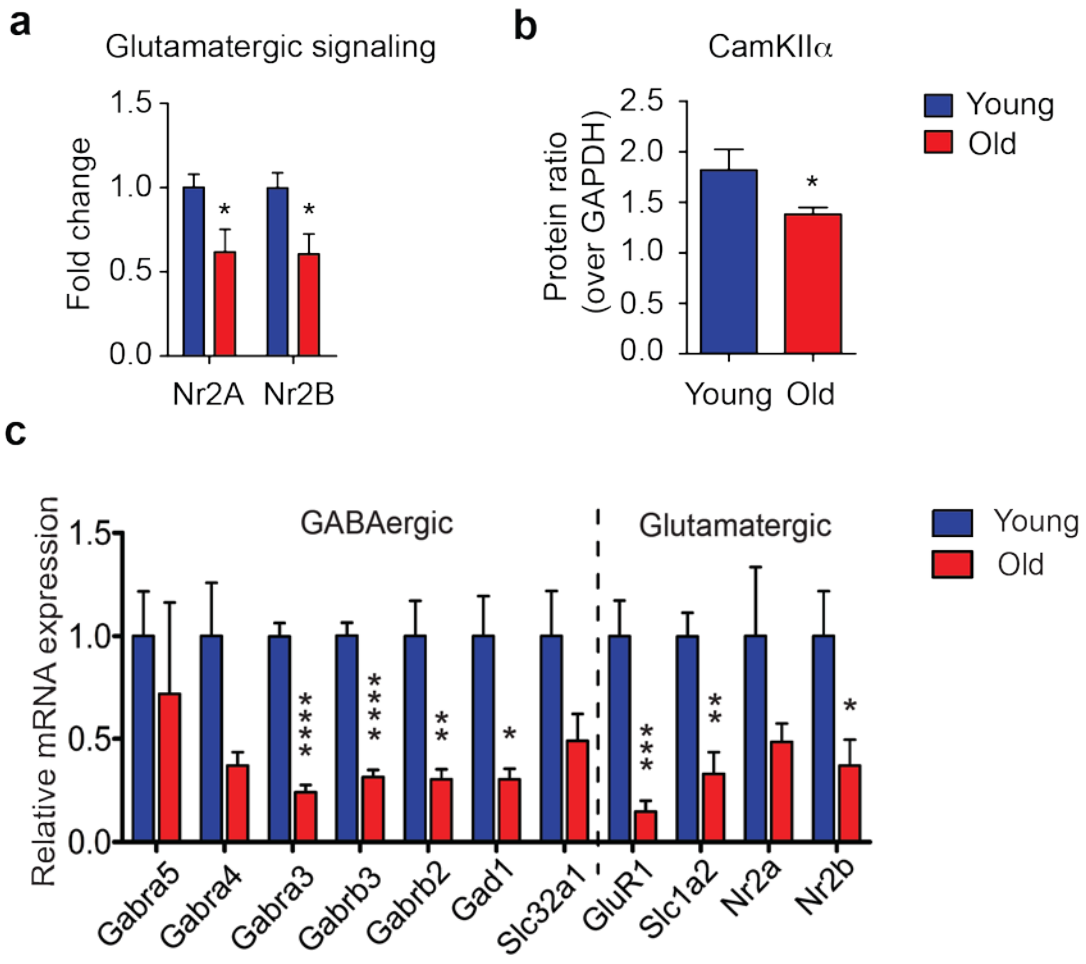

Figure 3.1. Aged mice show reduced glutamatergic and GABAergic signaling. (a) Expression of the NMDA receptor genes Nr2A and Nr2B are significantly reduced in the hippocampus of old mice, as compared to young controls (t-test, n=14 young, 5 old). (b) Western blot densitometry demonstrates that levels of CamKIIα, a downstream product of NMDAR activation, is significantly decreased in old age (t-test, n=5 young, 7 old). (c) Expression of GABAergic genes and glutamatergic genes including $GABA_A$ subunits, the GABA synthesis enzyme Gad1, the vesicular transport protein Slc32a1, the AMPA receptor subunit Glur1, the glutamate transporter Slc1a2, and NMDA receptor subunits, are significantly downregulated in the aged mouse hippocampus, compared to young (n = 4, t-test with Holm-Bonferroni correction). For all tests, *p<0.05, **p<0.01, ***p<0.005, ****p<0.001.

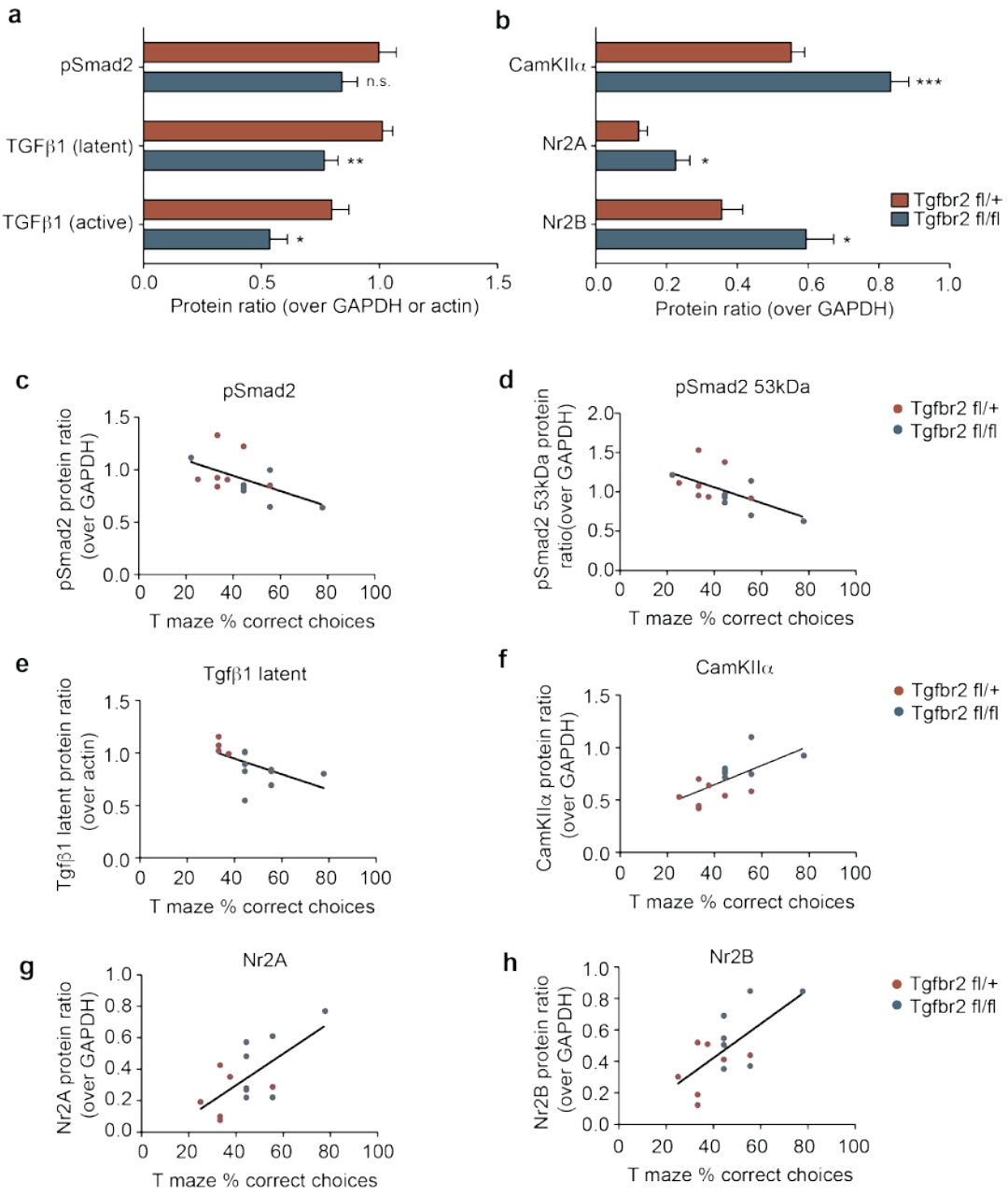

Figure 3.2. Middle-aged mice with an astrocytic TGFβR knockout show reduced inflammatory signaling and significant increase in NMDAR expression in the hippocampus. (a) Western blot densitometry of hippocampal tissue shows significant reduction in the active and latent forms of TGFβ1 but no change in pSmad2 (t-test, n=6 fl/+, 8 fl/fl). (b) Astrocytic TGFβR KO increased the protein expression of NR2A, NR2B, and CamKIIα (t-test, n= 7 fl/+, 7 fl/fl). (c-h) Correlation analyses of behavior and protein expression reveals that higher levels of total pSmad2 (Pearson's correlation, r^2=0.2947, p=0.0448, n=14), the pSmad2 53 kDa isoform (r^2=0.3577, p=0.0239, n=14), and the latent form of TGFβ1 (r^2=0.3065, p=0.0496, n=13) are correlated with worse performance in the T-maze, while higher levels of CamKIIα (r^2=0.4286, p=0.0111, n=14), NR2A (r^2=0.4343, p=0.0104, n=14), and NR2B (r^2=0.4461, p=0.0090, n=14) are correlated with better T-maze performance. For all tests, *p<0.05, **p<0.01, ***p<0.005.

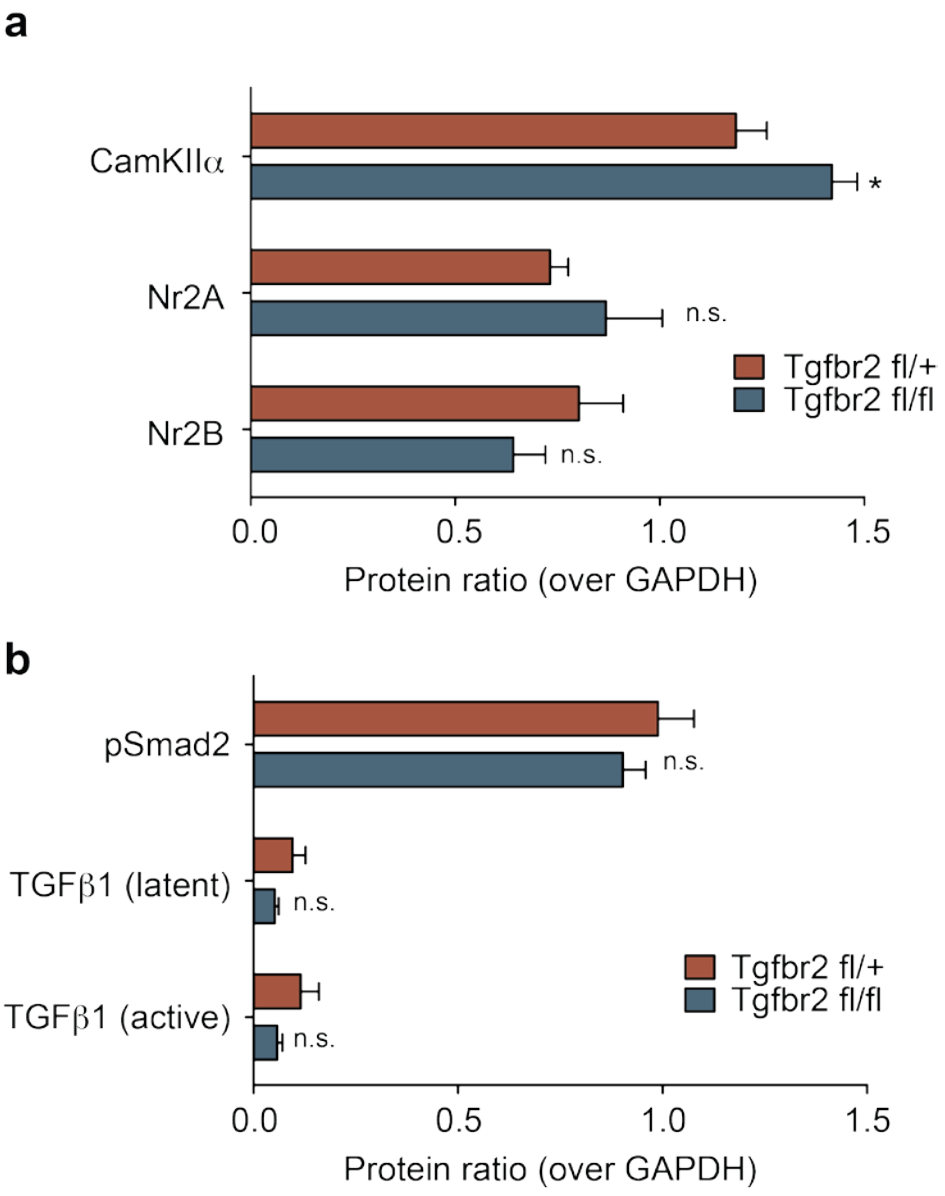

Figure 3.3. Astrocytic knock-out of TGFβR in 24 mo. old mice has modest effects on hippocampal CamKIIα, but no observable effect on TGFβ signaling. (a) Western blot densitometry shows that KO mice have increased downstream CamKIIα expression but no change in levels of NR2A or NR2B (t-test, n=7 fl/+, 7 fl/fl). (b) Astrocytic TGFβR KO did not produce significant differences in expression of pSmad2, active TGFβ1, or latent TGFβ1 (t-test, n=8 fl/+, 6 fl/fl). For all tests, *p<0.05.

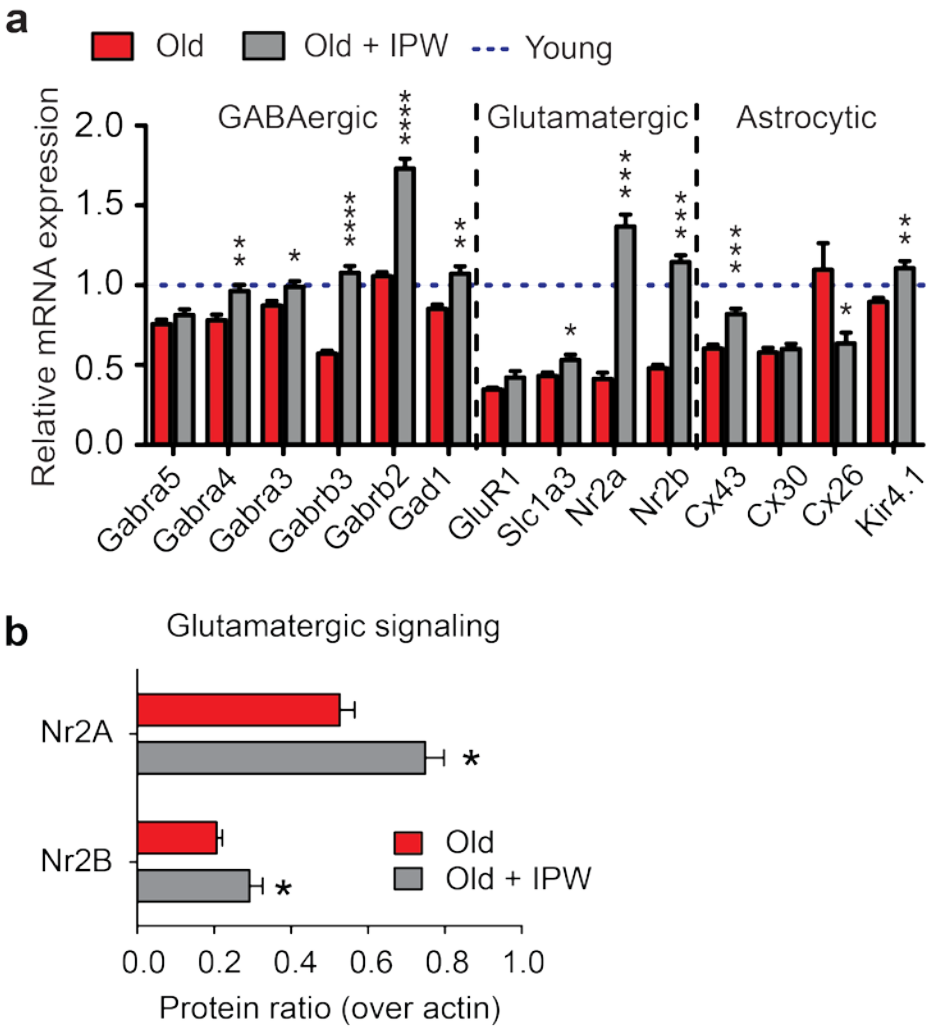

Figure 3.4. IPW treatment modulates GABAergic, glutamatergic, and astrocytic signaling in old mice. (a) Expression levels of selected glutamatergic, GABAergic, and astrocytic function genes is significantly increased 24 hours after a single i.p. injection of IPW (20 mg/kg), compared to aged vehicle-injected controls (t-test with Holm-Bonferroni correction, n = 8 old, 9 old + IPW). (b) 7 days of IPW treatment (daily single injection at 20 mg/kg) shows increased NR2A and NR2B hippocampal expression by western blot densitometry ((t-test, n=5 old, 5 old +IPW). For all tests, *p<0.05, **p<0.01, ***p<0.005, ****p<0.001.

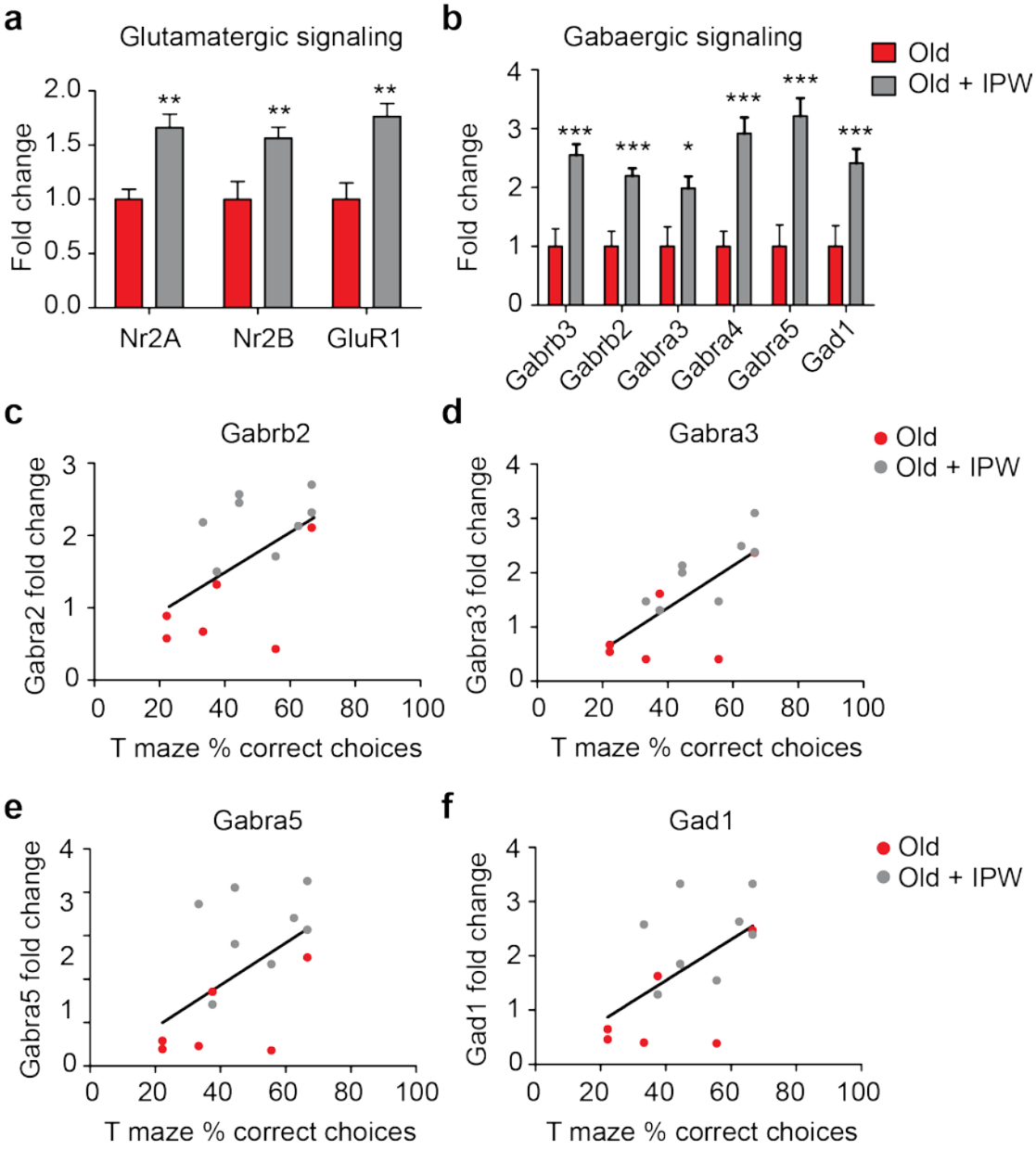

Figure 3.5. Two weeks of IPW treatment (daily single injection at 20 mg/kg) significantly increases glutamatergic and GABAergic signaling in the hippocampus of aged mice. IPW treatment in old mice increases expression of (a) glutamatergic genes Nr2A, Nr2B, and GluR1 and (b) gabaergic subunit genes gabrb3, gabrb2, gabra3, gabra4, gabra5, and gad1 (t-test, n=6 old, 9 old + IPW). (c-f) High levels of Gabrb2 (Pearson's correlation, r^2=0.3176, p=0.0358 n=14), Gabra3 (r^2=0.5272, p=0.0033, n=14), Gabra5 (r^2=0.3037, p=0.0411), and Gad1 (r^2=0.3351, p=0.0301) are positively correlated with better performance on the T-maze task. For all tests, *p<0.05, **p<0.01, ***p<0.005.

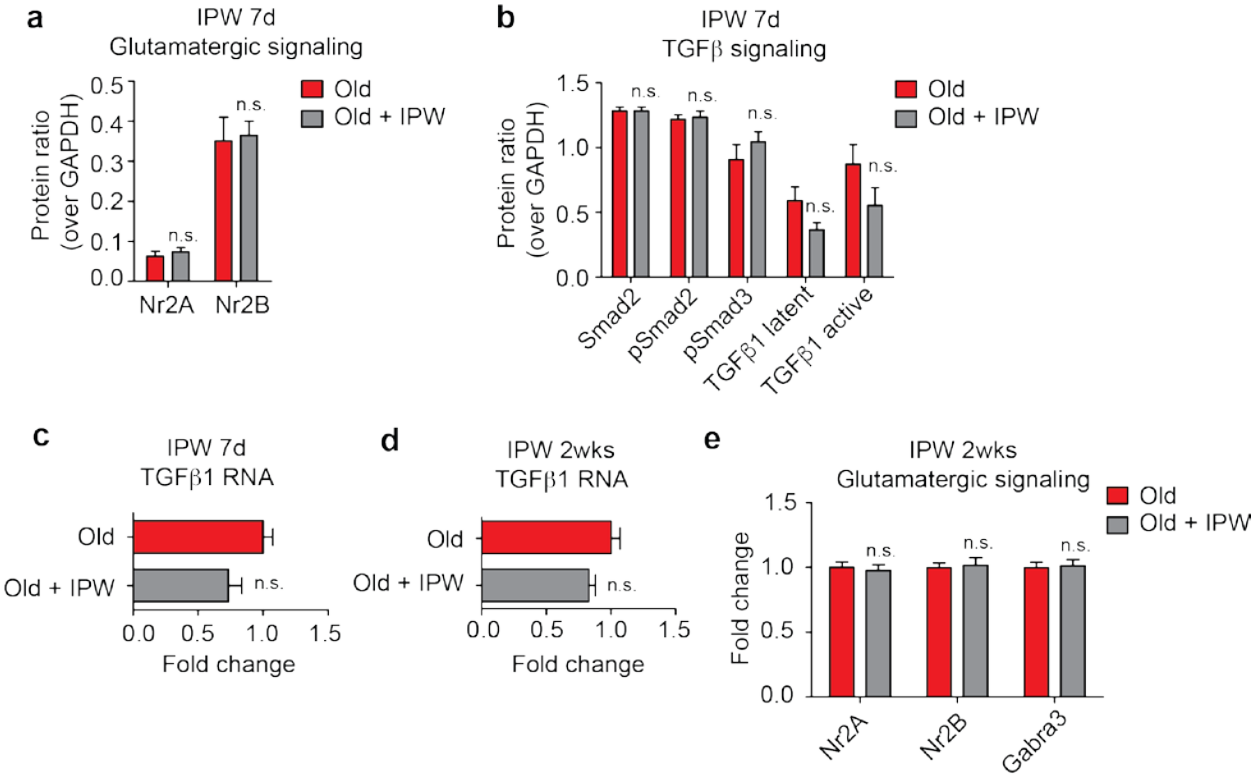

Figure 3.6. IPW treatment does not affect TGFβ signaling or glutamatergic signaling in the cortex. Western blot quantification shows no change in (a) NR2A or NR2B; or (b) TGFβ signaling or TGFβ levels after seven days of IPW treatment (t-test, n=5 old vehicle, 5 old + IPW). Gene expression of TGFβ1 similarly showed no difference in the cortex of IPW or vehicle treated old mice with either (c) 7 days of IPW or (d) 2 weeks of IPW (t-test, n=5 old + vehicle, 5 old + IPW). (e) Expression of genes implicated in glutamatergic and GABAergic signaling are unaffected in the cortex by 2 weeks of IPW treatment (t-test, n=6 old + vehicle, 9 old + IPW).

Chapter 4. Inhibition of TGF-beta signaling during aging restores expression of blood-brain barrier regulatory genes

4.1 Introduction

The blood-brain barrier (BBB) is a tightly controlled interface between the blood and the brain, with the central role of regulating transport of molecules through paracellular tight junctions between vascular cells [136]. This critical barrier maintains brain homeostasis, allowing healthy function of neurons and generally protects the brain parenchyma from acute insult, along with neurological diseases associated with vascular dysfunction, including traumatic brain injuries, Alzheimer's disease, stroke, epilepsy, and multiple sclerosis [137]. The essential process of BBB maintenance and regulation goes awry during aging and leads to a complex interaction of pathological activity in the brain[15,136] (Chapters 2 and 3).

Based on our previous studies, the efficacy of IPW treatment was surprisingly rapid, restoring normal ECoG activity within 24 hours and restoring youthful memory capacity within 7 days of treatment. This suggested that TGFβ signaling may directly impact neural function, likely via transcriptional regulation of downstream targets (Chapter 2). To test whether inhibition of TGFβ signaling could produce a rapid reversal of an “aged” transcriptional profile, we treated aged mice with a single dose of IPW, and 24 hours later quantified transcriptional changes in the target genes. After 24 hours, IPW caused significant changes, and often full reversal, in the majority of these target genes, including GABAergic and glutamatergic genes, as well as in genes regulating astrocyte function, including connexins that control connectivity within astrocytic networks and at neural synapses, and the inward rectifying potassium channel Kir4.1, which regulates neural excitability by buffering extracellular potassium released during neural firing. Similar results were seen again after 2 weeks of daily dosing, suggesting that initial changes to a transcriptional profile of neurotransmission remained potentiated (Chapter 3). Together, these studies showed that inhibition of chronic TGFβ signaling in aged mice can rapidly restore a “youthful” profile of neural and astrocytic gene expression. Our findings that IPW not only restores cognitive function but also expression levels of NMDAR and GABAR subunits suggests that the aging brain may retain considerable capacity for plasticity that is suppressed by BBB leakiness and inflammation, but can still be restored, indicating that it is still amenable to therapeutic intervention.

In this study, we further explore the potential of pharmacological TGFβ inhibition using the small molecule IPW. Specifically, we ask whether IPW has the potential to affect structural elements of the blood-brain barrier – the foundational genes which reflect regulation of tight junction efficacy and vascular cell function in the aging brain. If so, it would suggest that inhibiting TGFβ in the aging brain has remarkable potential to lower inflammatory load such that the BBB is able to be “repaired” to reduce age-related BBB permeability. To test this idea, we ran a preliminary study to look at specific tight junction and vascular cell marker genes after acute (24 hrs) and prolonged (2 weeks) treatment of single, daily doses.

4.2 Results

Acute and prolonged and inhibition of TGFβ selectively restores expression of BBB function genes in old mice

To gain a molecular readout of BBB status in the young and old hippocampus, we came up with a transcriptional profile of key BBB-related genes. To be able to infer a functional outcome of BBB, we specifically chose to look at genes that regulate the function of endothelial cell and pericytes, which line the blood vessels and act as the first line of defense for filtering and regulating access to components in blood serum, along with a host of essential tight junction genes – that are integral to the structure and function of the BBB, controlling paracellular transport and BBB permeability. For tight junction status, we probed a subset of claudin genes that are expressed in the brain (claudins-1, -3, -5, and -12); occludin-1; zonula occuldens-1 (ZO-1); TEK tyrosine kinase, endothelial (Tie-2); cluster of differentiation 31 or platelet endothelial cell adhesion molecule (CD31/Pecam-1); and endothelial-specific adhesion molecule (ESAM). For markers of pericytes, we probed beta-type platelet-derived growth factor receptor (PDGFRβ); and Desmin.

Additionally, we looked at glucose transporter 1, also known as solute carrier family 2, facilitated glucose transporter member 1 (Glut-1/slc2a1), for a readout of glucose transport since glucose uptake in the brain from the blood serum is regulated predominantly by Glut-1 [138]. In both mild cognitive impairment (MCI) and Alzheimer's disease (AD) the hippocampus is characterized by lower glucose metabolism, which precedes clinical symptoms, and is predictive of subsequent cognitive decline [139]. Decreased brain-glucose use also further correlates to patients with cognitive decline [139]. Our data show a predictable decline in Glut-1 expression during aging, which is nearly restored to young mouse levels with brief IPW treatment (ANOVA, $p=0.0026$) (Figure 4.1B).

Since previous research has suggested a role for vascular cells of the BBB in regulating brain immune responses [140,141], we also probed several immune markers – the chemokines chemokine (C-C motif) ligand 2, also known as chemoattractant protein 1 (CCL2/MCP1); and C-C motif chemokine 11, also known as eosinophil chemotactic protein (CCL11/eotaxin-1). CCL2 is upregulated in astrocytes and vascular cells in the hippocampus in pathological contexts [142,143] and accelerates neurocognitive dysfunction by promoting brain inflammation [144]. CCL11 is a circulatory factor that can infiltrate the hippocampus from the periphery during aging to negatively regulate the molecular substrates of cognitive function [145]. Our data indicates a decline in CCL11 levels during aging, with no effect of IPW (ANOVA, $p<0.0001$) (Figure 4.1C). We see an expected increase in CCL2 during aging, which is completely restored back to healthy levels 24 hours after IPW treatment (ANOVA, $p=0.0074$) (Figure 4.1C).

Tight junction components with reliable expression in the hippocampus of rodents have been shown to consist of ESAM, occludins, and brain claudins, and have all been localized to cell-cell borders of endothelial cells in the brain. Among the 24 claudin family proteins identified in mammals, the microvascular endothelium of the brain is known to expressed only claudins-1, -3, -5 and -12 [146,147]. Altered claudin expression has been reported to be differentially regulated in AD, vascular dementia, and related pathology [148] – and claudin-5 expression is considered to be an especially sensitive readout of BBB integrity [12]. For the claudin

gene cluster, we saw no change in the expression levels of Claudin-12 (ANOVA, p=0.1017); and decreased expression of Claudins-1 (p=0.0119) and 3 (ANOVA, p=0.0007), but no effect of old IPW treated mice compared to old vehicle controls (Figure 4.1A). Claudin-5 is highly expressed in the mouse hippocampus, and is normally localized at the BBB and is responsible for maintenance and function[149]. Interestingly, it has also been detected in surrounding astrocytes while being absent from the rat brain endothelium after BBB disruption [150]. Perhaps this reflects autophagy of tight-junction components by astrocytes in a pathological context similar to age-related BBB disruption [151]. Its deletion in mice results in size-dependent disruption of the BBB [152]. The attenuated expression of claudin-5 has recently been linked to BBB disruption and cognitive dysfunction of rats [153] and its dose-dependent therapeutic increase has been tied to favorable neurological outcomes [154], and in aging, BBB permeability is associated with alterations in claudin-5 [155]. Interestingly, TGFβ1 has been shown to exacerbate BBB permeability in a mouse model of hepatic encephalopathy via upregulation of a matrix metalloproteinase 9 (MMP9) and downregulation of claudin-5 [156]. Excitingly, our data clearly shows an age-related drop in claudin-5 in old animals, with drastic improvement of expression after both single dose of IPW (ANOVA, p<0.001) (Figure 4.1A), which maintained significantly elevated after 2 weeks of IPW treatment over levels of old control mice (p=0.0169) (Figure 4.2A).

Occludin-1, and ZO-1 are known to also be reliable and sensitive indicators of structural changes in the BBB in pathological contexts [157]. They are integral tight junction proteins that work together to maintain interaction with claudins and other structural elements of the BBB to form tight junction strands and regulate permeability [158]. In rats, expression of these genes was shown to change during aging [159]. In mice, the expression of these BBB proteins was found to be attenuated from young to 24 months of age [160]. Changes in these markers are also associated with BBB dysfunction during natural aging, and responsive to inflammatory changes [160]. Our results show no change in expression of ZO-1 during aging, or with IPW treatment after 24 hours (ANOVA, p=0.3809) (Figure 4.1A), but a marked increase in ZO-1 after 2 weeks of IPW in old animals compared to IPW treated (p=0.0002) (Figure 4.2A), indicating that a longer timescale of TGFβ inhibition might be necessary for increasing expression of this tight junction gene. For occludin-1, however, no change in young compared to old, or with IPW treatment, except for a small but significant decrease in expression when comparing young to old + IPW animals (ANOVA, p=0.0356) (Figure 4.1A). After 2 weeks, we also saw no changes in expression between old and old + IPW animals (p=0.4676) (Figure 4.2A).

One of the strongest effects after both 24 hours and 2 weeks of treatment was the expression of Tie-2, which declined during aging and was restored after single dose (ANOVA, p<0.0001) (Figure 1A), and remained elevated after 2 weeks of dosing in old vs old + IPW animals (p=0.0008) (Figure 4.2A). Tie-2 is a marker of endothelial cell function and its heterogenous expression in capillaries plays an essential role in context-specific remodeling of the microvasculature [161]. Increasing Tie-2 expression has been reported to induce vascular stabilization of the BBB after neurological insult [162], while its role in aging is largely unexplored.

Pecam-1 is an endothelial adhesion molecule also found on leukocytes [12], which can modulate endothelial cell activity to allow interaction with migrating leukocytes during inflammation [163]. It is also a general marker of BBB barrier function in maintenance [164]. Our data show a strong age-related decline in its expression, which is salvaged by IPW 24 hours after

injection (ANOVA, p<0.0001) (Figure 4.1A) and maintains elevated expression after 2 weeks in IPW-treated animals compared to controls (p=0.0239). The endothelial cell-cell adhesion factor, ESAM, has been shown to play an important role in modulating junctional tightness and regulating transendothelial trafficking [3]. Data in ESAM knock-out mice shows deficits in angiogenic function and endothelial cell-cell interaction [165]. There is not much known about how this factor changes during aging. Our data indicates that ESAM declines with age, and its expression is restored after 24 hours of single IPW injection (ANOVA, p<0.0001) (Figure 4.1A), and continues to stay elevated after 2 weeks of daily dosing (p=0.0061) (Figure 4.2A).

Among the different cell types of the neurovascular unit, pericytes have the most proximate anatomical association with brain endothelial cells, as they sit directly beneath a layer of the basement membrane. This proximity to the endothelium allows them to communicate with vascular endothelial cells both through secreted signaling factors and gap junctions [139]. This integral population of cells is absolutely essential for proper function of the BBB, which is evident from various studies showing higher transmembrane resistance and reduced permeability when they are co-cultured with endothelial cells compared to endothelial cells alone [166], and in vivo studies using PDGFRβ knock-out mice showing increased BBB permeability and related dysfunction in pericyte deficient animals [167,168]. Using two markers of pericyte function we observed an age-related decrease in both PDGFRβ and desmin during aging, which was rescued by a single dose of TGFβ inhibitor (PDGFRβ; ANOVA, p=0.0006) (desmin; ANOVA, p<0.0001) (Figure 4.1B). At two weeks, PDGFRβ expression did not change significantly (p=0.1694), but desmin levels remained high (p=0.004) (Figure 4.2B), suggesting changes in pericytes function at both timepoints.

Taken together, these results show the aged BBB is still susceptible to intervention and modulation, through the inhibition of TGFβ, a key secreted factor in the neurovascular unit. Even after just a single dose of IPW, many of the integral elements of the BBB were selectively restored to young mouse levels, and remained high in mice treated with IPW.

4.3 Discussion

In recent years, the idea of neurovascular coupling has drawn more attention in the field of neuroscience—rather than impose a strict divide between the pathology of neurons and the pathology of brain vasculature, a growing amount of evidence indicates that these two concepts are intricately connected, and pathological changes in the brain arise from a disruption in their carefully regulated symbiosis [12,169–171]. Studies have shown that this disruption becomes more prevalent in old age due to deterioration of the BBB, the primary interface between the CNS and the periphery [139,170–172].

Our prior research indicates that a small molecule TGFβ inhibitor could reverse age-associated pathological changes after BBB decline through a reduction in TGFβ signaling and subsequent restoration of key genes involved in glutamatergic and GABAergic signaling (Chapter 3). The present study examines whether TGFβ signaling affects BBB integrity. Astrocytic end-feet enclose almost the entirety of the parenchymal basal membrane found in capillaries [12], and are important for BBB maintenance and communication [169,170]. Furthermore, some evidence exists that endothelial cells and pericytes in the BBB may also be able to activate latent TGFβ or respond to astrocyte-activated TGFβ [173]. Specifically, we examined whether

inhibition of the inflammatory TGFβ signaling pathway could reverse cumulative BBB damage due to aging. Via BBB gene expression analysis, we found evidence that in aged mice, inhibiting TGFβ rescues integral aspects of BBB integrity including the loss of endothelial cell tight junctions, decrease in pericyte markers, and dysregulation of vascular cell interaction factors.

Not much is known about the role of TGFβ regulation of vascular dynamics in the aging brain. However, some evidence for a potential regulatory role comes from studies in younger animals. For example, in a model of peripheral inflammation in rats, a link between TGFβ and tight junction protein expression was systematically examined in young animals [174]. Induction of peripheral inflammation in rats lead to BBB permeability and decreased expression of tight junction proteins claudin-5, ZO-1, and occludin – the expression of which was recovered after dosing with a pharmacologically inhibitor of TGFβ [174]. In vitro, it has also been shown that TGFβ inhibition salvages expression of occludin and claudin 5 in human glioma endothelial cells [175]. Our data shows that in the aging brain, inhibition of TGFβ is sufficient to increase tight junction genes. Most notably, 24 hours following a single dose of IPW, claudin-5 was significantly upregulated in the hippocampus of aged mice to the same levels as young mice. Expression of claudin-5 remained elevated after 2 weeks of daily treatment. Claudin-5 is the most abundant of the claudin family in the BBB, and plays an important role in the regulation of permeability; genetic knockout of claudin-5 has been shown to relax the size-selectivity of tight junctions in the BBB, while transfection into formerly depleted endothelial cells had the rebounding effect of increasing selectivity [176]. Previous research in young adult mice has also demonstrated that TGFβ increases BBB permeability by downregulating claudin-5 through smad-dependent signaling [156]. In the aging brain, our data suggests a similar role for TGFβ inhibition in restoring tight junction genes.

The link between TGFβ signaling and vascular cells has not previously been examined during aging. TGFβ is known to be expressed in both pericytes as well as endothelial cells [177]. In human cells, TGFβ1 treatment decreased pericyte number due to a reduction in proliferation and also induced expression of many inflammatory genes [178], suggesting a detrimental role for TGFβ1 on human neurovasculature. Another recent study shed more light on the relationship between TGFβ and pericytes in the young brain, finding that TGFβ induces pericyte differentiation from progenitors in culture, and that TGFβR2 mutants showed deficient pericyte development in peripheral vasculature [179]. These data suggest that TGFβ has the ability to affect pericyte maturation and may play a similar role in pericyte turn-over during aging. TGFβ has also been reported to modulate the pericyte contractile phenotype, discovered through ablation of TGFβ signaling by retroviral infection with a truncated C-terminal intracellular kinase domain for TGFβR2, reducing pericyte proliferation [180]. When pericytes have proliferated and migrated to areas of angiogenesis, the adhesion between the pericytes and the endothelium has also been reported to be regulated by TGFβ signaling [181,182]. Evidence for this comes from data showing that pericyte TGFβ signaling produces extracellular matrix molecules whereas endothelial TGFβ signaling regulates pericyte adhesion by upregulating cadherin signaling [181]. Additionally, mice deficient in endothelial smad4, a mediator of the TGFβ signaling, have disrupted BBB integrity through destabilized endothelial-pericyte interactions [183]. Our data shows age-related decline of genes important for pericyte and endothelial cell function, along with their interactions. However, after TGFβ dosing we find restored levels of these markers,

highlighting a potential role for TGFβ in age-associated decline in vascular cell function, pericyte proliferation, and endothelial-pericyte interactions.

Interestingly, we found that TGFβ inhibition rapidly affected glucose transporter 1 (glut-1), which was significantly upregulated after a single dose of IPW. Deficiency of glut-1 suggests a dysregulated supply of glucose to the brain, and has been repeatedly implicated in loss of BBB integrity [171]. In the pathological brain, the balance between neural activity and cerebral blood flow is disrupted—for example, the Alzheimer's phenotype is characterized by a chronic depletion in glucose stores and an inability to clear away amyloid beta [12]. It's possible that a rapid increase in glucose transport is indicative of BBB repair, where energy sources such as glucose or fatty acids need to be replenished, to fuel increased metabolic requirements for BBB mending by vascular cells.

Could inhibition of TGFβ signaling, as a strategy to counteract the detrimental consequences of age- related BBB dysfunction, hold therapeutic potential? One of the major challenges (and causes of failure) in treating progressive neurological diseases is that patients decline over time, and thus may accumulate irreversible damage by the time of diagnosis. Considering that BBB dysfunction begins relatively early in aging, if it were necessary to chronically treat patients with TGFβ inhibitors to prevent future damage, that would present a considerable clinical challenge. However, we found that with brief daily dosing of the TGFβR inhibitor IPW, age-related pathological changes in BBB gene expression were reversed in the mouse brain. These results highlight the potential of TGFβ inhibition in the aging brain as a therapeutic intervention in vascular dysfunction during aging.

4.4 Methods

RT-qPCR. Total RNA was extracted from 200 mg of frozen mouse hippocampal tissue using TRIzol reagent (ThermoFisher Scientific #15596026), and further purified with DNA-free DNA Removal Kit (ThermoFisher Scientific AM1906). First-strand cDNA synthesis was performed from 1 µg isolated RNA template using iScript RT supermix (Bio-Rad #1708841). PCR products were amplified using a CFX96 Real-Time PCR System (Bio-Rad), and threshold cycles were detected using SsoAdvanced Universal SYBR Green Supermix (Bio-Rad #172-5271). Mean threshold cycles were normalized to 18s internal control, and relative gene expression levels were quantified using the 2-ΔΔCT method. Primer sequences were obtained from the NCI/NIH qPrimerDepot.

Statistics and data. Data collection and preparation was performed by researchers who were blind to experimental conditions, and the lead and corresponding authors were responsible for experiment design, conducting statistical analysis, and unblinding the final results. All graphs are plotted showing mean and SE. Two sample comparisons were performed by student's t-test and multiple group comparisons were conducted by ANOVA, followed by post-hoc testing to compare individual groups when a main effect was detected. For all inferential statistics, two-tailed tests were used and significance thresholds were set at $p<0.05$.

4.5 Figures

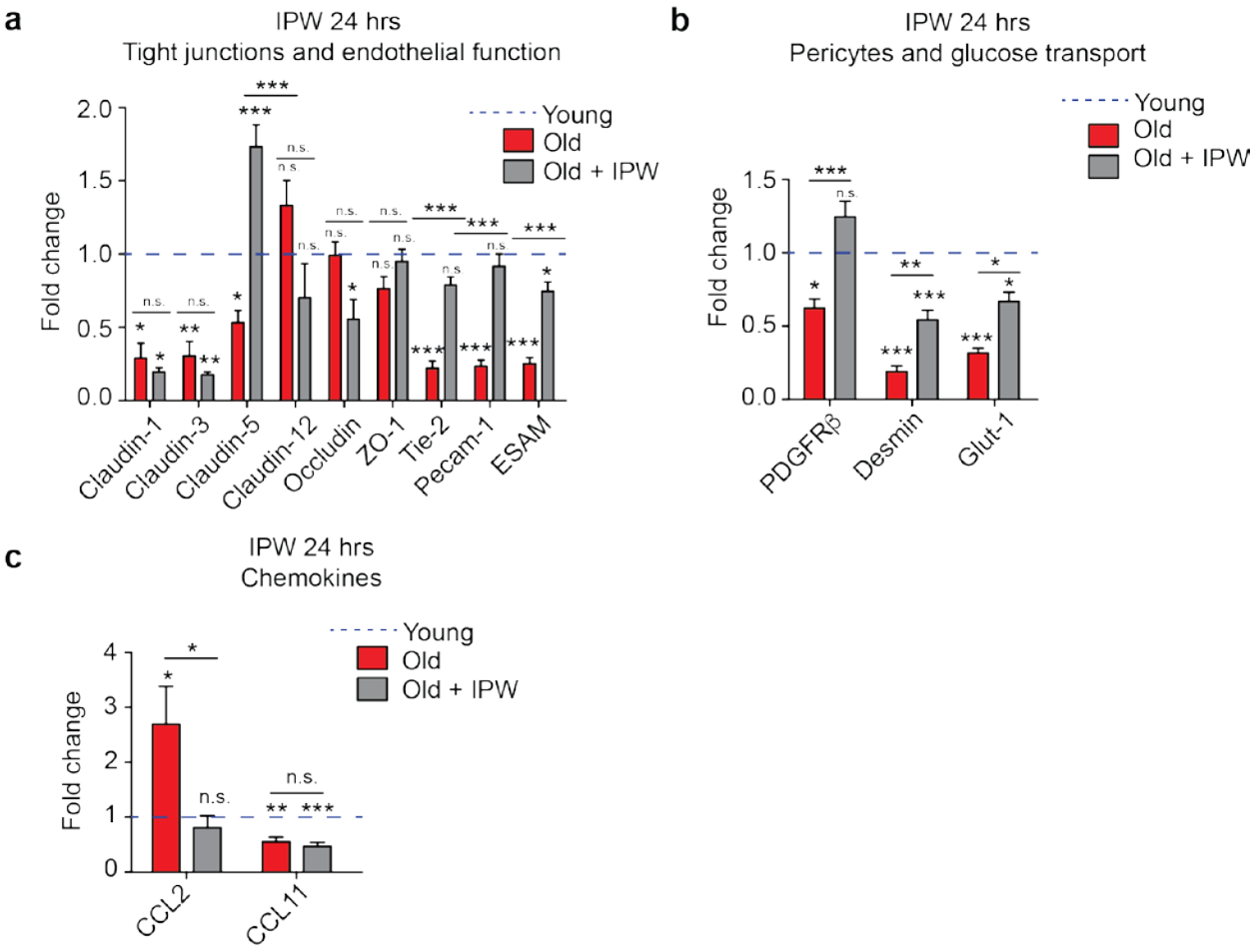

Figure 4.1. Single dose IPW treatment selectively improves age-related decline in BBB-associated genes. (a) Expression levels of selected tight junction-related genes, including claudins-1, -3, and -5, Tie-2, pecam-1, and ESAM is significantly downregulated in old mice, as compared to young mice. A single i.p. injection of IPW reverses the age-related downregulation in the tight junction genes claudin-5, Tie-2, pecam-1, and ESAM. (b) Expression levels of vascular cell markers and transport genes is significantly downregulated in old mice, as compared to young mice. IPW increases gene expression, as compared to aged mice with vehicle injection. (c) Old mice show increased expression of the chemokine CCL2, and reduced expression of the chemokine CCL11 in comparison to young mice. IPW reverses the upregulation of CCL2, but has no effect on CCL11. For all panels, dashed blue lines represent average expression levels in young mouse hippocampus. Gene expression of old and old+IPW is shown as fold change over young. Significance was determined by ANOVA with Tukey's test for multiple comparisons (n=10 young, n=8 old, n=8 old +IPW). For all tests, *p<0.05, **p<0.01, ***p<0.005.

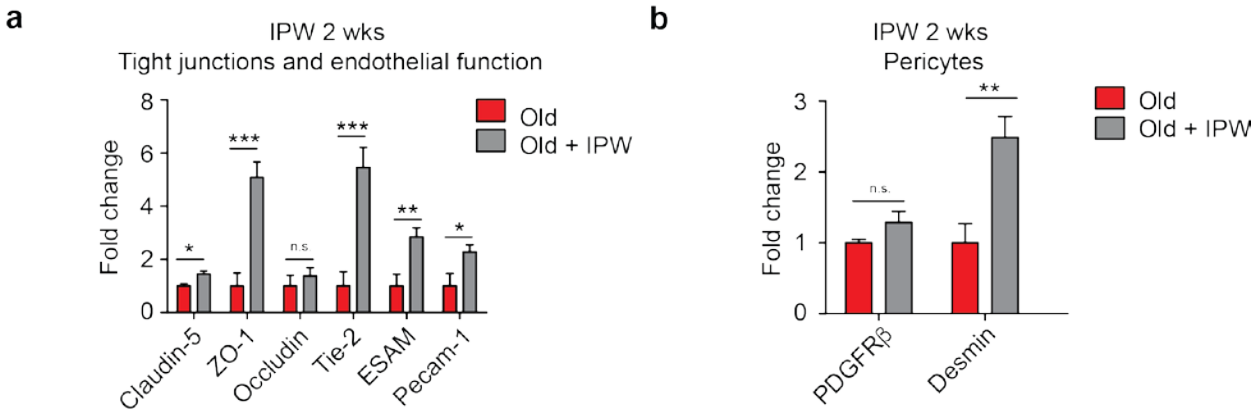

Figure 4.2. After 2 weeks of daily dosing, IPW treatment continues to selectively modify expression of tight junction and endothelial genes, along with pericyte markers in the aging mouse hippocampus. (a) Expression levels of selected tight junction genes is increased in aged mice two weeks of daily IPW i.p. injection, as compared to aged mice with vehicle injection. (b) Expression of pericyte marker desmin is increased in old mice with IPW treatment, as compared to old mice with vehicle control. Expression levels of pericyte marker PDGFRβ are unaffected by IPW treatment. Significance was determined by Student's T-test (n=6 old, n=9 old +IPW) *p<0.05, **p<0.01, ***p<0.005.

Chapter 5. Conclusion

In these studies, we report a provocative series of experiments that give new insight into how and why the brain deteriorates with age, addressing one of the most urgent, unanswered questions in neuroscience, and describing a therapeutic target that offers new hope for some most devastating neurological diseases of the aged brain, including dementias. During the advance into old age, the blood vessels of the brain start to lose their integrity. This disturbing phenomenon allows molecules from the blood to leak into the brain, compromising what is otherwise the most privileged and protected compartment of the body. Remarkably, the biological consequences of this vascular permeability have never been investigated. Here, we show for the first time that vascular decline in aging triggers an inflammatory, regulatory signaling cascade that severely disrupts normal neural function, causing downregulation of the major neurotransmission genes, aberrant neural activity, cognitive impairment, and decline of the structural elements of the blood-brain barrier. We show that this mechanism, which begins as early as middle age, accounts for some of the most notable and widely-seen changes associated with aging in the brain. Furthermore, we show that even brief intervention against this mechanism, with a targeted small molecule drug, reverses the deficits that we observed in aging mice, restoring youthful neural function, blood-brain barrier status, and cognitive capacity. These results provide an intuitive and straightforward new model to understand why the brain declines with age, and suggest that the aging brain may retain considerable capacity for plasticity, which may be chronically suppressed – but not irreversibly lost – by chronic leakiness of the blood vessels.

Highlights of the research are as follows: 1) In both humans and rodents, the integrity of the blood-brain barrier (BBB) declines with age. This vascular leakiness triggers an inflammatory response causing severe neural dysfunction. 2) Vascular permeability appears as early as middle age, making it one of earliest known triggers of brain aging, and increases in severity in old age. 3) The underlying mechanism is triggered when blood albumin crosses into the brain, where it activates transforming growth factor beta (TGFβ) signaling in astrocytes. This offers a simple explanation for gliosis in aging, one of the major hallmarks of dysfunction seen across research studies. 4) Experimental induction of this pathway in healthy young mice confers an aging brain phenotype, with gliosis, dysregulation of key neurotransmission genes, aberrant neural activity, decline of blood-brain barrier-related genes, seizure susceptibility and cognitive decline. 5) Inhibition of this pathway by two distinct mechanisms (a genetic knockout of TGFβ receptor in astrocytes, and a small molecule inhibitor of TGFβ receptors) in aged mice reverses these hallmarks of dysfunction, restoring a youthful phenotype including normal gliosis, expression of key neurotransmission genes, neural activity, blood-brain barrier regulatory genes, seizure susceptibility, and cognitive function.

Combined, the results presented in these studies suggest that age-related decline of the BBB induces astrocytic inflammatory signaling to cause neural dysfunction; yet, importantly, the aging brain retains the capacity for plasticity, as inhibition of this pathway reverses age-related phenotypes**.** This is demonstrated using MRI, electrocorticography (ECoG) recordings, RNA, protein, and behavioral analyses in rats, transgenic mouse lines, and humans.

There are still no effective treatments for most age-related neurological diseases, and the promising amyloid beta hypothesis has stalled with repeated failures in clinical trials. We

provide a desperately-needed new mechanism that defines a missing link between aging and disease in the brain, that is widespread and evolutionarily conserved, and that can effectively reverse dysfunction in the aged brain. Indeed, we all have a deep, personal stake in understanding, and developing interventions against, aging in the brain and the accompanying threats of cognitive decline and dementia. Therefore, it is my sincere hope that these studies are timely and impactful.

References

1. Morrison, J. H. & Baxter, M. G. The ageing cortical synapse: hallmarks and implications for cognitive decline. *Nat. Rev. Neurosci.* **13,** 240–50 (2012).
2. Bishop, N. A., Lu, T. & Yankner, B. A. Neural mechanisms of ageing and cognitive decline. *Nature* **464,** 529–535 (2010).
3. Zhao, Z., Nelson, A. R., Betsholtz, C. & Zlokovic, B. V. Establishment and Dysfunction of the Blood-Brain Barrier. *Cell* **163,** 1064–1078 (2015).
4. Abbott, N. J., Patabendige, A. A. K., Dolman, D. E. M., Yusof, S. R. & Begley, D. J. Structure and function of the blood-brain barrier. *Neurobiol. Dis.* **37,** 13–25 (2010).
5. Tibbling, G., Link, H. & Öhman, S. Principles of albumin and IgG analyses in neurological disorders. I. Establishment of reference values. *Scand. J. Clin. Lab. Investig.* **37,** 385–390 (1977).
6. Zlokovic, B. V. Neurovascular pathways to neurodegeneration in Alzheimer's disease and other disorders. *Nat. Rev. Neurosci.* (2011). doi:10.1038/nrn3114
7. Zeevi, N., Pachter, J., McCullough, L. D., Wolfson, L. & Kuchel, G. A. The blood-brain barrier: geriatric relevance of a critical brain-body interface. *J. Am. Geriatr. Soc.* **58,** 1749–57 (2010).
8. Rosenberg, G. A. Blood-Brain Barrier Permeability in Aging and Alzheimer's Disease. *J. Prev. Alzheimer's Dis.* **1,** 138–139 (2014).
9. Sweeney, M. D., Sagare, A. P. & Zlokovic, B. V. Blood–brain barrier breakdown in Alzheimer disease and other neurodegenerative disorders. *Nat. Rev. Neurol.* (2018). doi:10.1038/nrneurol.2017.188
10. Bien-Ly, N. *et al.* Lack of Widespread BBB Disruption in Alzheimer's Disease Models: Focus on Therapeutic Antibodies. *Neuron* **88,** 289–297 (2015).
11. Farrall, A. J. & Wardlaw, J. M. Blood–brain barrier: Ageing and microvascular disease – systematic review and meta-analysis. *Neurobiol. Aging* **30,** 337–352 (2009).
12. Zenaro, E., Piacentino, G. & Constantin, G. The blood-brain barrier in Alzheimer's disease. *Neurobiol. Dis.* **107,** 41–56 (2017).
13. Skillbäck, T. *et al.* CSF/serum albumin ratio in dementias: a cross-sectional study on 1861 patients. *Neurobiol. Aging* **59,** 1–9 (2017).
14. van de Haar, H. J. *et al.* Blood-Brain Barrier Leakage in Patients with Early Alzheimer Disease. *Radiology* **281,** 527–535 (2016).
15. Montagne, A. *et al.* Blood-Brain barrier breakdown in the aging human hippocampus. *Neuron* **85,** 296–302 (2015).
16. Montine, T. J. *et al.* Recommendations of the Alzheimer's disease-related dementias conference. *Neurology* **83,** 851–60 (2014).
17. Chin, J. & Scharfman, H. E. Shared cognitive and behavioral impairments in epilepsy and Alzheimer's disease and potential underlying mechanisms. *Epilepsy Behav.* **26,** 343–351 (2013).
18. Kam, K., Duffy, Á. M., Moretto, J., LaFrancois, J. J. & Scharfman, H. E. Interictal spikes during sleep are an early defect in the Tg2576 mouse model of β-amyloid neuropathology. *Sci. Rep.* **6,** 20119 (2016).
19. Palop, J. J. & Mucke, L. Epilepsy and Cognitive Impairments in Alzheimer Disease. *Arch.*

Neurol. **66,** 435 (2009).
20. Palop, J. J. *et al.* Aberrant excitatory neuronal activity and compensatory remodeling of inhibitory hippocampal circuits in mouse models of Alzheimer's disease. *Neuron* **55,** 697–711 (2007).
21. Haberman, R. P., Branch, A. & Gallagher, M. Targeting Neural Hyperactivity as a Treatment to Stem Progression of Late-Onset Alzheimer's Disease. *Neurotherapeutics* **14,** 662–676 (2017).
22. Fontana, R. *et al.* Early hippocampal hyperexcitability in PS2APP mice: role of mutant PS2 and APP. *Neurobiol. Aging* **50,** 64–76 (2017).
23. Yassa, M. A. *et al.* High-resolution structural and functional MRI of hippocampal CA3 and dentate gyrus in patients with amnestic Mild Cognitive Impairment. *Neuroimage* **51,** 1242–1252 (2010).
24. Cacheaux, L. P. *et al.* Transcriptome profiling reveals TGF-beta signaling involvement in epileptogenesis. *J. Neurosci.* **29,** 8927–35 (2009).
25. Braganza, O. *et al.* Albumin is taken up by hippocampal NG2 cells and astrocytes and decreases gap junction coupling. *Epilepsia* **53,** 1898–1906 (2012).
26. Kim, S. Y. *et al.* TGFβ signaling is associated with changes in inflammatory gene expression and perineuronal net degradation around inhibitory neurons following various neurological insults. *Sci. Rep.* **7,** 7711 (2017).
27. David, Y. *et al.* Astrocytic dysfunction in epileptogenesis: consequence of altered potassium and glutamate homeostasis? *J. Neurosci.* **29,** 10588–99 (2009).
28. Tomkins, O. *et al.* Blood-brain barrier breakdown following traumatic brain injury: a possible role in posttraumatic epilepsy. *Cardiovasc. Psychiatry Neurol.* **2011,** 765923 (2011).
29. Hay, J. R., Johnson, V. E., Young, A. M. H., Smith, D. H. & Stewart, W. Blood-Brain Barrier Disruption Is an Early Event That May Persist for Many Years After Traumatic Brain Injury in Humans. *J. Neuropathol. Exp. Neurol.* **74,** 1147–57 (2015).
30. Tagge, C. A. *et al.* Concussion, microvascular injury, and early tauopathy in young athletes after impact head injury and an impact concussion mouse model. *Brain* **141,** 422–458 (2018).
31. Shlosberg, D., Benifla, M., Kaufer, D. & Friedman, A. Blood-brain barrier breakdown as a therapeutic target in traumatic brain injury. *Nature Reviews Neurology* **6,** 393–403 (2010).
32. Cacheaux, L. P. *et al.* Transcriptome Profiling Reveals TGF- Signaling Involvement in Epileptogenesis. *J. Neurosci.* **29,** 8927–8935 (2009).
33. Weissberg, I. *et al.* Albumin induces excitatory synaptogenesis through astrocytic TGF-β/ALK5 signaling in a model of acquired epilepsy following blood–brain barrier dysfunction. *Neurobiol. Dis.* **78,** 115–125 (2015).
34. Bar-Klein, G. *et al.* Losartan prevents acquired epilepsy via TGF-β signaling suppression. *Ann. Neurol.* **75,** 864–875 (2014).
35. Levy, N. *et al.* Differential TGF-β Signaling in Glial Subsets Underlies IL-6–Mediated Epileptogenesis in Mice. *J. Immunol.* **195,** 1713–1722 (2015).
36. Bar-Klein, G. *et al.* Losartan prevents acquired epilepsy via TGF-β signaling suppression. *Ann. Neurol.* **75,** 864–75 (2014).

37. Weissberg, I. *et al.* Albumin induces excitatory synaptogenesis through astrocytic TGF-β/ALK5 signaling in a model of acquired epilepsy following blood-brain barrier dysfunction. *Neurobiol. Dis.* **78,** 115–125 (2015).
38. Salar, S. *et al.* Synaptic plasticity in area CA1 of rat hippocampal slices following intraventricular application of albumin. *Neurobiol. Dis.* **91,** 155–65 (2016).
39. Tomkins, O. *et al.* Blood-brain barrier disruption results in delayed functional and structural alterations in the rat neocortex. *Neurobiol. Dis.* **25,** 367–77 (2007).
40. Doyle, K. P., Cekanaviciute, E., Mamer, L. E. & Buckwalter, M. S. TGFβ signaling in the brain increases with aging and signals to astrocytes and innate immune cells in the weeks after stroke. *J. Neuroinflammation* **7,** 62 (2010).
41. El-Hayek, Y. H. *et al.* Hippocampal excitability is increased in aged mice. *Exp. Neurol.* **247,** 710–719 (2013).
42. Pineda, J. R. *et al.* Vascular-derived TGF-β increases in the stem cell niche and perturbs neurogenesis during aging and following irradiation in the adult mouse brain. *EMBO Mol. Med.* **5,** 548–562 (2013).
43. Tichauer, J. E. *et al.* Age-dependent changes on TGFβ1 Smad3 pathway modify the pattern of microglial cell activation. *Brain. Behav. Immun.* **37,** 187–196 (2014).
44. Yousef, H. *et al.* Systemic attenuation of the TGF-β pathway by a single drug simultaneously rejuvenates hippocampal neurogenesis and myogenesis in the same old mammal. *Oncotarget* **6,** 11959–11978 (2015).
45. Tarkowski, E. *et al.* Increased intrathecal levels of the angiogenic factors VEGF and TGF-β in Alzheimer's disease and vascular dementia. *Neurobiol. Aging* **23,** 237–243 (2002).
46. Rota, E. *et al.* Increased intrathecal TGF-β1, but not IL-12, IFN-γ and IL-10 levels in Alzheimer's disease patients. *Neurol. Sci.* **27,** 33–39 (2006).
47. Grammas, P. & Ovase, R. Cerebrovascular transforming growth factor-beta contributes to inflammation in the Alzheimer's disease brain. *Am. J. Pathol.* **160,** 1583–7 (2002).
48. Wyss-Coray, T. *et al.* Amyloidogenic role of cytokine TGF-beta1 in transgenic mice and in Alzheimer's disease. *Nature* **389,** 603–606 (1997).
49. Wyss-Coray, T., Lin, C., Sanan, D. A., Mucke, L. & Masliah, E. Chronic Overproduction of Transforming Growth Factor-β1 by Astrocytes Promotes Alzheimer's Disease-Like Microvascular Degeneration in Transgenic Mice. *Am. J. Pathol.* **156,** 139–150 (2000).
50. Wyss-Coray, T. *et al.* TGF-beta1 promotes microglial amyloid-beta clearance and reduces plaque burden in transgenic mice. *Nat. Med.* **7,** 612–618 (2001).
51. Endo, F. *et al.* Astrocyte-derived TGF-β1 accelerates disease progression in ALS mice by interfering with the neuroprotective functions of microglia and T cells. *Cell Rep.* **11,** 592–604 (2015).
52. Peters, S. *et al.* The TGF-β System As a Potential Pathogenic Player in Disease Modulation of Amyotrophic Lateral Sclerosis. *Front. Neurol.* **8,** 669 (2017).
53. Yan, J. *et al.* Obesity-and aging-induced excess of central transforming growth factor-β 2 potentiates diabetic development via an RNA stress response. *Nat. Med.* **20,** 1001–1008 (2014).
54. Tesseur, I. *et al.* Deficiency in Neuronal TGF-β Signaling Leads to Nigrostriatal Degeneration and Activation of TGF-β Signaling Protects against MPTP Neurotoxicity in Mice. *J. Neurosci.* **37,** 4584–4592 (2017).

55. Brionne, T. C., Tesseur, I., Masliah, E. & Wyss-Coray, T. Loss of TGF-beta 1 leads to increased neuronal cell death and microgliosis in mouse brain. *Neuron* **40,** 1133–1145 (2003).
56. Tesseur, I. *et al.* Deficiency in neuronal TGF- β signaling promotes neurodegeneration and Alzheimer ' s pathology. *J. Clin. Invest.* **116,** 3060–3069 (2006).
57. Erraji-Benchekroun, L. *et al.* Molecular aging in human prefrontal cortex is selective and continuous throughout adult life. *Biol. Psychiatry* **57,** 549–558 (2005).
58. Lu, T. *et al.* Gene regulation and DNA damage in the ageing human brain. *Nature* **429,** 883–891 (2004).
59. Haberman, R. P. *et al.* Prominent hippocampal CA3 gene expression profile in neurocognitive aging. *Neurobiol. Aging* **32,** 1678–1692 (2011).
60. Janota, C. S., Brites, D., Lemere, C. A. & Brito, M. A. Glio-vascular changes during ageing in wild-type and Alzheimer's disease-like APP/PS1 mice. *Brain Res.* **1620,** 153–168 (2015).
61. Chew, L.-J., DeBoy, C. A. & Senatorov, V. V. Finding degrees of separation: Experimental approaches for astroglial and oligodendroglial cell isolation and genetic targeting. *J. Neurosci. Methods* **236,** 125–147 (2014).
62. Cahoy, J. D. *et al.* A Transcriptome Database for Astrocytes, Neurons, and Oligodendrocytes: A New Resource for Understanding Brain Development and Function. *J. Neurosci.* **28,** 264–278 (2008).
63. Chew, L.-J., DeBoy, C. A. & Senatorov, V. V. Finding degrees of separation: Experimental approaches for astroglial and oligodendroglial cell isolation and genetic targeting. *J. Neurosci. Methods* **236,** 125–147 (2014).
64. Bar-Klein, G. *et al.* Imaging blood–brain barrier dysfunction as a biomarker for epileptogenesis. *Brain* (2017). doi:10.1093/brain/awx073
65. Brenner, R. P. *et al.* Computerized EEG spectral analysis in elderly normal, demented and depressed subjects. *Electroencephalogr. Clin. Neurophysiol.* **64,** 483–92 (1986).
66. Jackson, C. E. & Snyder, P. J. Electroencephalography and event-related potentials as biomarkers of mild cognitive impairment and mild Alzheimer's disease. *Alzheimer's Dement.* **4,** S137–S143 (2008).
67. Jeong, J. EEG dynamics in patients with Alzheimer's disease. *Clin. Neurophysiol.* **115,** 1490–1505 (2004).
68. Hauser, W. A., Annegers, J. F. & Kurland, L. T. Incidence of epilepsy and unprovoked seizures in Rochester, Minnesota: 1935-1984. *Epilepsia* **34,** 453–68
69. Jetter, G. M. & Cavazos, J. E. Epilepsy in the elderly. *Semin. Neurol.* **28,** 336–41 (2008).
70. Leppik, I. E. & Birnbaum, A. K. Epilepsy in the elderly. *Ann. N. Y. Acad. Sci.* **1184,** 208–224 (2010).
71. Ittner, L. M. *et al.* Dendritic Function of Tau Mediates Amyloid-β Toxicity in Alzheimer's Disease Mouse Models. *Cell* **142,** 387–397 (2010).
72. Ittner, A. *et al.* Site-specific phosphorylation of tau inhibits amyloid-β toxicity in Alzheimer's mice. *Science (80-.).* **354,** (2016).
73. Deacon, R. M. J. & Rawlins, J. N. P. T-maze alternation in the rodent. *Nat. Protoc.* **1,** 7–12 (2006).
74. Lalonde, R. The neurobiological basis of spontaneous alternation. *Neurosci. Biobehav. Rev.* **26,** 91–104 (2002).

75. Bannerman, D. M. *et al.* Regional dissociations within the hippocampus--memory and anxiety. *Neurosci. Biobehav. Rev.* **28,** 273–83 (2004).
76. Reisel, D. *et al.* Spatial memory dissociations in mice lacking GluR1. *Nat. Neurosci.* **5,** 868–73 (2002).
77. Braganza, O. *et al.* Albumin is taken up by hippocampal NG2 cells and astrocytes and decreases gap junction coupling. *Epilepsia* **53,** 1898–906 (2012).
78. Rabender, C. *et al.* IPW-5371 Proves Effective as a Radiation Countermeasure by Mitigating Radiation-Induced Late Effects. *Radiat. Res.* RR14403.1 (2016). doi:10.1667/RR14403.1
79. Burke, S. N., Wallace, J. L., Nematollahi, S., Uprety, A. R. & Barnes, C. A. Pattern separation deficits may contribute to age-associated recognition impairments. *Behav. Neurosci.* **124,** 559–573 (2010).
80. Murai, T., Okuda, S., Tanaka, T. & Ohta, H. Characteristics of object location memory in mice: Behavioral and pharmacological studies. *Physiol. Behav.* **90,** 116–24 (2007).
81. Ramasamy, A. *et al.* Genetic variability in the regulation of gene expression in ten regions of the human brain. *Nat. Neurosci.* **17,** 1418–1428 (2014).
82. Milikovsky, D. Z. *et al.* Electrocorticographic dynamics as a novel biomarker in five models of epileptogenesis. *J. Neurosci.* 2446–16 (2017). doi:10.1523/JNEUROSCI.2446-16.2017
83. Lam, A. D. *et al.* Silent hippocampal seizures and spikes identified by foramen ovale electrodes in Alzheimer's disease. *Nat. Med.* **23,** 678–680 (2017).
84. Vossel, K. A. *et al.* Incidence and impact of subclinical epileptiform activity in Alzheimer's disease. *Ann. Neurol.* (2016). doi:10.1002/ana.24794
85. Vossel, K. A. *et al.* Seizures and epileptiform activity in the early stages of Alzheimer disease. *JAMA Neurol.* **70,** 1158–66 (2013).
86. Cloyd, J. *et al.* Epidemiological and medical aspects of epilepsy in the elderly. *Epilepsy Res.* **68,** 39–48 (2006).
87. Schachter, S. C. *et al.* An evaluation of antiepileptic drug therapy in nursing facilities. *J. Am. Geriatr. Soc.* **46,** 1137–41 (1998).
88. Mattson, M. P. & Magnus, T. Ageing and neuronal vulnerability. *Nat. Rev. Neurosci.* **7,** 278–294 (2006).
89. Shi, Q. *et al.* Complement C3-Deficient Mice Fail to Display Age-Related Hippocampal Decline. *J. Neurosci.* **35,** 13029–13042 (2015).
90. Yeoman, M., Scutt, G. & Faragher, R. Insights into CNS ageing from animal models of senescence. *Nat. Rev. Neurosci.* **13,** 435–445 (2012).
91. Chow, H. & Herrup, K. Genomic integrity and the ageing brain. *Nat. Rev. Neurosci.* **16,** 672–684 (2015).
92. Herrup, K. The case for rejecting the amyloid cascade hypothesis. *Nat. Neurosci.* **18,** 794–799 (2015).
93. Cameron, B. & Landreth, G. E. Inflammation, microglia, and alzheimer's disease. *Neurobiol. Dis.* **37,** 503–509 (2010).
94. Chung, W.-S., Welsh, C. A., Barres, B. A. & Stevens, B. Do glia drive synaptic and cognitive impairment in disease? *Nat. Neurosci.* **18,** 1539–1545 (2015).
95. Liddelow, S. A. *et al.* Neurotoxic reactive astrocytes are induced by activated microglia.

Nature (2017). doi:10.1038/nature21029
96. Soreq, L. *et al.* Major Shifts in Glial Regional Identity Are a Transcriptional Hallmark of Human Brain Aging. *Cell Rep.* **18,** 557–570 (2017).
97. Clarke, L. E. *et al.* Normal aging induces A1-like astrocyte reactivity. *Proc. Natl. Acad. Sci. U. S. A.* **115,** E1896–E1905 (2018).
98. Chinta, S. J. *et al.* Cellular Senescence Is Induced by the Environmental Neurotoxin Paraquat and Contributes to Neuropathology Linked to Parkinson's Disease. *Cell Rep.* **22,** 930–940 (2018).
99. Chassidim, Y. *et al.* Quantitative imaging assessment of blood-brain barrier permeability in humans. *Fluids Barriers CNS* **10,** 9 (2013).
100. Veksler, R., Shelef, I. & Friedman, A. Blood–Brain Barrier Imaging in Human Neuropathologies. *Arch. Med. Res.* **45,** 646–652 (2014).
101. Weissberg, I. *et al.* Imaging Blood-Brain Barrier Dysfunction in Football Players. *JAMA Neurol.* **71,** 1453 (2014).
102. Weissberg, I., Reichert, A., Heinemann, U. & Friedman, A. Blood-Brain Barrier Dysfunction in Epileptogenesis of the Temporal Lobe. *Epilepsy Res. Treat.* **2011,** 1–10 (2011).
103. Seiffert, E. *et al.* Lasting blood-brain barrier disruption induces epileptic focus in the rat somatosensory cortex. *J. Neurosci.* **24,** 7829–36 (2004).
104. Milikovsky, D. Z. *et al.* Electrocorticographic Dynamics as a Novel Biomarker in Five Models of Epileptogenesis. *J. Neurosci.* **37,** 4450–4461 (2017).
105. Sharma, S., Rakoczy, S. & Brown-Borg, H. Assessment of spatial memory in mice. *Life Sci.* **87,** 521–536 (2010).
106. Salar, S. *et al.* Synaptic plasticity in area CA1 of rat hippocampal slices following intraventricular application of albumin. *Neurobiol. Dis.* **91,** 155–165 (2016).
107. Caraci, F. *et al.* Dysfunction of TGF-β1 signaling in Alzheimer's disease: Perspectives for neuroprotection. *Cell and Tissue Research* **347,** 291–301 (2012).
108. Yan, J. *et al.* Obesity- and aging-induced excess of central transforming growth factor-β potentiates diabetic development via an RNA stress response. *Nat. Med.* **20,** 1001–8 (2014).
109. Chang, K.-H., Wu, Y.-R., Chen, Y.-C. & Chen, C.-M. Plasma inflammatory biomarkers for Huntington's disease patients and mouse model. *Brain. Behav. Immun.* **44,** 121–127 (2015).
110. Diniz, L. P. *et al.* Astrocyte-induced synaptogenesis is mediated by transforming growth factor β signaling through modulation of d-serine levels in cerebral cortex neurons. *J. Biol. Chem.* **287,** 41432–41445 (2012).
111. Diniz, L. P. *et al.* Astrocyte transforming growth factor beta 1 promotes inhibitory synapse formation via CaM kinase II signaling. *Glia* **62,** 1917–1931 (2014).
112. Wang, N. *et al.* Active Calcium/Calmodulin-Dependent Protein Kinase II (CaMKII) Regulates NMDA Receptor Mediated Postischemic Long-Term Potentiation (i-LTP) by Promoting the Interaction between CaMKII and NMDA Receptors in Ischemia. *Neural Plast.* **2014,** 1–10 (2014).
113. Lau, C. G. & Zukin, R. S. NMDA receptor trafficking in synaptic plasticity and neuropsychiatric disorders. *Nature Reviews Neuroscience* **8,** 413–426 (2007).

114. Yashiro, K. & Philpot, B. D. Regulation of NMDA receptor subunit expression and its implications for LTD, LTP, and metaplasticity. *Neuropharmacology* **55,** 1081–1094 (2008).
115. Paoletti, P., Bellone, C. & Zhou, Q. NMDA receptor subunit diversity: Impact on receptor properties, synaptic plasticity and disease. *Nature Reviews Neuroscience* **14,** 383–400 (2013).
116. Magnusson, K. R., Brim, B. L. & Das, S. R. Selective vulnerabilities of N-methyl-D-aspartate (NMDA) receptors during brain aging. *Frontiers in Aging Neuroscience* **2,** (2010).
117. Wang, D., Jacobs, S. A. & Tsien, J. Z. Targeting the NMDA receptor subunit NR2B for treating or preventing age-related memory decline. *Expert Opin. Ther. Targets* **18,** 1121–1130 (2014).
118. Tang, Y. P. *et al.* Genetic enhancement of learning and memory in mice. *Nature* **401,** 63–69 (1999).
119. Brim, B. L. *et al.* Memory in aged mice is rescued by enhanced expression of the GluN2B subunit of the NMDA receptor. *Behav. Brain Res.* **238,** 211–226 (2013).
120. Coman, H. & Nemeş, B. New Therapeutic Targets in Alzheimer's Disease. *International Journal of Gerontology* **11,** 2–6 (2017).
121. Kurz, A. & Grimmer, T. Efficacy of memantine hydrochloride once-daily in Alzheimer's disease. *Expert Opin. Pharmacother.* **15,** 1955–1960 (2014).
122. Sgambato-Faure, V. & Cenci, M. A. Glutamatergic mechanisms in the dyskinesias induced by pharmacological dopamine replacement and deep brain stimulation for the treatment of Parkinson's disease. *Progress in Neurobiology* **96,** 69–86 (2012).
123. Giaume, C., Koulakoff, A., Roux, L., Holcman, D. & Rouach, N. Astroglial networks: a step further in neuroglial and gliovascular interactions. *Nat. Rev. Neurosci.* **11,** 87–99 (2010).
124. Haim, L. Ben & Rowitch, D. H. Functional diversity of astrocytes in neural circuit regulation. *Nat. Rev. Neurosci.* **18,** 31–41 (2017).
125. Leuba, G. *et al.* Pathological Reorganization of NMDA Receptors Subunits and Postsynaptic Protein PSD-95 Distribution in Alzheimer's Disease. *Curr. Alzheimer Res.* **11,** 86–96 (2014).
126. Bading, H. Therapeutic targeting of the pathological triad of extrasynaptic NMDA receptor signaling in neurodegenerations. *J. Exp. Med.* jem.20161673 (2017). doi:10.1084/jem.20161673
127. Zhu, X. *et al.* NMDA receptor NR2B subunits contribute to PTZ-kindling-induced hippocampal astrocytosis and oxidative stress. *Brain Res. Bull.* **114,** 70–78 (2015).
128. Carvajal, F. J., Mira, R. G., Rovegno, M., Minniti, A. N. & Cerpa, W. Age-related NMDA signaling alterations in SOD2 deficient mice. *Biochim. Biophys. Acta* **1864,** 2010–2020 (2018).
129. Zhao, X. *et al.* The effects of aging on N-methyl-d-aspartate receptor subunits in the synaptic membrane and relationships to long-term spatial memory. *Neuroscience* **162,** 933–945 (2009).
130. Yang, Y. *et al.* Compound Astragalus and Salvia miltiorrhiza Extract exerts anti-fibrosis by mediating TGF-β/Smad signaling in myofibroblasts. *J. Ethnopharmacol.* **118,** 264–270 (2008).
131. Topic, B. *et al.* Impaired maze performance in aged rats is accompanied by increased density of NMDA, and 5-HT1A, and α-adrenoceptor binding in hippocampus.

Hippocampus **17,** 68–77 (2007).
132. Koh, M. T., Rosenzweig-Lipson, S. & Gallagher, M. Selective GABAA5 positive allosteric modulators improve cognitive function in aged rats with memory impairment. *Neuropharmacology* **64,** 145–152 (2013).
133. Hausrat, T. J. *et al.* Radixin regulates synaptic GABAA receptor density and is essential for reversal learning and short-term memory. *Nat. Commun.* **6,** 6872 (2015).
134. McQuail, J. A., Frazier, C. J. & Bizon, J. L. Molecular aspects of age-related cognitive decline: The role of GABA signaling. *Trends in Molecular Medicine* **21,** 450–460 (2015).
135. Huang, D. *et al.* Glutamate-glutamine and GABA in brain of normal aged and patients with cognitive impairment. *European Radiology* 1–7 (2016). doi:10.1007/s00330-016-4669-8
136. Popescu, B. O. *et al.* Blood-brain barrier alterations in ageing and dementia. *J. Neurol. Sci.* **283,** 99–106 (2009).
137. Blanchette, M. & Daneman, R. Formation and maintenance of the BBB. *Mech. Dev.* **138,** 8–16 (2015).
138. Oldendorf, W. Brain uptake of radiolabeled amino acids, amines, and hexoses after arterial injection. *Am. J. Physiol. Content* **221,** 1629–1639 (1971).
139. Erickson, M. A. & Banks, W. A. Blood-brain barrier dysfunction as a cause and consequence of Alzheimer's disease. *J. Cereb. Blood Flow Metab.* **33,** 1500–13 (2013).
140. Bell, R. D. *et al.* Pericytes Control Key Neurovascular Functions and Neuronal Phenotype in the Adult Brain and during Brain Aging. *Neuron* **68,** 409–427 (2010).
141. Hill, J., Rom, S., Ramirez, S. H. & Persidsky, Y. Emerging Roles of Pericytes in the Regulation of the Neurovascular Unit in Health and Disease. *J. Neuroimmune Pharmacol.* **9,** 591–605 (2014).
142. Gruol, D. L., Vo, K. & Bray, J. G. Increased astrocyte expression of IL-6 or CCL2 in transgenic mice alters levels of hippocampal and cerebellar proteins. *Front. Cell. Neurosci.* **8,** 234 (2014).
143. Song, Y. *et al.* Aging enhances the basal production of IL-6 and CCL2 in vascular smooth muscle cells. *Arterioscler. Thromb. Vasc. Biol.* **32,** 103–9 (2012).
144. Kiyota, T. *et al.* CCL2 Accelerates Microglia-Mediated Aβ Oligomer Formation and Progression of Neurocognitive Dysfunction. *PLoS One* **4,** e6197 (2009).
145. Villeda, S. A. *et al.* The ageing systemic milieu negatively regulates neurogenesis and cognitive function. *Nature* **477,** 90–94 (2011).
146. Tsukita, S., Furuse, M., Tsukita, S. & Furuse, M. Occludin and claudins in tight-junction strands: leading or supporting players? *Trends Cell Biol.* **9,** 268–73 (1999).
147. Morita, K., Sasaki, H., Furuse, M. & Tsukita, S. Endothelial claudin: claudin-5/TMVCF constitutes tight junction strands in endothelial cells. *J. Cell Biol.* **147,** 185–94 (1999).
148. Romanitan, M. O. *et al.* Altered expression of claudin family proteins in Alzheimer's disease and vascular dementia brains. *J. Cell. Mol. Med.* **14,** 1088–100 (2010).
149. Matter, K. & Balda, M. S. Holey barrier. *J. Cell Biol.* **161,** 459–460 (2003).
150. Yang, Y., Estrada, E. Y., Thompson, J. F., Liu, W. & Rosenberg, G. A. Matrix Metalloproteinase-Mediated Disruption of Tight Junction Proteins in Cerebral Vessels is Reversed by Synthetic Matrix Metalloproteinase Inhibitor in Focal Ischemia in Rat. *J. Cereb. Blood Flow Metab.* **27,** 697–709 (2007).

151. Zlokovic, B. V. The blood-brain barrier in health and chronic neurodegenerative disorders. *Neuron* **57,** 178–201 (2008).
152. Nitta, T. *et al.* Size-selective loosening of the blood-brain barrier in claudin-5–deficient mice. *J. Cell Biol.* **161,** 653–660 (2003).
153. Wang, B. *et al.* Blood-brain Barrier Disruption Leads to Postoperative Cognitive Dysfunction. *Curr. Neurovasc. Res.* **14,** 359–367 (2018).
154. Greene, C. *et al.* Dose-dependent expression of claudin-5 is a modifying factor in schizophrenia. *Mol. Psychiatry* (2017). doi:10.1038/mp.2017.156
155. Kaur, J., Tuor, U. I., Zhao, Z. & Barber, P. A. Quantitative MRI Reveals the Elderly Ischemic Brain is Susceptible to Increased Early Blood—Brain Barrier Permeability Following Tissue Plasminogen Activator Related to Claudin 5 and Occludin Disassembly. *J. Cereb. Blood Flow Metab.* **31,** 1874–1885 (2011).
156. McMillin, M. a *et al.* TGFβ1 exacerbates blood–brain barrier permeability in a mouse model of hepatic encephalopathy via upregulation of MMP9 and downregulation of claudin-5. *Lab. Investig.* **0,** 1–11 (2015).
157. Yang, Y. & Rosenberg, G. A. MMP-Mediated Disruption of Claudin-5 in the Blood–Brain Barrier of Rat Brain After Cerebral Ischemia. in 333–345 (Humana Press, Totowa, NJ, 2011). doi:10.1007/978-1-61779-185-7_24
158. Fanning, A. S., Jameson, B. J., Jesaitis, L. A. & Anderson, J. M. The tight junction protein ZO-1 establishes a link between the transmembrane protein occludin and the actin cytoskeleton. *J. Biol. Chem.* **273,** 29745–53 (1998).
159. Mooradian, A. D., Haas, M. J. & Chehade, J. M. Age-related changes in rat cerebral occludin and zonula occludens-1 (ZO-1). *Mech. Ageing Dev.* **124,** 143–6 (2003).
160. Elahy, M. *et al.* Blood-brain barrier dysfunction developed during normal aging is associated with inflammation and loss of tight junctions but not with leukocyte recruitment. *Immun. Ageing* **12,** 2 (2015).
161. Kelly-Goss, M. R. *et al.* Dynamic, heterogeneous endothelial Tie2 expression and capillary blood flow during microvascular remodeling. *Sci. Rep.* **7,** 9049 (2017).
162. Chen, J., Cui, X., Zacharek, A. & Chopp, M. Increasing Ang1/Tie2 expression by simvastatin treatment induces vascular stabilization and neuroblast migration after stroke. *J. Cell. Mol. Med.* **13,** 1348–1357 (2009).
163. Vestweber, D. How leukocytes cross the vascular endothelium. *Nat. Rev. Immunol.* **15,** 692–704 (2015).
164. Huntley, M. A., Bien-Ly, N., Daneman, R. & Watts, R. J. Dissecting gene expression at the blood-brain barrier. *Front. Neurosci.* **8,** 355 (2014).
165. Ishida, T. *et al.* Targeted disruption of endothelial cell-selective adhesion molecule inhibits angiogenic processes in vitro and in vivo. *J. Biol. Chem.* **278,** 34598–604 (2003).
166. Nakagawa, S. *et al.* Pericytes from Brain Microvessels Strengthen the Barrier Integrity in Primary Cultures of Rat Brain Endothelial Cells. *Cell. Mol. Neurobiol.* **27,** 687–694 (2007).
167. Bell, R. D. *et al.* Pericytes Control Key Neurovascular Functions and Neuronal Phenotype in the Adult Brain and during Brain Aging. *Neuron* **68,** 409–427 (2010).
168. Armulik, A. *et al.* Pericytes regulate the blood-brain barrier. *Nature* **468,** 557–61 (2010).
169. Iadecola, C. The Neurovascular Unit Coming of Age: A Journey through Neurovascular Coupling in Health and Disease. *Neuron* **96,** 17–42 (2017).

170. McConnell, H. L., Kersch, C. N., Woltjer, R. L. & Neuwelt, E. A. The Translational Significance of the Neurovascular Unit. *J. Biol. Chem.* **292,** 762–770 (2017).
171. Zhao, Z., Nelson, A. R., Betsholtz, C. & Zlokovic, B. V. Establishment and Dysfunction of the Blood-Brain Barrier. *Cell* **163,** 1064–1078 (2015).
172. Pitkänen, A. *et al.* Advances in the development of biomarkers for epilepsy. *Lancet Neurol.* **15,** 843–856 (2016).
173. Beck, K. & Schachtrup, C. Vascular damage in the central nervous system: A multifaceted role for vascular-derived TGF-β. *Cell and Tissue Research* **347,** 187–201 (2012).
174. Ronaldson, P. T., Demarco, K. M., Sanchez-Covarrubias, L., Solinsky, C. M. & Davis, T. P. Transforming growth factor-beta signaling alters substrate permeability and tight junction protein expression at the blood-brain barrier during inflammatory pain. *J. Cereb. Blood Flow Metab.* **29,** 1084–98 (2009).
175. Ishihara, H. *et al.* Endothelial Cell Barrier Impairment Induced by Glioblastomas and Transforming Growth Factor β_2 Involves Matrix Metalloproteinases and Tight Junction Proteins. *J. Neuropathol. Exp. Neurol.* **67,** 435–448 (2008).
176. Gonçalves, A., Ambrósio, A. F. & Fernandes, R. Regulation of claudins in blood-tissue barriers under physiological and pathological states. *Tissue Barriers* **1,** e24782 (2013).
177. Armulik, A., Genové, G. & Betsholtz, C. Pericytes: Developmental, Physiological, and Pathological Perspectives, Problems, and Promises. *Dev. Cell* **21,** 193–215 (2011).
178. Rustenhoven, J. *et al.* TGF-beta1 regulates human brain pericyte inflammatory processes involved in neurovasculature function. *J. Neuroinflammation* **13,** 37 (2016).
179. Yamazaki, T. *et al.* Tissue Myeloid Progenitors Differentiate into Pericytes through TGF-β Signaling in Developing Skin Vasculature. *Cell Rep.* **18,** 2991–3004 (2017).
180. Sieczkiewicz, G. J. & Herman, I. M. TGF-beta 1 signaling controls retinal pericyte contractile protein expression. *Microvasc. Res.* **66,** 190–6 (2003).
181. Winkler, E. A., Bell, R. D. & Zlokovic, B. V. Central nervous system pericytes in health and disease. *Nat. Neurosci.* **14,** 1398–1405 (2011).
182. Obermeier, B., Daneman, R. & Ransohoff, R. M. Development, maintenance and disruption of the blood-brain barrier. *Nat. Med.* **19,** 1584–1596 (2013).
183. Li, F. *et al.* Endothelial Smad4 Maintains Cerebrovascular Integrity by Activating N-Cadherin through Cooperation with Notch. *Dev. Cell* **20,** 291–302 (2011).